The horizontal added mass of a suction bucket jacket

J.H.A. Stokkermans

Technische Universiteit Delft

TU Delft

The horizontal added mass of a suction bucket jacket

by

J.H.A. Stokkermans

to obtain the degree of

Master of Science in

Offshore and Dredging Engineering

at Delft University of Technology,
In cooperation with Royal Boskalis N.V.
Papendrecht, The Netherlands.

To be defended publicly on June 21st, 2018 at 14h00.

Student number:	1524305	
Project duration:	July 1st, 2017 – June 21st, 2018	
Thesis committee:	Prof.dr. ir. A.P. van 't Veer	TU Delft, Chairman
	Ir. J. den Haan	TU Delft
	Ir. P. Hendrickx	Royal Boskalis N.V.
	Ir. O. Sainz Avila	Royal Boskalis N.V.

”There is no shortcut to success,
you have to take the scenic route”

J.H.A. Stokkermans
Delft, June 2018

Contents

Abstract

The new rapidly growing wind energy market has been moving to offshore waters the last few years. New techniques and growing experiences make it possible to move to challenging offshore domains and towards harsher conditions and deeper waters. From the oil & gas industry a lot of expertise is already available on support structures.
The focus in this thesis is on the installation of a jacket type sub-structure for an offshore wind turbine. In more detail: the *horizontal added mass for suction bucket jackets* during installation was studied, from the moment the bucket touches the water till the buckets are fully submerged. This is a period during installation with a lot of uncertainties and unknowns, especially inside the buckets.

A suction bucket jacket is identical to the commonly known jacket type support structure, however, at the bottom of each leg a suction anchor is attached. For a structure of about 60[m] in height and 1000[tonne], these anchors have a rough dimension of 8-9[m] in diameter and have similar heights. Note that the combined mass of the enclosed water inside the buckets can almost reach twice the weight of the dry structure.

Figure 1: Suction bucket jackets.

A benchmark suction bucket with dimensions 10[m] in diameter, 10[m] in height and a wall thickness of 10[cm] was used to design a scale model of 50[cm] diameter, 62.5[cm] in height and a wall thickness of 0.5[cm]. This corresponds to a Froude scaling factor of 1:20.

The experiments were executed at the hydrolab at Boskalis, Papendrecht. A tank of 20x3.5x3[m] was available there to execute the experiments.
The water-depth in the tank was 1.12[m].
During the experiments a vertical pipe segment was forced to oscillate at a known frequency. The pipe was attached to a guiding system, restraining all motions but the surge direction. The applied force by the actuator was measured by a load-cell attached at the point where the crankshaft was connected to the pipe. Simultaneously a LBT-sensor measured the position of the pipe versus time.
The experiments were done for the following settings for draft and scale model wave period range, each experiment was executed three times to reduce the error:

Full scale	wave periods	11	10	9	8	7	6	5	4	
Series	**Configuration**	Period	[s]							
D_1	Draft= 0	2.46	2.24	2.01	1.79	1.57	1.34	1.12	0.89	(3x)
D_2	Draft= $\phi/4$	2.46	2.24	2.01	1.79	1.57	1.34	1.12	0.89	(3x)
D_3	Draft= $\phi/2$	2.46	2.24	2.01	1.79	1.57	1.34	1.12	0.89	(3x)
D_4	Draft=$3\phi/4$	2.46	2.24	2.01	1.79	1.57	1.34	1.12	0.89	(3x)
D_5	Draft= ϕ	2.46	2.24	2.01	1.79	1.57	1.34	1.12	0.89	(3x)

The data was filtered and analyzed with the use of the linear Least Squares Method (LSM). The raw data was fitted by adjusting the amplitude and phase of a sinusoidal fit signal. The amplitude and phase provide information on the relation between damping and added mass in the system.
Finally the results added mass (and damping) were checked with the theoretical potential theory.

While for all frequencies the added mass stayed more or less constant for each draft, during sloshing the added mass decreased. The damping was more or less constant for all drafts at low frequency, but at a wave period of 9[s] the damping start to increase for deeper drafts.
Sloshing occurred at the shortest two periods. This had a significant impact on the damping and added mass terms. At sloshing the added mass decreased rapidly with 40%, while the damping increased up to 300%.

Acknowledgments

Hereby I would like to thank several people who made writing my thesis possible in the first place and/or made my time at Boskalis even more pleasant. First of all I would like to thank Peter Hendrickx, for giving me the opportunity to write my thesis with this beautiful company called Boskalis. Right from the start this felt like a warm bath, the perfect timing of an 'afdelingsuitje' the second week I started at Boskalis was the perfect way to get to know the people I would spend 40 hours per week with for almost a year.
I want to show my immense gratitude to Oscar Sainz Avila, for the very informative moments we had. If I passed by when I had a problem or question, you made time to solve the issue together right on the spot. Your ability to explain problems in a very clear way and distill the problem to basic mathematical equations are what I could not have hoped more for in a mentor.
I want to thank Panagiotis Antonakas for answering a lot of my questions and guidance in the early stages of my research.

Professor Van 't Veer, thanks for facilitating my graduation and your visit to the hydrolab of Boskalis.

During the experiments I got a lot of help from; Maurice Teeuw, Gerrit Verheul, Illker Balaban and Niels Scheffer, thanks for providing me with knowledge, experience and making sure all the equipment and facilities were available, so it was possible to execute the experiments at all.
A special thanks to Marius Schipper, for all the countless times I had practical troubles with building my test set-up, you were my helping hand out.

I want to thank Joost den Haan for his time and support regarding some programming problems I faced in the later stages of my thesis and thanks for being part of my exam committee.
Hereby I want to thank Boy Körver for his inexhaustible support during the final stage of my thesis. Thanks for keeping me on track and kindly forcing me to make a strict planning and stick to it, this is the support I needed in the final stage of my thesis.

Then I want to say thank you Igor Zuikov, Cathelijne van Steensel, Hans van Loon and Reinoud Hoes for their input and answers to my questions during my thesis. Of course thanks to all the other graduate students at Boskalis for having interesting discussions and interesting conversations which made my time at Boskalis even better.
I want to thank my house mates for our conversations, their support and understanding during my thesis.

And then finally, last but definitely not least, special thanks to my girlfriend, family and friends for their support and understanding during the thesis. Especially during the final part, but through the years as well.

For now my eyes are on the very near future, I will go experience what Norway is like during my summer internship at Equinor (former Statoil) in Stavanger. Where I will study the hydro and mooring forces of floating solar energy platforms!

Nomenclature

a	Wave amplitude	$[m]$
A_{ij}	Added mass	$[kg]$
B_{ij}	Damping	$[\frac{kg}{s}]$
C_A	Added mass constant	[-]
C_D	Damping constant	[-]
C_{ij}	Restoring force	$[\frac{kg}{s^2}]$
C_M	Inertia constant	[-]
d	Waterdepth	$[m]$
D	Draft	$[m]$
EOM	Equation of motion	
F	Force	$[N]$
F_n	Froude number $F_n = \frac{v}{\sqrt{gL}}$	[-]
FFT	Fast fourier transform	
g	Gravity constant =9.81	$[\frac{m}{s^2}]$
Hz	Hertz	$[s^{-1}]$
k	Wavenumber $k = \frac{2\pi}{\lambda}$	$[m^{-1}]$
KC	Keulegan Carpenter number	[-]
LSM	Least Squares Method	
M	Mass	$[kg]$
R_n	Reynolds number $Re = \frac{\rho VL}{\mu} = \frac{VL}{\nu}$	[-]
RPM	Rotations Per Minute	$[s^{-1}]$
SWL	Still water level	[m]
T	Wave period	$[s]$
v	Velocity	$[\frac{m}{s}]$
WRD	Wave radiation damping	[-]
x	Displacement in x-direction	$[m]$
$\dot{x}$	Velocity in x-direction	$[\frac{m}{s}]$
$\ddot{x}$	Acceleration in x-direction	$[\frac{m}{s^2}]$

Symbols

λ	Wavelength	[m]
ρ_{sw}	Density seawater = 1025	$[\frac{kg}{m^3}]$
ρ_{fw}	Density freshwater =1000	$[\frac{kg}{m^3}]$
ω	Frequency	$[\frac{rad}{s}]$
ϕ	Phase shift, Bucket diameter	[°], [m]

1 Introduction

1.1. Energy transition

These days the world is on the verge of a large energy transition, conventional oil & gas is slowly replaced by cleaner energy sources such as photo-voltaic (solar) and wind energy.
Wind energy can be divided in two sections, *onshore* and *offshore* divisions. Both divisions have their advantages and disadvantages. The installation and maintenance of onshore wind energy is less expensive due to smaller structures, accessibility and is exposed less to environmental forces.
At offshore locations the wind is usually stronger, resulting in more efficient wind turbines. This comes with the costs of, for example, higher installation and maintenance expenditures.
Nowadays the resistance is growing in the public opinion about onshore wind turbines. The wind turbines are blamed to produce visual pollution and produce a lot of noise and rapid moving shades on the ground. Additionally, for example in the Netherlands, available land space for large wind parks is limited. This all together results in a trend of wind energy moving towards offshore locations. Technical developments and increasing experience in this relatively new business, providing access to deeper waters to install new wind parks in, this increases the possibilities to develop new wind parks offshore.

Last year (2017) was an incredible good year for offshore wind energy. A record of 4,331 MW new offshore wind power was installed across nine markets globally. This represents an increase of 95% compared to the 2016 market. Overall, there is now a capacity of 18,814MW of installed offshore wind power in 17 markets around the world.
The offshore wind market is concentrated in a few locations across the globe. At the end of 2017, nearly 84% (15,780MW) of all offshore installations were located in the waters off the coast of eleven European countries. The remaining 16% is located largely in China, followed by Vietnam, Japan, South Korea, the United States and Taiwan.
The world's largest offshore wind market is located in primarily the UK, this accounts for just over 36% of installed capacity, followed by Germany in the second place with 28.5%. China comes third in the global offshore rankings with just under 15%. Denmark now accounts for 6.8%, the Netherlands 5.9%, Belgium 4.7% and Sweden 1.1%. The rest of the installed power is mainly divided over countries such as Vietnam, Finland, Japan, South Korea, the US, Ireland, Taiwan, Spain, Norway and France [16].

According to Shell's Global Energy resources database, China could produce ten times more wind energy offshore than producing on land. This gives an insight on what the potential of offshore wind energy could be in the future for certain countries [28].

The wind industry is growing and is moving towards offshore environments, the investments in offshore wind overtook the investments made in onshore wind in 2016. The investments for onshore wind decreased by about 5% to €9.4bn, while offshore wind investments increased by 22% to €43bn. Combined this resulted in an increase of 5% on investments in wind energy in 2016 compared to a year earlier [35]. By 2015 there was an approximate of 131GW of installed wind power onshore and about 11GW offshore, this is Europe's third largest energy source, covering 15,6% of Europe's consumption

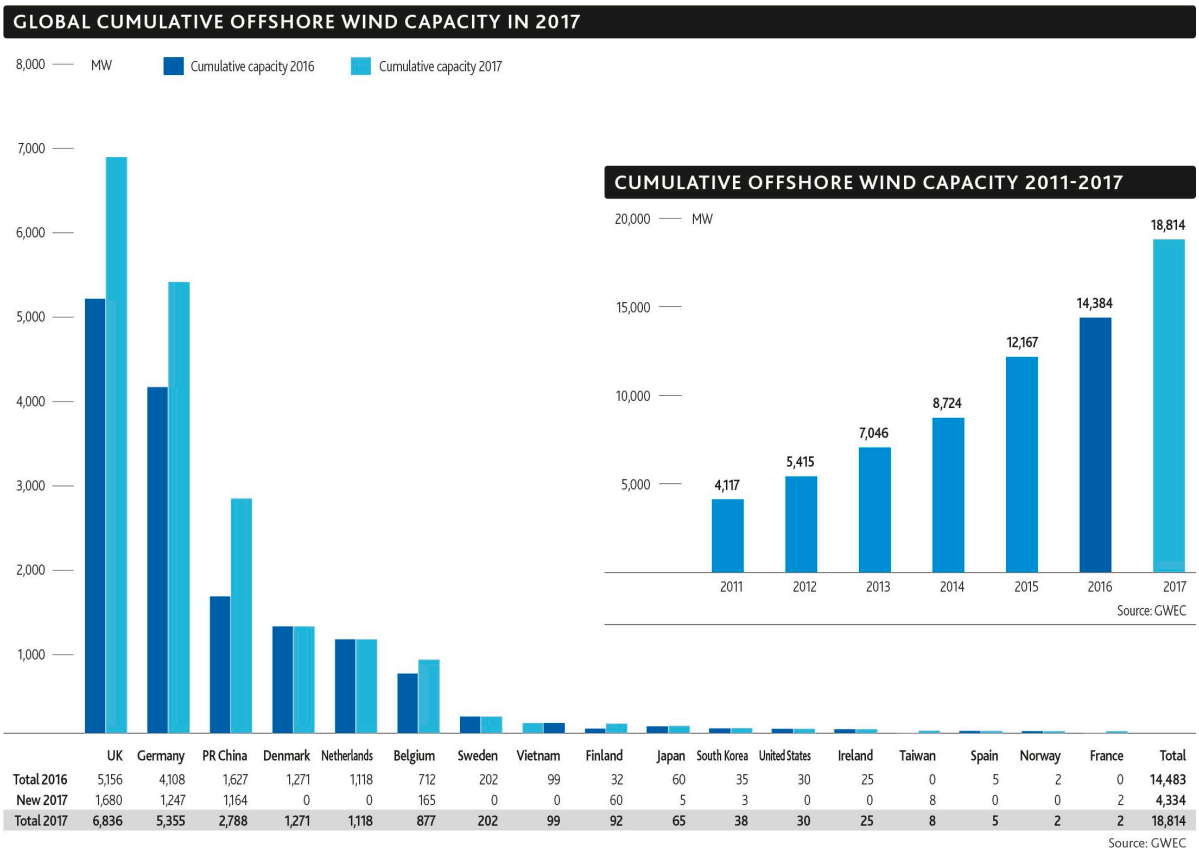

	UK	Germany	PR China	Denmark	Netherlands	Belgium	Sweden	Vietnam	Finland	Japan	South Korea	United States	Ireland	Taiwan	Spain	Norway	France	Total
Total 2016	5,156	4,108	1,627	1,271	1,118	712	202	99	32	60	35	30	25	0	5	2	0	14,483
New 2017	1,680	1,247	1,164	0	0	165	0	0	60	5	3	0	0	8	0	0	2	4,334
Total 2017	**6,836**	**5,355**	**2,788**	**1,271**	**1,118**	**877**	**202**	**99**	**92**	**65**	**38**	**30**	**25**	**8**	**5**	**2**	**2**	**18,814**

Source: GWEC

Figure 1.1: Global cumulative wind capacity in 2017

[35]. By 2016, 12.5GW of wind power was added, roughly 11GW onshore and 1,5GW offshore. Together with this transition, the offshore wind energy is also moving towards deeper waters. The limit of the ongoing increasing diameter of the conventional monopiles is expected to be reached in the near future. Fabrication, transportation and installation becomes more complex for the larger and heavier monopiles. Other, stiffer and lighter structures, such as jackets, become increasingly interesting alternatives [17] [10] [31] [11].

Because this industry in growling rapidly it is interesting for Boskalis to do research on the installation of offshore wind turbines. This thesis is focused on the installation of offshore wind support structures, and more specific *the installation of suction bucket jackets* as support structures for offshore wind turbines.

1.2. Strategy of Boskalis

The strategy of Boskalis is designed to ”benefit from the key macro-economic drivers that fuel global demand in their selected markets: global trade, increasing energy consumption, population growth and the challenges of changing climate conditions” [5].
Recently Boskalis’ new converted vessel, the Bokalift 1 (previously called the Finesse) was released. Bokalift 1, due to its origin as a heavy transport vessel, has a very large strong deck, making it an ideal vessel to transport and install offshore wind turbine support structures.

Boskalis’ clients are considering the use of jacket tripod structures as a support structure for offshore wind turbines in ’deeper’ water (+-60m structures). At some point there will be a trade-off between the heavy monopiles who require thicker walls to withstand (increasing) environmental loading and its own weight. The alternative are the more stiff and lighter jacket support structures which are (slightly) more complex to fabricate and transport. Then within the jacket-type-substructures there are the **suction bucket jackets**.

Figure 1.2: Suction Bucket Jackets on transport

1.3. Installation of support structures

For offshore wind energy it is required to have a large number of structures for a certain (offshore) wind project, while the conservative oil & gas project requires just a few production platforms. For (offshore) wind turbines there is a variance of types of support structures, most of them come from the oil & gas industry, which is an experienced party in offshore support structures. Only bottom founded type of structures are discussed in this thesis. For offshore wind energy, the installation costs are a significant part of the overall costs, therefore it is interesting to study any possible improvements in the installation process. Better understanding of the forces on the substructure can reduce over-estimations and benefit the workability of the installation vessels and finally reducing costs.

Monopiles

Monopiles are the most conventional support structure for on- and offshore wind turbines. Easy to design and manufacture, the installation is straight forward by hammering or driving the monopile into the soil/seabed.
However, expected is that the maximum installable water depth for this kind of wind support structure is soon to be reached. Monopiles are near its maximum available production size. Larger monopiles can buckle or become oval under their own weight and production is no longer possible for the required wall thickness. No hammers are available that are large enough to install monopiles of >10m and larger diameter monopiles produce more noise during installation (+200dB), which can be harmful for the environment. [29]

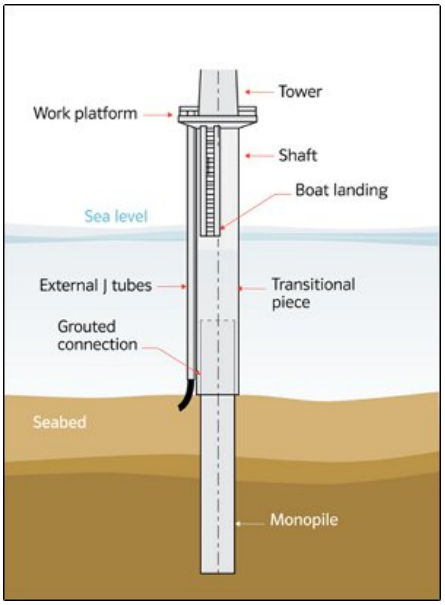

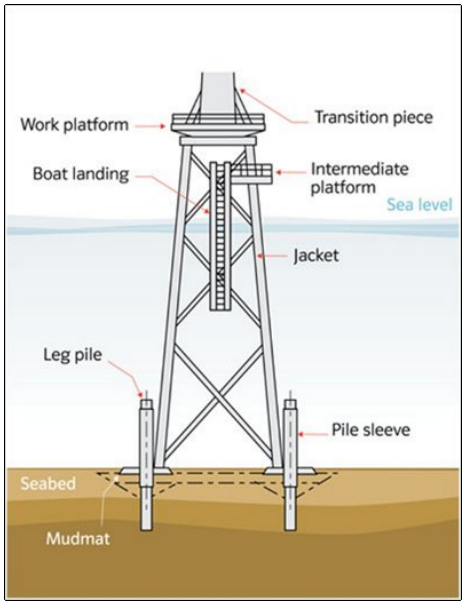

Figure 1.3: a) Monopile support structure. b) Jacket support structure. [1]

Conventional Jackets

A jacket support structure is a structure with (usually) three or four legs connected with slender braces and beams (see figure 1.3b). Once the frame is put on the seabed, piles are hammered through the legs, or through the pile sleeves to connect the structure to the seabed [1].
Jacket structures are more stiff and less steel is required for production than monopiles. Jackets are transparent structures to most sea states and its wide base provides a large resistance to the over-turning moment acting up on it. But they are more complex to produce, so there is a break even point (water depth and sea-states) from where jackets become more favorable than monopiles.
The oil & gas industry has a lot of experience with jacket structures (very common offshore platform). In addition to that, the oil & gas sector has more conservative regulations due to hazards than typically needed for wind energy structures. Therefore a lot of experience and knowledge is available for jacket installations.

Suction bucket Jackets (SBJ)

Suction bucket jackets are applicable in similar water depths as the regular jacket structures. It also has the same properties such as stiffness and overturning moment resistance.
SBJ have some advantages. They can be installed in one operation. No additional hammering is needed, which also reduces under water noise. The SBJ is placed on the seabed, due to its own weight it penetrates the seabed a bit already. Then the buckets are pumped to under pressure by the pre-installed pumps on the buckets. Due to this under pressure the buckets penetrate the seabed further and realize a firm connection [27] [7]. This process can be completely reversed in case of decommissioning. Suction bucket jackets do give restrictions on seabed characteristics, soft soil is needed for the suction buckets to be able to penetrate the seabed.

Splash-zone

During the installation of suction bucket jackets, when the buckets go through the splash-zone, there is a moment of large uncertainties. Several effects come into play, such as: trapped air inside the buckets, dynamic buoyancy forces, incoming waves introduce external forces (including slam loads) on the system. These forces are in horizontal and vertical direction and mostly coupled. This creates a very complex system.

In this thesis the focus is on the horizontal effects, more specific the added mass relations regarding the suction buckets in the splash-zone. The suction buckets are quite big, roughly 10[m] in diameter and 10[m] height. These sizes give large capabilities for possible damping and added mass effects.

Figure 1.4: Suction Bucket Jacket installation through the splash zone

In the following figures the anchoring process is shown in more detail. The pre-installed pumps creating an under-pressure inside the buckets. This under-pressure results in a net force dragging the SBJ into the seabed.

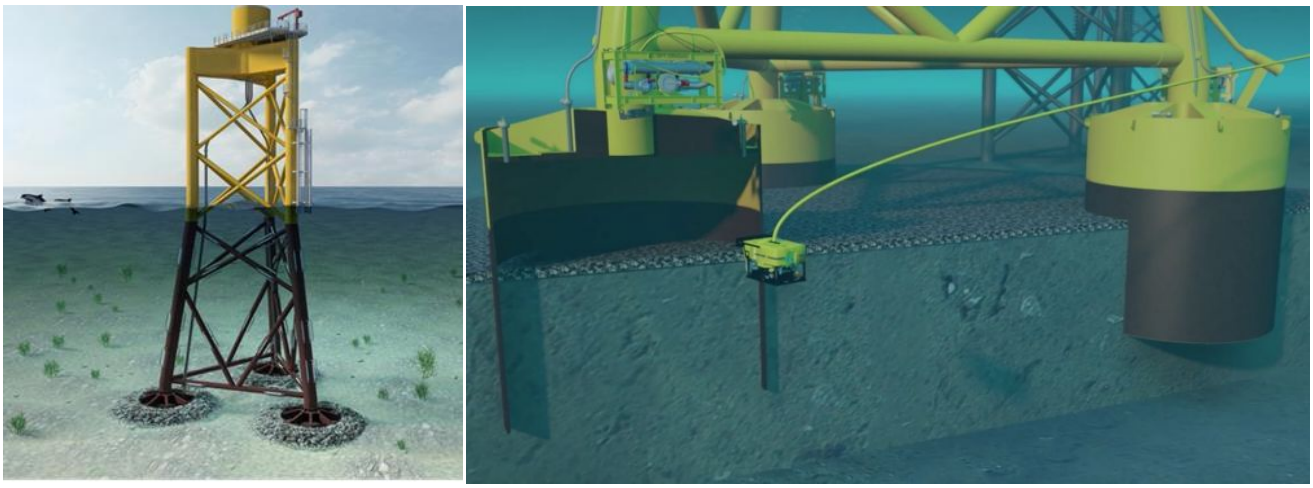

Figure 1.5: a) SBJ support structure installed b) Pumps at work, dragging the SBJ into the seabed

Advantages of SBJ
• Significant reduction of the foundation cost, due to minimal seabed preparation.
• Environmentally friendly installation process (low noise).
• Transport and installation in one procedure.
• Suitable for water depths of 30-60m
• Fully and easy to decommission

Installation process
1. The suction bucket jacket is lowered to the seabed with pumps pre-installed on the buckets.
2. An under pressure is applied to the buckets by individual suction pumps.
3. The hydrostatic pressure difference and the weight of structure causes the buckets to penetrate the soil.
4. The suction pumps are recovered to the installation vessel.
5. A thin layer of concrete is injected between seabed and bucket lid. [**?**]

Figure 1.6: Installed SBJ support structure

1.4. Added mass and its uncertainty

"Added mass" is a term often used in hydrodynamics and can be "visualized" as a mass of water being "stuck" to the body under consideration. A more scientifically justified description would be the forces that are in phase with acceleration (therefore inertial, hence mass equivalent) due to complex hydrodynamic interactions. [25]

Added mass effects inside and outside the buckets are expected.
Because of the large size of the buckets (roughly 10[m] in diameter and 10[m] in height), combined with the fact SBJ consists of three to four buckets, this can result in a large potential horizontal added mass inside the buckets. A simple calculation shows that when the volume of the combined buckets is multiplied with the density of sea water the potential added mass of the volume inside the buckets is:

$$A_m = 3 \cdot \rho \cdot H \cdot \frac{\pi}{4} \cdot D^2 = 3 \cdot 1025 \cdot 10 \cdot \frac{\pi}{4} \cdot 10^2 = 2415099[kg] = 2415.1[tonne]$$

While a SBJ typically weights about 1000 tonne. The added mass inside only, could be up to 2.4 times its intrinsic mass.

The outside added mass can be calculated using the known theories:
1. Morison equation [reversed and only for slender (compared to wavelength) bodies] [22].
2. Diffraction theory.

Because it is unknown which part of this volume has to be considered "trapped" inside the bucket, a conservative approach is taken and the full volume inside the bucket is assumed to be "trapped".
The amount of added mass is expected to be wave **frequency dependent** and and of course **draft dependent**.

1.5. Scope of the thesis

The scope of this research is to achieve an understanding on how the horizontal added mass (inside) of a SBJ is dependent on **draft(T)** and **frequency(ω)**.
More specifically, from the moment the SBJ touches the waterline, until the bucket is fully submerged. This will be studied for the most dominant frequencies that can be found in the north sea (JONSWAP spectrum).

The added mass can be considered to consist of an added mass outside and an added mass inside the bucket. Especially the contribution of the added mass inside the bucket is a large unknown at the moment. The outside added mass can be estimated quite accurately using known theories, for example the diffraction theory.

The (horizontal) added mass plays an important role in the maximum offlead and sidelead of the crane, which are limiting factors in the workability of crane vessels.
The SBJ can be modeled as a double pendulum when hanging in the crane. The eigen-frequency is dependent on the moment of inertia of the system. The three suction buckets have a non-negligible influence on the double pendulumn eigen-frequency due to the large dimensions of the buckets, which are roughly 10[m] high and 10[m] in diameter.
No previous experiments are available to rely on for determining the added mass in horizontal direction for open vertical cylinders that pierce the water surface.

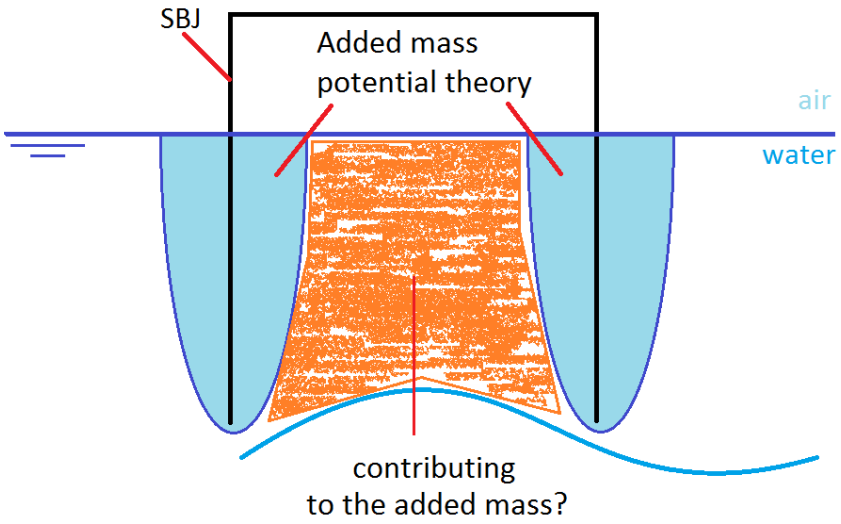

Figure 1.7: Schematic cross section of a suction bucket and its expected added mass

Hypothesis
Low frequencies allow water to flow around the bucket edges easily into the cavity of the bucket, possibly reducing the inertia term.
For obvious reasons it can be assumed that the further the bucket is submerged the more water can be assumed to be ”trapped” inside and contribute to the inertia term.

Hornsea One and Aberdeen Offshore Wind Project

The Hornsea One Project and the Aberdeen Offshore Wind Project can be used as a benchmark for this study. The Hornsea One is an offshore wind project 120km offshore Hornsea, United Kingdom. Hornsea One consists of 174 wind turbines of 7MW each, resulting in an installed power of 1,128MW. It is located at water depths varying from 24 to 37m. For support structures SBJ’s were initially considered.
The Aberdeen Project is an offshore wind project with 11 SBJ’s of 8.4MW, with a combined capacity of 93.2 MW. Located 2.4km offshore at a water depth of 19-32[m]. These are the second most powerful installed wind turbines to date [1] [36] [26].

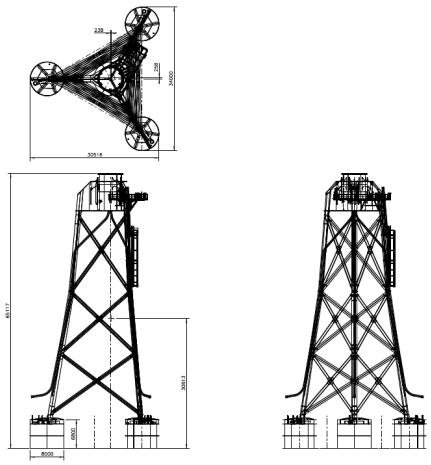

Figure 1.8: Hornsea SBJ proposal

Aberdeen SBJ installation

1.6. Experiments

Experiments are intended to provide a more realistic view on these relations than available software can provide. Every type of software usually has its flaws, for example it is often based on linear potential theory and excludes the viscous effects. When sloshing comes into play, the software becomes inaccurate because this is a highly non-linear effect. Experiments can hopefully provide a more realistic insight on the hydrodynamic response.
Although the post processing of the experiments is also based on linearizations, the non-linear effects are measured and are present in the raw obtained data.
Chosen is to go for a model scale because a full scale experiment is far more expensive. There is no (spare) SBJ available, the experiments could not be executed on shore and it is not sure whether there is a crane vessel plus crew available for executing the experiments.
Close attention needs to be paid to scaling effects to correctly represent the full scale SBJ in the experiments.

The model scale experiment can be described as follows:
A hollow pipe segment will be forced by an actuator to undergo a forced harmonic oscillation, purely in surge motion.
The dry weight (M_0) and the applied displacement in time (frequency (ω) and amplitude($\hat{x}$)) are known.
The measured force on the bucket by the actuator ($F(t)$) and its corresponding displacement $x(t)$.
Dry tests provide the friction in the system.
All known and measured values together make it possible to finally determine the added mass of the water inside and around the bucket.

The next stage is to determine the relation between added mass inside the SBJ and its draft (T). Same goes for the relation between the added mass and the applied frequency/diameter ratio ($\frac{\omega}{D}$).

Further on in the report more information is given on the parameters of the experiments, the chosen values and the to be expected results for the specific variables.
In chapter two is explained which theories are used to finally derive the added mass and the damping for the SBJ. In chapter 3 details can be found on the experimental set-up, practical information about the set-up and used sensors and equipment. In chapter 4 the data from the experiments is analyzed. In chapter 5 the analyzed results of the experiments are presented. Discussions and conclusions can be found in chapter 6. Finally recommendations for future studies are made in chapter 7.

2

Methods and Theories

In this chapter the methodology is explained how the full size suction bucket is replicated in a scale model. Finally, the assumptions and theories are explained on which the analysis is based to obtain the final results.

2.1. Assumptions

As described in Offshore Hydromechanics [22] all flows are treated as being potential flows. This is a mathematical way of describing the laws of fluid mechanics in a simplified version. Basic flow properties are defined: the medium being **non-viscous**, **incompressible**, **continuous** and **homogeneous**. These statements together can be derived to the so called potential theory, in short, the velocity of a particle in a flow is equal to the derivative if the potential function ($\Phi(x, y, z)$ in that direction.

$$u = \frac{\partial \Phi}{\partial x},\ v = \frac{\partial \Phi}{\partial y},\ w = \frac{\partial \Phi}{\partial z}$$

See Offshore Hydromechanics by Journee for more background information on the potential theory [22].

For linear (Airy) waves the potential function can be described as:

$$\phi = \frac{g\zeta_a}{\omega} \frac{\cosh k(z+d)}{\cosh(kd)} \cos(\omega t - kx\cos(\beta) - ky\cos(\beta)) \qquad [m^2/s]$$

The particle velocity can be obtained via $\vec{v} = \vec{\nabla}\phi$.
For the vertical particle velocity this becomes;

$$\vec{v} = \omega\zeta_a e^{kz} \cos(\omega t - kx\sin(\beta) - ky\sin(\beta)) \qquad [m/s]$$

If this theory is isolated to the effect of one single bucket, the beta term(β) drops out due to symmetry. If the space origin is chosen in the center of the bucket the x and y term vanishes likewise. The equations describe the undisturbed wave in the center of the bucket. Resulting in the following equations:

$$\zeta = \zeta_a \sin(\omega t) \qquad [m]$$

$$\phi = \frac{g\zeta_a}{\omega} \frac{\cosh k(z+d)}{\cosh(kd)} \cos(\omega t)) \qquad [m^2/s]$$

$$\vec{v} = \omega\zeta_a e^{kz} \cos(\omega t) \qquad [m/s] \tag{2.1}$$

With boundary conditions:
1. Continuity condition, incompressibility, irrotationality
2. Seabed boundary (no penetration of the seabed)
3. Free surface dynamic boundary condition
4. Free surface kinematic boundary condition.
5. Radiation condition
6. Symmetric or anti-symmetric condition

Potential Theory
The wave potential function ($\Phi(x, y, z)$ $[m^2/s]$) should fulfill the following statements [22]:
1. Continuity condition, incompressibility, irrotationality.
2. Seabed boundary (no penetration of the seabed).
3. Free surface dynamic boundary condition.
4. Free surface kinematic boundary condition.

Assumed is that the wave slope being very small and it is sinusoidal shaped. A result of these general assumptions is that the dispersion relation holds:

$$\omega^2 = kg \cdot \tanh(kh) \tag{2.2}$$

This relation is later used to calculate the wave group velocity and wave reflection times in the tank.

2.2. Hydrodynamic Forces
The forces acting up on the structure can be divided into two categories: the *Excitation forces* and the *Radiation forces*.

Excitation forces
Structures in waves will experience loads. These forces can be estimated using two types of forces: the *Froude-Krylov Forces* and the *Diffraction forces*[13] [12].
- The excitation forces are the forces acting up on the structure due to incoming waves, the pressure field integration over the wetted surface of the undisturbed wave are called Froude-Krylov forces.
- The forces required by the structure to disturb the incoming waves are called diffraction forces.

Froude-Krylov Forces
The Froude-Krylov forces are the forces induced by the unsteady pressure fields generated by the *undisturbed incident waves*.

$$\vec{F}_{FK} = -\int\int_{S_W} p\vec{n}ds \tag{2.3}$$

Where:
$\vec{F}_{FK}$ Froude–Krylov force
S_w Structure's wetted surface
p Undisturbed wave pressure
$\vec{n}$ Structures normal vector vector (pointing into the water)

Diffraction forces

Diffraction forces are the forces required by the floating structure to disturb the incoming waves. These potentials have to satisfy the earlier presented boundary conditions.
McCamy and Fuchs (1954) [17] derived an analytical expression for wave diffraction on vertical cylinders. This led to the inertia coefficient C_m in the Morison equation of:

$$C_m = \frac{4A(ka)}{\pi(ka)^2}$$

Where:

$$A(ka) = \sqrt{J_1'^2 + Y_1'^2}$$

a = radius cylinder
k = wave number
$J_1'^2$ and $Y_1'^2$ are derivatives of the Bessel functions of order one and two.

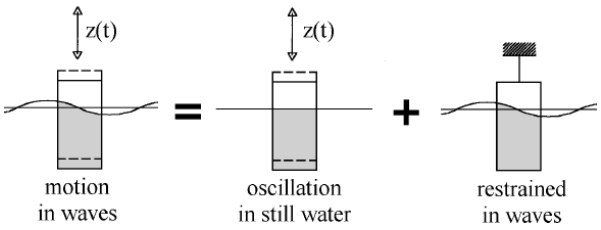

Figure 2.1: Superposition excitation forces

Because the Froude-Krylov forces and the diffraction forces are linear, they can be added using superposition, this results in the total motions due to incoming waves. This is shown in figure 2.1 (albeit in the vertical direction, the same holds for horizontal directions). On the left hand side the superposition is shown for the loads, while on the right hand side the loads are separated into *diffraction loads* and *wave radiation loads*.

Radiation forces

In this thesis a forced oscillation is studied, therefore no incoming waves and hence no incoming wave forces are present. The reaction forces are determined by measuring the force needed to oscillate the model at a certain, forced, frequency.

Added mass

The force required to move the bucket and its added mass according to the forced oscillation, is studied in this research. From this the added mass is extracted. Expected is that there is a dependency on the draft of the bucket and a (slight) dependency on the frequency.

Wave radiation forces

While forcing the bucket to undergo a harmonic oscillation with a determined frequency, it is inevitable to generate waves. These waves have a non-zero amplitude and therefore contain energy. This will contribute to the damping (B), which later is determined together with the added mass.

2.3. Parameters

Full scale

Proposed and even installed suction bucket jacket projects such as Hornsea One and Aberdeen Offshore can be used as benchmark projects. The proposed Hornsea project consisted of suction buckets of 6.8[m] in height and 8[m] in diameter, while the jacket was 65.1[m] in total. Aberdeen consisted of suction buckets of 11.5[m] in height and 10.05[m] diameter, while the jacket was 61.3[m] in total. See figure 1.8 for drawings and a photo of the mentioned SBJs.
For this thesis a reference full scale model will be used containing suction buckets to be of 10[m] in height and 10[m] in diameter. Unfortunately no hydrodynamic data is available for either of these projects. A scale model of 1:20 will be used, which corresponds a 10[m] full scale diameter to a 50[cm] model scale.

2.4. Scaling Laws

2.4.1. Reynolds Scaling

When viscous and inertia forces are of importance, Reynolds scaling has to be used. For example in pipe flows and when flows are creating wake formations behind a body. It indicates the importance of viscous effects within the system. Low Reynolds numbers indicate dominance of viscous effects and high Reynolds numbers indicate turbulence flows. Stationary water flows are not considered to have a large direct influence on the added mass [22].

2.4.2. Froude Scaling

When free surface effects, and thus gravity forces, are part of the system, Froude scaling should be applied. In Froude scaling the ratio of inertia (or pressure) forces versus gravity forces is preserved [32]. The added mass is proportional to the forces and accelerations. The force and the displacement is what will be measured during the experiments. Inertia forces are studied, therefore Froude scaling is used to scale the model. The Froude number should be kept constant for both the full scale suction bucket and the model scale bucket.

$$F_n = \sqrt{\frac{inertia\ or\ pressure\ forces}{gravity\ forces}} \tag{2.4}$$

A dimension analysis is done for this equation. Obviously, the Froude number is a dimensionless number, but it can give insight on how scaling for different dimensions relate to each other.
Every scaling factor α is the relation of the model dimension divided by the full scale dimension.
For example the dimension length: $\alpha_L = \frac{L_{model}}{L_{full}}$. Other scaling factors are present for the; velocity V, wave period T, gravity constant g and density constant ρ.

$$F_n = \sqrt{\frac{\alpha_\rho \cdot \alpha_V^2 \cdot \alpha_L^2}{\alpha_\rho \cdot \alpha_L^3 \cdot \alpha_g}} = \sqrt{\frac{\alpha_L^2 \cdot \alpha_L^2}{\alpha_L^3 \cdot \alpha_T^2}} = \sqrt{\frac{\alpha_L}{\alpha_T^2}} = \frac{\sqrt{\alpha_L}}{\alpha_T} = [-] \tag{2.5}$$

$\alpha_g = 1$ Since the gravity (and thus α_g) can not (easily) be changed.
$\alpha_\rho = 0.976 \approx 1$ The density scaling factor is approximately 1.
Fresh water will be used in the tank ($1000[kg/m^3]$), while offshore salt water is present ($1025[kg/m^3]$).

The fact that relatively cold water ($6°C$) is used, which is close to the highest density point of $4°C$, compensates slightly for this error. It is good to be aware of these errors but it is chosen to not compensate for this small deviation in the practical and theoretical scaled density.

$$F_n = \frac{V}{\sqrt{gL}} \tag{2.6}$$

V Relative velocity
g Gravity constant
L Characteristic length model

From equation 2.5 the time-relation $\alpha_T = \sqrt{\alpha_L}$ holds. As a result;

Time scales with $\alpha_T = \sqrt{\frac{L_{real\ scale}}{L_{model\ scale}}}$

Preferred is to represent the full scale object in the experiment as good as possible, three distinct similarities properties can be determined:

- **Geometric similarity** Model has uniform dimension proportions to the prototype (the same shapes)
- **Kinematic similarity** Velocities in the model are proportional to those in the prototype
- **Dynamic similarity** Forces and accelerations are proportional to those in the prototype

Each of these similarities should be met as much as possible in the model scale.

2.5. Linearity of System

Several theories are based on linearity characteristics. The equation of motion is linearized. This is only valid for small displacements. As derived in Offshore Hydromechanics [22], the amplitude of the forced oscillation should be well below one third of the bucket diameter.
Frequencies below produced breaking waves, inside the bucket visible as sloshing, can be linearized. Sloshing will introduce non-linearities which will be linear approximated in the post processing process.

Keulegan Carpenter number

Garbis H. Keulegan and Lloyd H. Carpenter described in their paper that was published in 1958 the drag and inertia terms of plates and cylinders in an oscillating flow [23].
Their Keulegan-Carpenter (KC) number is a dimensionless quantity describing the relative relation between drag forces and inertia forces. In other words, for small KC numbers the inertia is dominant, which is a linear domain. While larger KC values (3<KC<15) indicate drag dominance, which is a non-linear effect, for this non-linear domain the drag effect is often linearized. For 15<KC<45 it is impossible to avoid the full Morison equation including the non-linear drag. For KC>45 the drag effect is the dominant factor, the vortex shedding frequency becomes high compared to the wave frequency. The flow starts to behave like a uniform flow (current). Inertia effects can be neglected in this situation [22]. See figure 2.2 for illustrated KC values. Aimed for is to stay within small KC values during the experiments [18].
The KC number is a measure of the water particle orbital amplitude, with respect to the cylinder diameter. This shows the relationship of the circumference of the wave particle path to the structure diameter. [33]

$$KC = \frac{VT}{L} \tag{2.7}$$

Where:
V Amplitude of flow velocity
T Period of oscillation
L Characteristic length of object

As stated in Offshore Hydromechanics [22] the relation is linear if [amplitude oscillation < 3·D] [17] [13] which can be interpreted as the maximal forced oscillation amplitude $x_{max}(t) << \frac{1}{3}$ of the diameter of the bucket. Together with the requirement that the slope of the waves has to be low (sinusoidal waves, no wave breaking) it is assumed that linear properties are present.
When energy is accumulated in an eigen-mode inside a volume with rigid boundaries, the standing wave amplitude increases. This effect keeps on going till the critical wave steepness is reached. At this point waves start to break, this effect is also known as *sloshing*. Sloshing is a highly non-linear

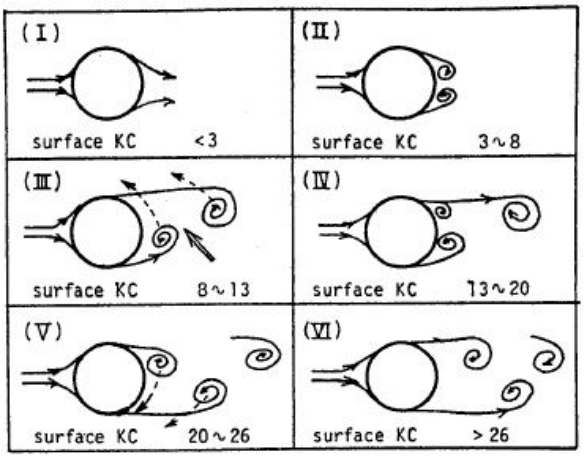

Figure 2.2: Illustrated KC regimes [Iwagaki, et al. (1983)]

effect. When this comes into play the sloshing effect should be linearized to comply with the theories again, or other post process methodologies should be taken to describe the effects properly.

2.6. Equation of Motion

Assumed is that the system is completely free in any direction, it does not experience any constraint in any direction. The free system will then have 6 degrees of freedom (DOF). Hence the matrices in the equation of motion (EOM) are [6x6] and the vectors $\vec{X}$ and $\vec{F}$ are [1x6] vectors. (i=6,j=6)

Equation of motion:

$$\left[M_{ij} + A_{ij}\right] \cdot \ddot{\vec{x}} + \left[B_{ij}\right] \cdot \dot{\vec{x}} + \left[C_{ij}\right] \cdot \vec{x} = \sum \vec{F}_{extern}$$

M_{ij} is a constant for i=j, namely the rest mass of the system M_0 and zero elsewhere. In the model this is the mass of the pipe segment and its attached moving components.

B_{ij} is the damping term, this can roughly be divided in friction terms in the system (e.g. friction in the rails of the model) and an hydro damping term.

$$\left[B_{ij}\right] = \left[B_{ij}\right]_{system} + \left[B_{ij}\right]_{hydro} \tag{2.8}$$

Because there is no restoring force in the horizontal direction, C is set to zero, resulting in the following equation:

$$\left[M_{ij} + A_{ij}\right] \cdot \ddot{\vec{x}} + \left[B_{ij}\right] \cdot \dot{\vec{x}} + = \sum \vec{F}_{extern}$$

The suction bucket is axis-symmetric and will only move in surge motion in the test set-up, so the vector and matrix notation can be removed. The general equation can be rewritten for the suction bucket model in surge direction as:

$$(M_0 + A) \cdot \ddot{x} + B \cdot \dot{x} = F_{extern}(t) \tag{2.9}$$

Where:

M_0	Intrinsic mass of all moving parts	this is measured to be 21,5 [kg].
A	Added mass	
B	Damping term	frequency dependent.
C	Spring term	no restoring force in surge motion, this term reduces to zero.
$F(t)$	Force	applied by the actuator to the model.
$x(t)$	Displacement	forced oscillation in surge direction, known amplitude and frequency.
T	Draft	draft of bucket.

Dimensionless Added Mass

DNV RP-H103[34] defines the dimensionless added as:

$$Added\ mass[-] = \frac{Added\ mass}{\rho \cdot Volume\ pipe} = \frac{A}{\rho \cdot \frac{\pi}{4} D^2 T} = [-] \tag{2.10}$$

This is convenient to compare added mass properties of different drafts to each other and to possible other experiments found in literature.
Expected is that the dimensionless added mass scales approximately linear with depth, deeper drafts provide more surface to interact with the water. Geometric effects may deviate slightly from this linear assumption.

Dimensionless Damping

The damping term can be made dimensionless by:

$$D_{dimless} = \frac{Damping}{\rho V \sqrt{\frac{g}{D}}} = \frac{Damping}{\rho \frac{\pi}{4} D^2 \sqrt{\frac{g}{D}}} = \frac{Damping}{\rho \frac{\pi}{4} D^{\frac{3}{2}} \sqrt{g}} = [-] \tag{2.11}$$

Expected is that this damping term decreases for increasing drafts, wave radiation damping is expected tot be the dominant effect. Because this takes place at the air-water interface this effect decreases with depth. When the damping is divided by its submerged volume the ratio will decrease.

2.7. Data filtering

Once the to be studied frequency range is determined and the scaling properties are known, the equation of motion can be determined to estimate the expected results. The experimental set-up can then be determined and the experiments can be executed. When the raw data is available, the results need to be filtered to reduce errors before conclusions can be drawn from the results. Several filtering methodologies are available, of which several are discussed below.

2.7.1. Fast Fourier Transform (FFT)

The damping can be found easily when the displacement signal is started at the point where the phase is zero. The Fast Fourier Transform gives a complex function, which contains of a real and an imaginary part.The damping will increase for increasing frequency. The real and imaginary part can be separated. The real part gives the added mass versus frequency relation, while the imaginary part gives information about the damping versus frequency relation.

2.7.2. Linear Least Squares Method

Assumed is an harmonic response signal. Just as the forced input signal, but with a different amplitude $\hat{F}$ and with a phase difference ϕ compared with the input signal. The input displacement signal can be described as:

$$x(t) = \hat{x}\cos(\omega t)$$

While the force response signal is expected to be:

$$x(t) = \hat{F}\cos(\omega t + \phi)$$

The system can, after some rewriting, be described as the following mathematical system (see section 4.4) for the complete derivation:

$$[A]\ \vec{b} = \vec{F} \tag{2.12}$$

This is a linear fit method, however, for experimental results this system usually has no exact values for the vector b such that the system gives valid solutions. Therefore the vector b is solved to the point where it gives the best approximation of the solution, the best fit. This is done by solving the quadratic minimization problem.

$$error = (Ab - F(t))$$

Because the area between the function and the fit needs to be minimized the square is taken (negative values are not allowed to cancel positive values):

$$error^2 = (Ab - F(t))^2$$

Morison Approach

The Morison equation is a gentle method to calculate the *outside* forces on stationary slender cylinders in a non-stationary medium. The Morison equation can be described as:

$$F = \underbrace{\rho\, C_m \frac{\pi}{4} D^2\, \dot{u}}_{F_I} + \underbrace{\frac{1}{2}\rho\, C_d\, D\, u\, |u|}_{F_D} \tag{2.13}$$

Where:

ρ Water density
u Flow velocity
C_m Inertia coefficient
C_d Damping coefficient
D Diameter cylinder.

The total force is a combined force of the inertia force (F_I) and the drag force (F_I). One of the limits of the Morison equation is that it is only valid for slender cylinders, so to say, the relation $\frac{D}{\lambda} < [0.1 - 0.2]$ must hold [13][22].

2.8. Forced Oscillation test

Vertical motions

A forced oscillation experiment is an easy way of determining the added mass and damping terms of a body. A vertical forced oscillation test for a buoy is described in Offshore Hydromechanics by Journeé and Massie [22]. The forced heave oscillation test set-up can be seen in fig 2.4. The buoy is defined by the forced vertical motion, described as:

$$z(t) = z_a \sin(\omega t)$$

z_a is the amplitude of the buoy, ω is the (forced) oscillation frequency.
The heave forces are correlated to the vertical displacement, the forces measured by the transducer are:

$$F(t) = F_a \sin(\omega t + \epsilon_{FZ})$$

F_a is the amplitude of the applied force, ϵ_{FZ} is the phase shift between displacement and force in the vertical direction.

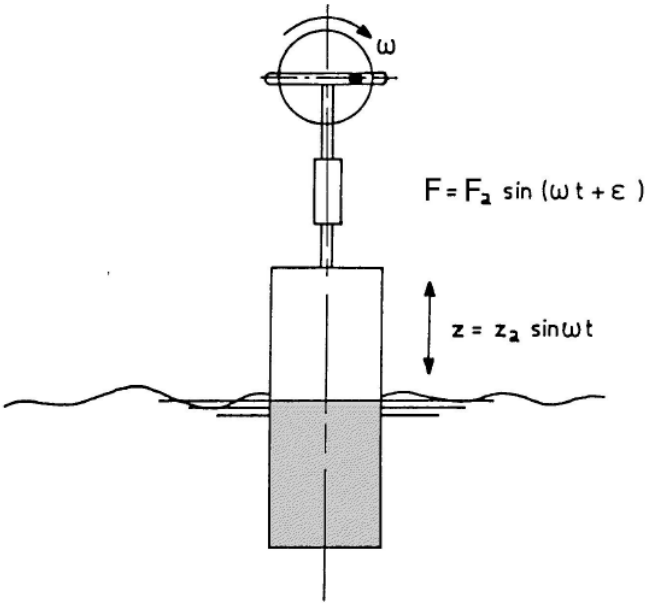

Figure 2.4: Forced Oscillation Test

The linear equation of motion (EOM) is given by:

$$\boxed{(m+a)\ddot{z} + b\dot{z} + cz = F_a \sin(\omega t + \epsilon_{FZ})} \tag{2.14}$$

Where z=$z(t)$ and the derivatives follow from the forced oscillation input:

$z(t) = z_a \sin(\omega t)$
$\dot{z}(t) = \omega z_a \cos(\omega t)$
$\ddot{z}(t) = -\omega^2 z_a \sin(\omega t)$
This can be implied in the EoM and simplified to obtain:

$$z_a[-(m+a)\omega^2 + c]\sin(\omega t) + z_a b\omega \cos(\omega t) = F_a cos(\epsilon_{FZ}) \sin(\omega t) + F_a \cos(\omega t)\sin(\epsilon_{FZ})$$

This can be separated by taking specific times where the cosine or sine functions drop out. At $\omega t = \frac{\pi}{2}$ and $\omega t = 0$, to find values for the added mass (a) and the damper term (b), since they are $assumed$ to be perfectly out of phase:

$\omega t = \frac{\pi}{2} \quad \rightarrow \quad a = \frac{c - \frac{F_a}{z_a}\cos(\epsilon_{FZ})}{\omega^2} - m$

$\omega t = 0 \quad \rightarrow \quad b = \frac{c - \frac{F_a}{z_a}\sin(\epsilon_{FZ})}{\omega}$

From geometry the spring term can be determined for this vertical walled cylinder:
$c = \rho g A_w$

2.9. Translation to forced surge oscillation

For horizontal forced oscillation the same theory can be applied as the vertical forced oscillation explained previously. One important difference should be noted: there will not be a restoring force, hence c will be zero, $c = 0$. This results in the following superposition of hydro-mechanical and wave loads [22].

The forced displacement is harmonic and known, this can be written as:

$$x(t) = \hat{x}\cos(\omega t) \tag{2.15}$$

Where:
- $\hat{x}$ amplitude of harmonic oscillation, equal to half of the maximal stroke of the actuator
- ω is the known and forced frequency [rad/s]
- t time [s]

The related reaction force has to have the same frequency (ω). Since this is a physical model which is not ideal, there will be friction, drag and wave radiation damping. Therefore the reaction force will experience a phase shift (ϕ) additional to the 90° phase shift the force and displacement already have. This results in the theoretical force equation with the unknown phase shift ϕ and the unknown amplitude $\hat{F}$.

$$F(t) = \hat{F}\cos(\omega t + \phi) \tag{2.16}$$

Where;

$\hat{F}$	maximal amplitude of the force signal	[N]
ω	known forced frequency	[rad/s] (equal to the signal x(t))
t	time	[s]
ϕ	unknown phase shift between x(t) and F(t)	[rad/s]

With the least squares method $\hat{F}$ and ϕ can be fitted to the data set. For more details on this fitting method see the chapter *Post Processing*.

Horizontal added mass

The DNV RP-H103 regulation [34] state that for lifting through the splash-zone the following effects play a role in horizontal direction:
Inertia force due to moving object:

$$F_{I,i} = -(M\delta_{ij} + A_{ij})\ddot{x}_j \qquad [N]$$

M = intrinsic mass [kg]
δ_{ij} = 1 if i=j, else 0
A_{ij} = added mass in direction i due to acceleration in direction j
x_j = acceleration in direction j

Because in the experiments only surge motion is allowed this problem simplifies to the 1D problem described in equation 2.9 (this time no damping is left out of the equation).
The added mass is usually expressed in term is an *dimensionless* added mass coefficient C_A^{ij} defined by:

$$A_{ij} = \rho C_A^{ij} V_R$$

Where:
ρ = density of water
V_R = Volume of body

When an object moves in the vicinity of the free surface, radiation gravity waves are generated, damping the original motions. This is called the wave damping force, or wave radiation force:

$$F_{WDF} = B_{ij}\dot{x_j} \qquad [N]$$

Where:
B_{ij} = wave generation damping coefficient $[\frac{kg}{s}]$
$\dot{x_j}$ = object velocity near free surface $[\frac{m}{s}]$

According to the guidelines ”DNV-RP-H103 Modelling and analysis of marine operations” [34], wave damping effect vanishes when the wavelength is much larger or much smaller than the object characteristics dimension. Because the wavelength is dependent on the frequency, this relation can be expressed in the wave period:

$$T >> \sqrt{\frac{2\pi D}{g}} \qquad [s]$$

2.10. Validation methods

The conventional approach to this kind of problems in full scale is make an computational model (Ansys) of the buckets and find its properties regarding added mass and damping. The properties are then loaded to an Orcaflex model and launch waves of a certain spectrum and direction to it. One of the approaches is that all of the water inside the buckets is considered trapped.

Computational Fluid Dynamics (CFD)
CFD is, compared to experiments, a cheap solution to study hydrodynamic effects. Although it should be stated that computation times can become extremely long.

CFD is based on the following concepts:
General transport equations, mass conservation, momentum conservation and energy conservation.
Navier-Stokes equations and modeling simplifications.

CFD results are largely dependent on assumptions made prior to the computation. Grid definition and grid sizes are of big importance. The grid should be refined around the object, especially at sharp edges.
CFD using the panel method is unfortunately still unable to model viscous effects. Boundary conditions are impossible to meet in CFD when wave breaking takes place and water and air (compressible and incompressible fluids) mix. All these effects with unknown influences are taken into account doing scale experiments, giving it in this sense a more realistic result.

Experiments
Experiments will be executed to study the hydrodynamic effects.
A scale model of a full scale SBJ will be build and experimented with, more information on scaling properties can be found in the next chapter. A forced oscillation with a known frequency range are executed, while the displacement and force on the bucket will be measured versus time.
Finally, the experiment results are compared to the damping and added mass analysis from Ansys.

It is chosen to do experiments with a physical scale model of the suction buckets to get the most realistic results for the added mass in real size suction buckets. All hydro effects that are taking place are covered, including the non-linear effects. These effects will be linearized during the post processing method.

3

Experimental set-up

In this chapter, the test set-up will be explained in detail. Which characteristics are present, which sensors are used, what kind of actuator and other equipment is needed to execute the experiments and what outcomes may be expected.
All the experiments are executed in the hydrolab at Boskalis Papendrecht. There a towing tank is available for the experiments. A movable bridge is present to cross the tank. The set-up is attached to this bridge. The tank has dimensions of 20[m]x3.5[m]x3[m] (LxWxH). At one side of the tank a ladder is present, at the other side of the tank a large sheet is hung into the water to act as a wave damper to reduce wave reflections. The water depth in the tank was 1.12[m], this due to the frame dimensions, position of the window in the tank and the height of the bridge.

3.1. Frame design

A specific frame was designed for this experiment. In attachment A.1 detailed technical drawings and assembly drawings can be found of the designed frame.

The requirements for this frame were as follows:
• To be safe. No risk of injury or risk of electronics being exposed to water.
• The frame has to be able to guide the surge motion and support of the bucket.
• Adjustable in draft. If possible from the bridge, instead from within the tank, this is a plus.
• Minimal friction in the guiding system (rails) is required, because this influences the accuracy of the experiments.
• No penetration of still water level (SWL). This can result in wave reflections interfering with the test set-up.
• All sensors have to be able to be attached to the frame and/or pipe.
• The frame need to be as stiff as possible, especially in surge motion.

The yellow frame tubes go through the green casing tubes, here a bolted connection holds the frame at the right draft. Holes are pre-drilled at the right drafts of the bucket, this way there is no need to change the water depth at different drafts of the bucket during the experiments. The frame can be lowered and lifted by a hand tackle accessible from the bridge.

3.2. Set-up Characteristics

The set-up is equipped with several sensors. The crankshaft is connected to a load-cell on the pipe, this sensor gives the applied force on the pipe. A BTL magnetostrictive linear position sensors is attached to the frame, a magnet connected to the pipe will slide over the needle of the BTL-sensor (without touching it) and tracks the displacement of the bucket in time. These two sensors give the relation between the applied force and the resulting displacement in time. From this the velocity and acceleration can be determined.
As a cross check an accelerometer is attached to the pipe segment, to validate if the applied force (minus damping terms) contributes to the acceleration. This can be seen in figure 3.2.

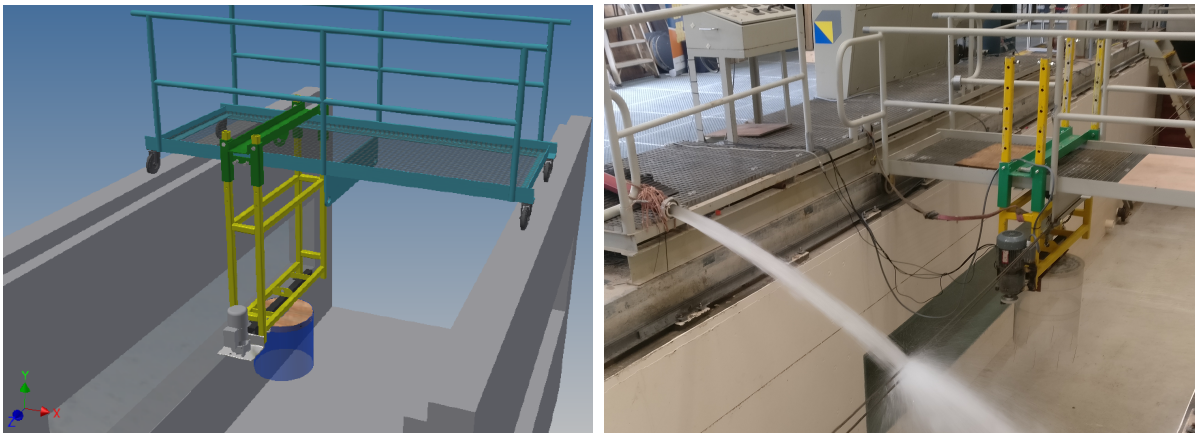

Figure 3.1: Technical drawing of the frame set-up and realized frame when tank is being filled.

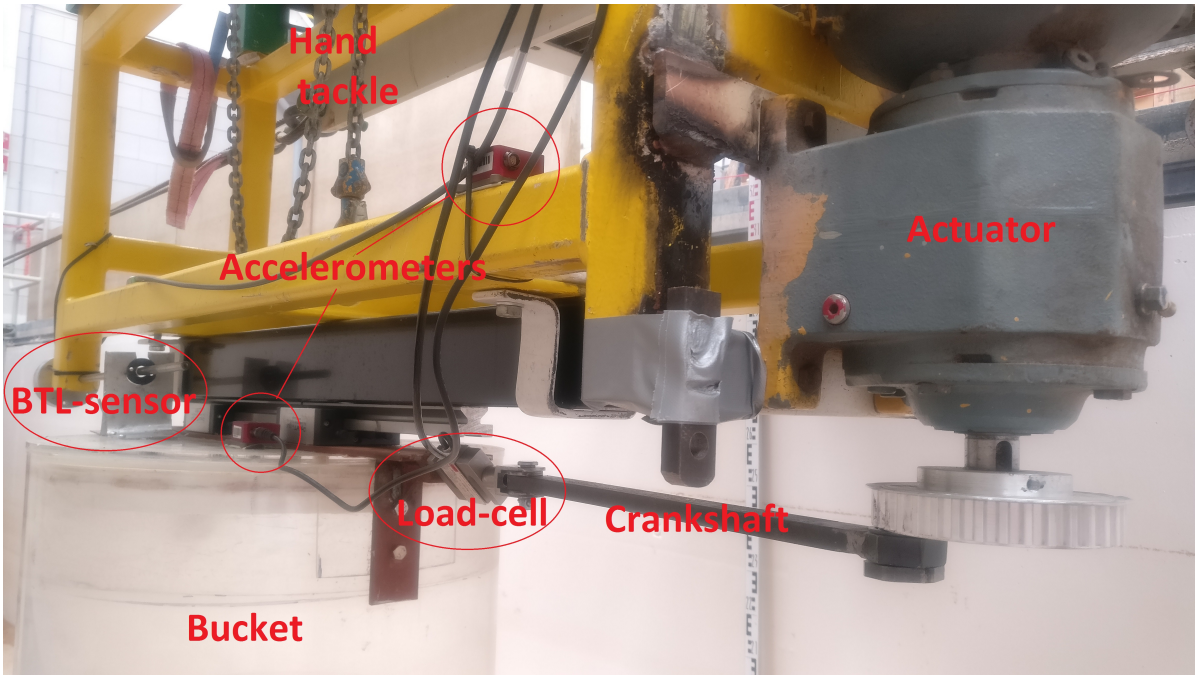

Figure 3.2: Actuator, crankshaft, load-cell, bucket, railing system, accelerometers (in red) and BTL-sensor

Error reduction

It is of great importance to minimize errors and uncertainties as much as possible. The rails were lubricated to reduce mechanical friction before all experiments are started. Two trolley cars were used to fixate the pipe to the guiding system, this to reduce pitching motions (which is in line with the applied force). The shape of the trolleys makes sure motions in all other directions, but surge, are restricted. Each sensor is calibrated. Reflection times were calculated so interference of possible reflected waves can be excluded by stopping the tests before a certain wave is reflected.

3.3. Scale Models

Scale models become more accurate with increasing size. But a large model is more prone to boundary influences as the tank has limited dimensions. Wall reflections and influences from the bottom can become non-negligible.
The suction buckets of a SBJ need to be represented as good as possible in the scale model, while keeping in mind the scaling factors that are discussed in the previous chapter. Two different diameter pipe segments are available, a 50[cm] diameter pipe and a 39[cm] diameter pipe. Both with a wall thickness of 5[mm]. The stroke of the forced oscillations in the experiments will be 8.3[cm] (0.0415[m] amplitude) in both cases. This is possible because the amplitude of the oscillation does not have influence on the added mass [22]. More details are discussed below.
Initially a bucket intrinsic mass of 30[kg] was estimated. It later turned out to be 21,5[kg]. This had effect on the initial power requirement calculations. It was a conservative mass estimate where the actual mass is used in the power requirement calculations below and therefore became slightly lower.

3.3.1. Bucket 1: 39[cm]

The 39 [cm] diameter pipe is obviously less wide in diameter, therefore the model could be slightly less accurate since viscous terms can become more dominant than they are supposed to be in the full scale situation (the model is Froude scaled and not necessarily Reynolds scaled as well).
These are called scaling effects and should be avoided as much as possible. Because the full scale characteristics are set to be 10[m] in diameter and a wall thickness of 10[cm] this pipe segment is relative to the full scale situation too thick walled. Unfortunately pipes with such a diameter are not fabricated with thinner walls.

Froude scalings factor

The Froude scaling factor should be kept identical in the full scale case and the model scale. Here is an example of how a typical full scale wave can be converted into the model case.
In the previous chapter Methods and Theories the Froude number is explained. In equation 2.5, the scaling for time and length is explained.
Length scales with:

$$\alpha_L = \left(\frac{T_{full\ scale}}{T_{model\ scale}}\right)^2 = \frac{10}{0.39} = 25.64$$

Time scales with:

$$\alpha_T = \sqrt{\frac{L_{full\ scale}}{L_{model\ scale}}} = \sqrt{\frac{10}{0.39}} = 5.06$$

The frequency in the scale model becomes:

scale = 1 : 25.64	**Full scale**	**Model0.39**	ω
max	4 [s]	0.79[s]	7.95 [rad/s]
min	11 [s]	2.17 [s]	2.90[rad/s]

Power requirement 39[cm] bucket

The required torque of the actuator is estimated at $\tau = 16.8[Nm]$. This is based on the following assumptions:

1:25.64 scale	**Full scale**	**Model**
Diameter	10 [m]	39 [cm]
wall thickness	0.1 [m]	0.5 [cm]
Period	4-11 [s]	0.79-2.17 [s]
ω	1.57-0.57 [rad/s]	7.95-2.90 [rad/s]
Amplitude	N/A	4.15 [cm]
Mass	N/A	21.5 [kg]

To determine the maximal required power at maximum acceleration, the displacement function x(t) needs to be derived twice in time:

$$x(t)_{max} = |a_0 e^{i\omega t}| = a_0 = 0.0415\ [m]$$

$$\dot{x}(t)_{max} = |\omega a_0 e^{i\omega t}| = a_0\omega = 0.33\ [m/s]$$

$$\ddot{x}(t)_{max} = |-(\omega)^2 a_0 e^{i\omega t}| = a_0\omega^2 = 2.63\ [m/s^2]$$

The maximum required torque from the actuator can be estimated through:

$$\vec{\tau} = \vec{R} \times \vec{F}$$

$$\vec{R} = a_0 = 0.0415\ [m]$$

$$\vec{\tau} = \vec{a_0} \times ((M_0 + A)\ddot{x})$$

The intrinsic mass and the added mass $(M_0 + A)$ is initially assumed as the density times the displaced (closed) volume of the bucket. Here done for fully submerged situation at Draft=0.39[m].
According to Keulegan and Carpenter [23], the C_M number is 2.0 for small displacement oscillatory waves, which is the case in the experiment. Therefore for initial dimension estimates a 100% added mass is considered outside. This results in density times the volume inside the bucket $+100\%$ added mass outside, plus the dry weight of the bucket which is 21.5[kg].
The $\ddot{x}_{max}$ is calculated by deriving the $x(t)$ twice with an arm of 4.15[cm] and a minimum period of 0.89[s] as is done above:

$$M_0 + a = m_{dry} + 2\rho V = 21.5 + 2 \cdot 1000 \cdot 0.39 \cdot \left(\frac{\pi}{4}\right) \cdot 0.39^2 = 114.68[kg]$$

If the arm $\vec{a_0}$ is assumed to be 4.15[cm]:

$$\vec{\tau} = 0.0415 \times ((114.68) \cdot 2.63) = 12.51[Nm]$$

To go from torque to power the following equation is applied:

$$\frac{J}{s} = \frac{torque \cdot 2\pi}{T} = \frac{12.51 \cdot 2\pi}{0.79} = 99.55Watt = \textbf{0.10 kW}$$

The actuator has an output power of 0.18kW. This is sufficient for this experiment if the power factor of $\phi = 0.77$ is taken into account. The required power by the actuator then becomes:
0.10/0.77**= 0.129kW**

3.3.2. Bucket 2: 50[cm]

The 50[cm] pipe has exactly the geometric similarity as the full scale case. The diameter and wall thickness are both exactly scaled with the Froude scaling factor. This has the advantage that effects are more accurate compared to the full scale reference model.
The 50[cm] pipe is assumed small enough compared to the tank dimensions such that influences of the walls and the bottom are small.

Froude scalings factor
The same full scale Froude scaling factor is applicable here:
Length scales with

$$\alpha_L = \left(\frac{T_{full\ scale}}{T_{model\ scale}}\right)^2 = \frac{10}{0.5} = 20.0$$

Time scales with

$$\alpha_T = \sqrt{\frac{L_{full\ scale}}{L_{model\ scale}}} = \sqrt{\frac{10}{0.5}} = 4.47$$

1:20 scale	**Full scale**	**Model0.39**	ω
max	4 [s]	0.89 [s]	7.06 [rad/s]
min	11 [s]	2.46 [s]	2.55[rad/s]

The same derivation applies here, for the 50[cm] pipe, as for the 39[cm] pipe:

Power requirement
The required torque of the actuator is estimated at $\tau = 18.7[Nm]$. This is based on the following assumptions:

1:20 scale	**Full scale**	**Model**
Diameter	10 [m]	50 [cm]
wall thickness	0.1 [m]	0.5 [cm]
Period	4-11 [s]	0.89-2.46 [s]
Amplitude	N/A	4.15 [cm]
Mass	N/A	21.5 [kg]

To determine the maximal required power at maximum acceleration, the displacement function x(t) needs to be derived twice in time:

$$x(t)_{max} = |a_0 e^{i\omega t}| = a_0 = 0.0415\ [m]$$

$$\dot{x}(t)_{max} = |\omega a_0 e^{i\omega t}| = a_0\omega = 0.29\ [m/s]$$

$$\ddot{x}(t)_{max} = |-(\omega)^2 a_0 e^{i\omega t}| = a_0\omega^2 = 2.07\ [m/s^2]$$

The required torque from the actuator can be determined through:

$$\vec{\tau} = \vec{R} \times \vec{F}$$

$$\vec{\tau} = \vec{R} \times ((M_0 + A)\ddot{x})$$

$(M_0 + A)$ is initially assumed as the density times the displaced (closed) volume of the bucket, (done for fully submerged situation at Draft=0.5[m]).
According to Keulegan and Carpenter [23], the C_M number is 2.0 for small displacement oscillatory

waves, which is the case in the experiment. Therefore for initial dimension estimates a 100% added mass is considered outside [19]. This results in density times the volume inside the bucket $+100\%$ added mass outside the bucket, plus the dry weight of the bucket which is 21.5[kg]:

$$M_0 + A = 2\rho V + m_{dry} = 21.5 + 2 \cdot 1000 \cdot 0.5 \cdot \left(\frac{\pi}{4}\right) \cdot 0.5^2 = 217.8[kg]$$

If the arm $\vec{R}$ again is assumed to be half of the stroke, which is 8.3[cm]:

$$\vec{\tau} = 0.0415 \times ((217.8) \cdot 2.07) = 18.7[Nm]$$

To go from torque to power the following equation is applied:

$$\frac{J}{s} = \frac{torque \cdot 2\pi}{T} = \frac{18.7 \cdot 2\pi}{0.89} = 132.1\ Watt = \textbf{0.132kW}$$

The actuator has an output power of 0.18kW. This is sufficient for this experiment. If the power factor of $\phi = 0.77$ is taken into account, the required power is 0.132kW/0.77 **= 0.171kW**.
This is close to the maximum power available from the actuator, therefore it is chosen to take the first more powerful available actuator, which is 1.5kW. This way the power will definitely not be an issue and if necessary higher frequencies could be tested as well without changing the actuator.

Preferred model scale
The **50[cm] pipe** is chosen as the preferred scale model. As the geometric similarities (wall thickness) better fits the full scale case than the 39[cm] model. Together with less scaling effects due to a larger model scale and a sufficient actuator which still can easily reach its required power output.

NOTE: The amplitude is not of importance for the added mass. Only it is required to stay within linear region (see explanation KC values in chapter Method & Theories). This is the case when amplitude $<< \frac{1}{3}$ bucket diameter, which is clearly the case and even better for the 50[cm] diameter pipe than for the 39[cm] pipe.

3.4. Test Matrix

As discussed earlier, the experiments will cover waves of 4-11[s] (full scale). Typical waves experienced in the North Sea are 3-9[s] [4]. Waves will break when they reach their critical steepness, shorter waves have a lower critical wave amplitude and therefore can not contain a lot of energy. The energy that a wave contains is directly related to its amplitude [19]. See figure 3.3 for a typical J0NSWAP spectrum and the frequency range that will be covered by the experiments.

Series	**Conf.**	Period [s]								
		11	10	9	8	7	6	5	4	
D_1	Draft=0	2.46	2.24	2.01	1.79	1.57	1.34	1.12	0.89	(3x)
D_2	Draft=$\frac{\phi}{4}$	2.46	2.24	2.01	1.79	1.57	1.34	1.12	0.89	(3x)
D_3	Draft=$\frac{\phi}{2}$	2.46	2.24	2.01	1.79	1.57	1.34	1.12	0.89	(3x)
D_4	Draft=$\frac{3\phi}{4}$	2.46	2.24	2.01	1.79	1.57	1.34	1.12	0.89	(3x)
D_5	Draft=ϕ	2.46	2.24	2.01	1.79	1.57	1.34	1.12	0.89	(3x)

Repetition of experiments
To increase the accuracy of the experiments, each test will be repeated three times. The results (added mass and damping separately) are summed up and the average is taken from the results after post processing. Uncertainty bars are plotted in the graphs to visualize the reliability of each test result.
The standard error will reduce according to the relation:

$$standard\ error = \frac{s}{\sqrt{N}} \approx 0.58 \cdot s$$

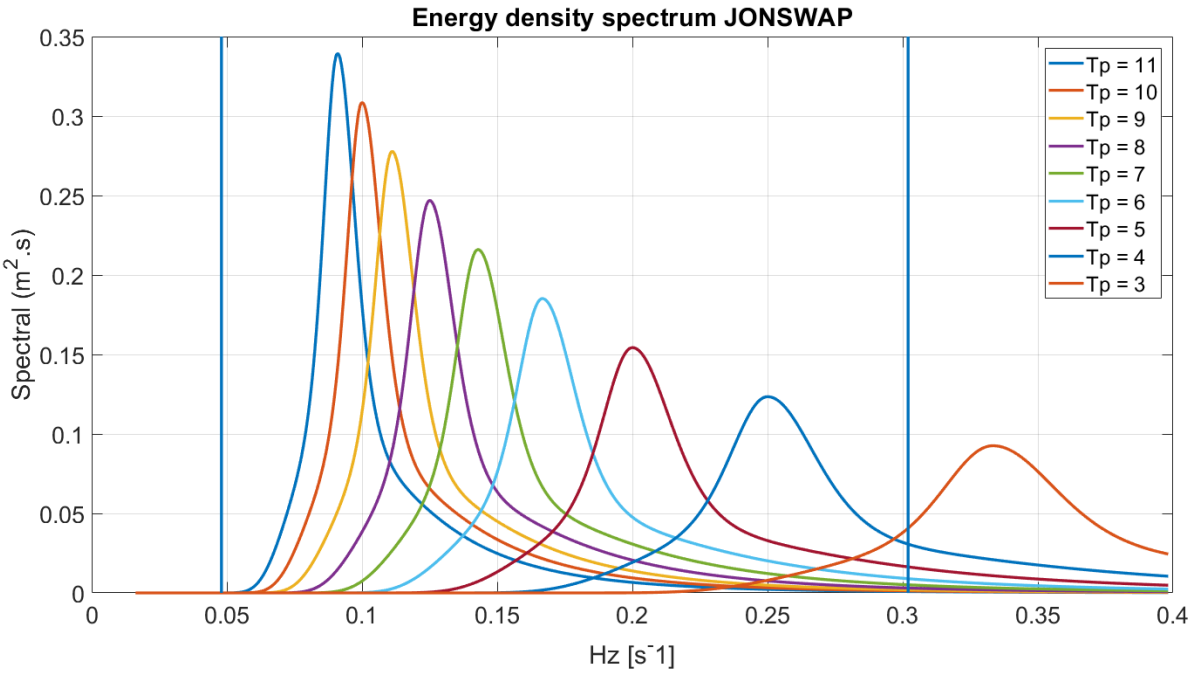

Figure 3.3: JONSWAP spectrum for full scale waves.
Left and right verticals indicate the tested spectrum range.

N is the number of experiments and s is the standard deviation. With N=3, the standard error is reduced by over 40%. The standard error is displayed as uncertainty bars in the added mass and damping graphs.

Bucket drafts

The draft is chosen to be the following fractions of the diameter ϕ: 0, $\frac{\phi}{4}$, $\frac{\phi}{2}$, $\frac{3\phi}{4}$, ϕ. In absolute values this represents drafts of; 0[cm], 12.5[cm], 25[cm], 37.5[cm] and 50[cm]. This to cover the situations no draft, bucket halfway submerged and submerged at the point where the draft is equal to the bucket diameter. Two drafts in between are added to increase the visibility of the trend.

Configuration	Draft [cm]
Draft 1	0.00
Draft 2	12.5
Draft 3	25.0
Draft 4	37.6
Draft 5	50.0

Table 3.1: Draft numbers and corresponding drafts in [cm].

The last intended draft $\frac{5D}{4}$(62.5[cm]) was unfortunately not possible to experiment with, the load-cell was not watertight for longer periods which would definitely be the case for this draft. Due to this fact the fully submerged set-up was not tested. This is an important test because assumed is that the full volume inside the bucket can be considered trapped when the bucket is fully submerged. The deepest tested draft now still contains a few centimeters of air, this allows waves to break inside the bucket and introduces non-linear effects (sloshing).
The draft can be changed using a hand tackle, that is accessible from the bridge and therefore it is not necessary to go into the water/tank to change the draft. All controllers are located behind a window in the tank. All tests are clearly visible from the side at SWL through the window.

3.4.1. Wave Reflection times

It should be mentioned that the tank has finite borders, therefore wave reflections could play a role if test-series last a while. Therefore it is necessary to calculate the wave reflection times to be aware of the moment when reflected waves can start to interfere with the test set-up. A Matlab function is written to calculate the wave reflection times for certain wave periods, the Matlab script is included in the attachments (Attachment 3.2). The derivation used in the script is explained below.

The model scale wave periods follow from the Froude scaling. The dispersion relation from equation 2.2 is applicable. This equation can be used such that the wave phase velocity can be determined [19].

$$c = \sqrt{\frac{g}{k} \cdot \tanh(kd)} \ [m/s] \tag{3.1}$$

$$n = \frac{1}{2}\left(1 + \frac{kd}{\sinh(2kd)}\right) \ [-]$$

Where:
d = water depth of tank, 1.12[m]
k = wavenumber [m^{-1}]

Note:
For shallow water $n \approx 1$
For intermediate water $\frac{1}{2} < n < 1$
For deep water $n = \frac{1}{2}$

The group velocity of the wave then can be determined using the relation:

$$c_g = n \cdot c \ [m/s] \tag{3.2}$$

From this relation the wavelength can be found using an iterative process:

$$\lambda = \frac{gT^2}{2\pi} \tanh\left(\frac{2\pi d}{\lambda}\right) \tag{3.3}$$

Where:
g = gravity constant 9.81 [m/s^2]
T = wave period [s]

The deep water limit of equation 2.2 when $d \to \infty$ gives:

$$\omega^2 = g \cdot k$$

This can be rewritten to the wavenumber k and the wavelength λ:

$$kd = \frac{2\pi}{\lambda} d \ [-]$$

$$k = \frac{2\pi}{\lambda} \ [m^{-1}]$$

$$\lambda = \frac{gT^2}{2\pi} \ [m]$$

If the wave group velocities are identified for each frequency, the wave reflection times can be calculated. The total wave reflection times per frequency can be found in table 3.2.

Wave periods full scale	[s]	11	10	9	8	7	6	5	4
Wave periods	[s]	2.46	2.24	2.01	1.79	1.57	1.34	1.12	0.89
Wave length (λ)	[m]	9.44	7.83	6.31	5.00	3.85	2.80	1.96	1.24
$k_0 d$	[-]	0.74	0.90	1.12	1.41	1.83	2.51	3.59	5.69
n	[-]	0.68	0.65	0.62	0.58	0.55	0.52	0.50	0.50
c_g	[m/s]	2.07	1.93	1.75	1.54	1.31	1.07	0.88	0.69
$t_{reflection}$	[s]	**9.68**	**10.35**	**11.421**	**13.00**	**15.30**	**18.63**	**22.77**	**28.78**

Table 3.2: Wave reflection times per frequency

3.4.2. Deflection in structure

The deflection of the structure due to the exerted force by the actuator is calculated. If, as a benchmark, a maximum allowable deflection of 1% of the displacement of the bucket is assumed, an allowable constructional deflection of 0.8mm is allowed.
Will the deflection of the structure stay within this range with the expected forces?
The following equation gives the needed relation:

$$\delta = \frac{EI}{L^3} F$$

δ = 0.0008[m]
L = 1.8[m]
$F = m \cdot \ddot{x}$ = 217.8 [kg]· 2.07 $[m/s^2]$
F = 450.8[N] (entire structure)
F = 112.7[N] (1 out of 4 beams)
E_{steel} = 209[GPa]

The required resistance area moment of intertia is:

$$I_{xx} = \frac{\delta \cdot L^3}{F \cdot E}$$

$$I_{xx} = \frac{0.0008 \cdot 1.8^3}{112.7 \cdot 210 \cdot 10^9} = 1.97 \cdot 10^{-16} [m^4]$$

In the frame beams of 40mmx40mmx4mm are used, they each provide an area moment of inertia I_{xx} of:

$$I_{xx} = \frac{bh^3 - (b - 2w)\,(h - 2w)^3}{12}$$

$$I_{xx} = \frac{0.040^4 - (0.040 - 2 \cdot 0.004)\,(0.04 - 2 \cdot 0.004)^3}{12} = 1.26 \cdot 10^{-7} [m^4]$$

Note that this provides an excess of a moment of inertia. Take into account that the frame has four horizontal braces in the surge direction on two different heights, this introduces a considerable extra stiffness in this direction. The frame also has four beams in the sway direction. Deflection of the frame due to the applied force of the actuator is considered negligible. However, this still will be monitored by an accelerometer connected to the frame. The accelerations of the frame in all directions should at all times be close to zero.
The total frame will be more than stiff enough to not deflect more than 1% of the displacement. This is not considered as a possible uncertainty in the test set-up.

3.5. Sensors and Equipment

Load-cell

AE Sensors, AE-B3G-C3-250kg-6B, Range:-250kg/+250kg, Accuracy: 0.0875[kg] (0.035%)

The load-cell has a range of -250[kg] (tension) to +250[kg] (compression). This is sufficient since an estimated maximum force of 450.8[N] (45.95[kg]) is expected. The load-cell is connected to the pipe, on the other end it is attached with a swivel to the crankshaft. This way it will measure the force applied by the actuator to the pipe segment purely in surge motion.

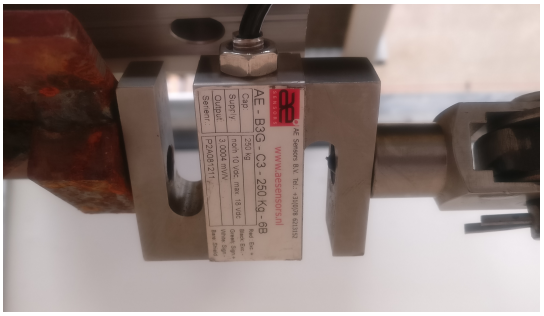

Figure 3.4: Load-cell to measure applied force by actuator to bucket

Calibration

There was a certificate of calibration present with this sensor. Although a check was done with a weight of 35.7 [kg] and two scales, this was within margin. A second check was done with another weight of 95[kg], which was again within margin.

BTL sensor

Balluff, MicroPulse linear Transducer - BTL5, Range: 0-50[cm], Accuracy: 100μm.

The BTL sensor is a sensor that will measure the displacement of the pipe versus time. The sensor is attached to the yellow (stationary frame). To measure the displacement, a magnet is attached to the pipe and will slide over the needle of the sensor. Due to a changing magnetic flux in the needle the displacement can be measured very accurately. A risk here is that if there appears a roll motion the magnet will touch the BTL sensor, this may introduce an additional friction.

Figure 3.5: BTL sensor, with magnet (in black)

Calibration

The BTL sensor was calibrated by measuring the maximal physical stroke the pipe was able to make. This was compared to the difference between the minimum and maximum value the BTL sensor gave. Which again was well within margin (8.3[cm] versus 8.2[cm]).

Accelerometer

SBG Sensors, Ellipse2-A

Two SBG accelerometers are used to find the accelerations of the frame, to check if the frame is really stationary as it should be. The other accelerometer is attached to the bucket and monitors the accelerations of the pipe. An SBG sensor logs the accelerations in x-,y- and z-direction. Both sensors are aligned so that the x-direction will coincide with the direction of displacement due to the applied force in surge direction. The accelerations in this direction will be expected to be minor, especially for the frame, but also dominant compared to the other directions.

Figure 3.6: Accelerometer, one attached at the bucket and one at the frame, both aligned such that x-direction points in direction of motion.

Calibration

This sensor was not calibrated, since the acceleration was not used for data collection. The sensors were used to check if any resonances took place while and in between tests. It was also used to check if waves were damped out before starting a new experiment.

3.5.1. Actuator

SEW, R42 DT901-4 TF, Range: 0-1.5kW 174[r/min], Power-factor: cos(ϕ)=0.77

The output frequency of the actuator is an unknown variable. Since this is dependent on many characteristics of the system it is very important to calibrate the actuator.

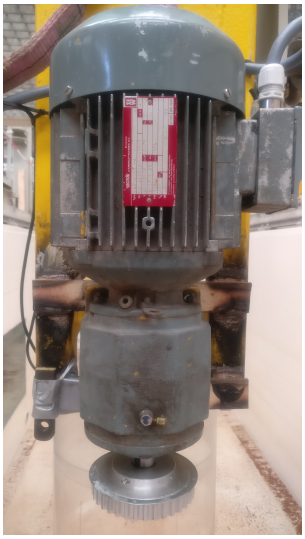

Figure 3.7: Actuator for the forced oscillation (1.5kW).

Powerfactor (PF_D) $\cos(\phi)$, gives an insight on the efficiency of the actuator. This function gives the ratio between the real power (P) (dissipated power by the load) in Watt (W) and the reactive power (Q) in volts-amperes reactive (VAR) [24]:

$$PF_D = \frac{P}{S} = \cos(\delta_1 - \theta_1) = \cos\phi$$

The apparent power then becomes $(S) = \frac{P}{\cos\phi}$

Number of Poles which is an unknown number:

$$N = \frac{2 \cdot 60 \cdot f}{p}$$

RPM Number of rotations per minute (rpm) output due to certain RPM input. The actuator has a gearbox attached to reduce its output RPM to lower frequencies. The relation input/output frequency is unknown.

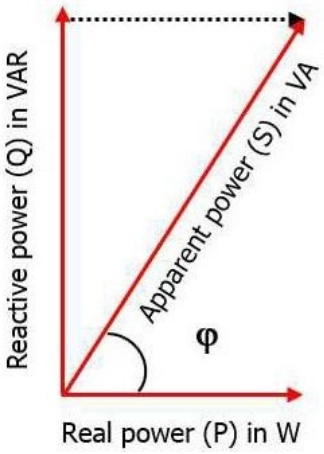

Figure 3.8: Representation of the vector relationship between real, apparent and reactive power.

Figure 3.9: MIDI master, actuator frequency regulator

3.5.2. Frequency regulator

SIEMENS, MIDIMASTER, Range: 0-7.5kW 0-60[Hz]

The frequency regulator has a display which can be set to show the output frequency in one decimal. This is unfortunately not very accurate. That is why a workaround method is developed. The output frequency is corresponded to an output voltage on the range 0-20[V]. This is directed back into the data acquisition device which can read up to four decimals. Since there are many factors that have influence on the output frequency of the actuator, it is chosen to calibrate the voltage of the actuator output frequency manually.

3.5.3. Other system details

Accuracy sensors

The accuracy of each sensor is given by the manufacturer. The calibration is done to make sure there is no offset in the data and there is a nice linear relation. It is important to know the accuracy of each sensor and know how this affects the final answer. It is important to know the reliability of the final answer, how does the accuracy of the sensors and the used methodology influence this. Calibration of the sensors is key here.

3.6. Hammer test

To determine the eigen-frequencies for each specific draft, a hammer test is done. Hitting the frame and letting it oscillate freely provides the impulse response spectrum once the FFT of the force signal is taken. The impulse response spectrum gives insight on which frequencies are prone to resonance, the impulse response is large for these specific frequencies.

Ideally the impulse response is zero for all frequencies. Even though, such an infinite stiff system does not exist. More practical, the impulse response should be as low as possible and constant (no dominant peaks are present) over the frequency range at which the experiments will be done. As can be seen in the attachments (section C.4) the response for the to be tested frequencies (0.41-1.12[Hz]) is almost constant and fairly low. All eigen-frequencies of the frame (visible as sharp peaks in the FFT spectrum) are well above the highest test frequencies and its first multiple harmonics. Thereby no resonance is expected during the experiments that can have influence on the measured accelerations and/or Force signal.

The Matlab script for the determination of the hammer test frequency domain can be found in the appendix.

3.7. Dry test

A dry test is done to find the mechanical friction properties of the system. The friction term (incorporated in the damping term B) is determined together with its frequency dependency. Doing this provides information later on when the actual experiments are done. At this moment it is known what part of the determined damping is (mechanical) friction and thus the remaining damping is due to wave radiation damping and due to viscous effects. (see equation 4.30)
A second dry test was done to find the dynamic friction for the slowest possible harmonic oscillation. It turned out that the friction was more or less frequency independent. The friction was determined again at a period for which the displacement was just right out of the slip and stick region. Here the bucket performed a clean sinusoidal oscillation, this was at a period of 35[s]. Here the friction force could be determined the most accurate.
The friction force measured in the load-cell here was about 3.6[kg] (35.3[N]).

Geometry

Because a single suction bucket is axis-symmetrical, the surge motion can in theory be decoupled from all other motions. Because experiments have to deal with practical (non-ideal) effects this might not be the case. This is monitored with two accelerometers both for three directions $\hat{x}$, $\hat{y}$ and $\hat{z}$ (surge, sway and heave).
The n= values, identifying the water depth region, for the set-up are ranging from 0.5002 up to 0.6891. A n-value of n=0.5 represents deep water and therefore no interaction with the bottom of the tank is assumed. The value n = 0.6891 represents intermediate water depth. Due to characteristics of the tank, bridge and tank window, it was not possible to increase the water depth to reduce bottom influence. But taken into account pure surge motion could (theoretically) be decoupled from the other motions, this effect due to the intermediate water depth (and even not yet *shallow* water depth region), is assumed to be small.
Wall reflections originated perpendicular to the direction of motion (resp. sway and surge directions) are assumed small. The bucket radiates waves with an intensity related to the bucket's normal vector related to the surge motion. At 90° and 270° (positive and negative sway direction) this is purely parallel, therefore the bucket's normal vector product with surge direction is zero. This is stated in 'Water wave radiation problem by a submerged cylinder' by Sheng-chao Jiang et al. (recommended article for submerged cylinders) [21].
Theoretically no waves are produced in this direction. Although this is a theoretical theorem, in practice this might not be 100% valid (e.g. when roll resonances take place), it is assumed that reflections in this direction are small. From a visual check through the window of the tank, perpendicular to the surge motion, this assumption is confirmed.

4

Post Processing

To extract the final inertia coefficient (C_M) from the obtained data, the data needs to be post processed. The relation $C_M = 1 + C_a$, where C_a is the added mass coefficient, holds. The added mass can be determined using different kind of methods. Each method has its advantages and disadvantages. The different methods are explained and discussed below.

4.1. Post Processing Methodologies

As described earlier in section 2.7, different kind of filtering methodologies are available. The Morison approach, the Fourier series method and the linear least squares method are explained here.

4.1.1. Morisons Method

From equation 2.13 the damping and inertia terms can be separated because these two factors are 90° out of phase. Rewriting the equation and taking the moments when one of the parts is zero each part can be determined. By nature the velocity and the displacement of a harmonic oscillation are 90° out of phase. This results in the damping and the inertia coefficients:

$$C_D = \frac{2F}{\rho D \cdot u_a|u_a|} \qquad at\ t\ where\ \ \dot{u} = 0$$

$$C_M = \frac{4F}{\pi\rho D^2 \cdot u_a\omega} \qquad at\ t\ where\ \ u = 0$$

An elegant and simple way to determine the C_D and C_M by hand, although this can become dangerous as the accuracy might lack sufficiently due to the fact that the drag and inertia term are in practice not 100 % out of phase. Additionally only two time points are studied instead of the entire data set to find the C_D and C_M coefficients, this will introduce inaccuracies.

4.1.2. Fourier Series Approach

Two Fourier series are compared, similar terms on the motion series and the force series. This is a straightforward process once the $F(t)$ signal is known. The inertia force component is related to the b_1 term, while the drag is related to the a_1 term [22].

$$C_D = \frac{3\pi}{4\rho D} \cdot a_1$$

$$C_M = \frac{4}{\pi D^2 \rho} \cdot \frac{b_1}{\omega u_a}$$

Where:
$a_1 = \frac{8}{3\pi} \cdot A \approx 0.849 \cdot A$. This is the velocity dependent Fourier amplitude (kg/m^2)
b_1 = the acceleration dependent Fourier amplitude (Nm)

This method is more accurate than the Morisons method as it this uses the entire time domain data set to obtain the Fourier coefficients. One thing to mention is that this is based on a linear system, so this will introduce some inaccuracies.

4.1.3. Least Squares Method

The least squared method treats the Morisons equation as if it is a computational approximation. The function $F(t, C)_D, C_{Mcomputed})$ is fitted, adjusting the linear coefficients C_D and C_M. The C_D and C_M have to be determined. This can be done by using the minimal residual difference function:

$$R\,(C_D, C_M) = \int_0^T [F(t)_{measured} - F\,(t, C_D, C_M)]^2 dt$$

The next thing to do is to minimize the function by adjusting the C_D and C_M until a minimum value is found. This can be done analytically and therefore it is possible to set both derivatives equal to zero: $\frac{\partial R}{\partial C_D} = 0$ and $\frac{\partial R}{\partial C_M} = 0$.
The experiment will be *inertia dominated*, the drag phenomenon is relatively small. Therefore the final C_D value might be less reliable. The least squares method can be an accurate method to reduce noise over the measured data and find the added mass and damping terms.

4.1.4. Weighted Least Squares Method

The theory behind the weighted least squares method is the same as the previous method but more specifically applied to a specific region of interest. For example, near a force peak to determine the resulting force more precisely. To improve the fitting close to the peak force is to weight the difference in the $R\,(C_D, C_M)$:

$$R\,(C_D, C_M) = \int_0^T [F(t)_{measured}]^2 \cdot [F(t)_{measured} - F\,(t, C_D, C_M)]^2 dt$$

Aimed is for a steeper graph for the error function $R\,(C_D, C_M)$, so a more precise minimum can be defined for $R\,(C_D, C_M)$.
Note, the residual function $R\,(C_D, C_M)$ is not required to be dimensionless. Most important is the relative value compared to other values for different chosen C_D, C_M values.
Mention the experiment will be *inertia dominated*, the drag phenomenon is relatively small. Therefore the final C_D value might be less reliable.
Finally the preferred processing method will be executed in Matlab to post process the data before analyzing the results.

4.2. Assumptions and Variables

The post processing methods are based on several assumptions. The mentioned theories are valid, or even only valid, for linear regions. This results in restrictions for the input data. The assumptions made to validate the used theories are described here.

4.2.1. Assumptions

Water:

- Water is assumed to be incompressible
- The flow is assumed to be irrotational, i.e. no shear force is present in water
- Airy waves (linear waves)

Suction Bucket:

- Bucket is scaled with a factor 1:20, 10[m] prototype is represented by a ϕ=50[cm] model
- Periods are assumed linear, 4-11[s] waves are scaled to 0.89-2.46[s] oscillation periods.
- Drafts till suction buckets are fully submerged in 5 steps:

- 0[cm]
- 12.5[cm]
- 25[cm]
- 37.5[cm]
- 50[cm]

4.2.2. Variables

Independent Variables

The independent variables are: Draft (T), Frequency (f) and Duration (t).
More than one independent variable may introduce uncertainties. This is expected not to be a problem since the effects of draft and excitation frequency are assumed to be uncoupled and hence can be studied separately.
Each combination of independent variables is tested separately three times to obtain reliable results by taking the average value after post processing each of them individually.
The duration of each test will be 30 seconds, but action needs to be taken when reflections become significant and interact with the model. This is something to be aware of and has been discussed in the previous chapter.

Controlled Variables

The controlled variables are: Amplitude ($\hat{x}(t)$), Diameter bucket (ϕ), Density water (ρ_w), Temperature water (T) (6°), Dimensions towing tank ($LxHxB$), (reduced) reflection effects.
All the known and/or chosen constant parameters of the set-up which will not change during the experiments.

Dependent Variables

The dependent variables are: Applied force (F), Mechanical friction in the guiding system ($F_{friction}$), actuator power output (P) and displacement ($x(t)$).
These are the unknown output parameters of the system. The relation between the applied force and the displacement will give the added mass and damping for each draft and frequency.

4.3. Data Analysis

To analyze the data the *linear least squares method* is used. It is the most elegant and accurate method for these experiments that uses the entire dataset. A check is done with the FFT to see if any resonances are present. Also a hammer test is done to understand what the natural frequencies of the test set-up are. No natural frequencies are within range of the to be tested frequencies. As a result it is assumed safe to use test these frequencies and post process them with the linear least squares method.

4.4. Matlab Approach

Mathematical structure of the problem

From the chapter *Methods and Theories* it is known that for the displacement signal and the force signal the following equations hold:

$$x(t) = \hat{x}\cos(\omega t) \tag{4.1}$$

$$F(t) = \hat{F}\cos(\omega t + \phi) \tag{4.2}$$

To solve this computationally, the system is described as a linear equation of a matrix and vectors:

$$[A]\,\vec{b} = \vec{F} \tag{4.3}$$

To solve the matrix-vector equation in Matlab by tuning ϕ and $\hat{F}$, the equation has to be rewritten.

Mathematical (re)formulation

According to Euler this can be rewritten as:

$$x(t) = \hat{x}\cos(\omega t) = \hat{x}\mathbb{R}\{e^{i\omega t}\} \tag{4.4}$$

and

$$F(t) = \hat{F}\cos(\omega t + \phi) = \hat{F}e^{i(\omega t+\phi)} = \hat{F}\mathbb{R}\{e^{i\omega t}e^{i\phi}\} \tag{4.5}$$

When these equations are filled into the equation of motion and are simplified:

$$(-\omega^2(M_0 + A)) + i\omega B)\hat{x}e^{i\omega t} = \hat{F}e^{i\omega t}e^{i\phi} \tag{4.6}$$

The right hand side of the equation can be rewritten as:

$$\hat{F}e^{i\omega t}e^{i\phi} = \hat{F}[\cos(\omega t) + i\cos(\omega t)] \cdot [\cos(\phi) + i\sin(\phi)] \tag{4.7}$$

Which again rewrites itself to:

$$\hat{F} \cdot [\cos(\omega t) + i\sin(\omega t)] \cdot [\cos(\phi) + i\sin(\phi)] = \tag{4.8}$$

$$\hat{F} \cdot [\cos(\omega t)\cos(\phi) + i\cos(\omega t)\sin(\phi) + i\sin(\omega t)\cos(\phi) - \sin(\omega t)\sin(\phi)] \tag{4.9}$$

If it is assumed that the forced displacement $x(t)$ is a cosine function, the real part needs to be taken from the last equation, resulting in the equation:

$$\mathbb{R}\{\hat{F} \cdot [\cos(\omega t) + i\sin(\omega t)] \cdot [\cos(\phi) + i\sin(\phi)]\} = \tag{4.10}$$

$$\hat{F} \cdot [\cos(\omega t)\cos(\phi) - \sin(\omega t)\sin(\phi)] \tag{4.11}$$

When this equation is filled in into equation 4.6 this results to the final equation;

$$(-\omega^2(M_0 + A)) + i\omega B)\hat{x}e^{i\omega t} = \hat{F} \cdot [\cos(\omega t)\cos(\phi) - \sin(\omega t)\sin(\phi)] \tag{4.12}$$

Solution to the mathematical structure

This can be written in the form given in 4.3, where

$$[A] = \begin{bmatrix} \cos \omega t_1 & -\sin \omega t_1 \\ \cos \omega t_2 & -\sin \omega t_2 \\ \dots & \dots \\ \cos \omega t_n & -\sin \omega t_n \end{bmatrix} \tag{4.13}$$

$$\vec{b} = \begin{bmatrix} \hat{F} \cos(\phi) \\ \hat{F} \sin(\phi) \end{bmatrix} \tag{4.14}$$

$$\vec{F} = \begin{bmatrix} F(t_1) \\ \dots \\ F(t_n) \end{bmatrix}_{dataset} \tag{4.15}$$

This is another form of equation 4.6 which can be solved by Matlab. Once $\vec{b}$ is known, there are two equations with two unknowns. This system can be solved. First $b(2)$ and $b(1)$ are divided by each other to obtain the phase shift (ϕ)

$$\frac{b(2)}{b(1)} = \frac{\hat{F} \sin(\phi)}{\hat{F} \cos(\phi)} = \frac{\sin(\phi)}{\cos(\phi)} = \tan(\phi) \tag{4.16}$$

$$\phi = atan\left(\frac{b(2)}{b(1)}\right) \tag{4.17}$$

Once, this is known, $\hat{F}$ can be found:

$$\hat{F} = \frac{b(1)}{\cos(\phi)} = \frac{b(2)}{\sin(\phi)} \tag{4.18}$$

$$(-\omega^2(M_0 + A)) + i\omega B)\hat{x} = \hat{F}e^{i\phi} \tag{4.19}$$

Again rewrite the exponent in cosine and sine functions according to Euler:

$$(-\omega^2(M_0 + A)) + i\omega B)\hat{x} = \hat{F}[cos(\phi) + i \sin(\phi)] \tag{4.20}$$

Fit method - Least squares method

For a single data set this means that the area between the data and the fit should be minimal:

$$(norm)_{min} = \left(\sum_{i=1}^{n} |x_i - y_i|^2\right)^{\frac{1}{p}}_{min}$$

For this case the norm of power 2 should be used since it is about the area between the two graphs. The norm-2 function is called the Euclidean distance. The least squares method is fitting $\hat{F}$ and ϕ such that the Euclidean distance is minimal [9].

$$(Euclidean\ distance)_{min} = \sqrt{\left(\sum_{i=1}^{n} |x_i - y_i|^2\right)}$$

$$\epsilon = \vec{F} - [A]\vec{b} \tag{4.21}$$

Positive and negative area between signals are not allowed to cancel each other out, therefore the squared notation is used.

$$\epsilon^2 = \left(\vec{F} - [A]\vec{b}\right)^2 \tag{4.22}$$

To solve the least squares method the error function should be minimized [9]

$$S(b) = \sum_{i=1}^{m} |F_i - \sum_{j=1}^{n} A_{ij} b_j|^2 = |\left[F\right] - \left[A\right]\vec{b}|^2 \tag{4.23}$$

The minimum is found when the gradient is zero. The partial derivatives are:

$$\frac{\partial S}{\partial b_j} = 2\sum_{i=1}^{m} \epsilon_i \frac{\partial \epsilon_i}{\partial b_j} \qquad (j = 1, 2, \dots, n) \tag{4.24}$$

and

$$\frac{\partial \epsilon_i}{\partial b_j} = -A_{ij} \tag{4.25}$$

Substitution of the expressions into the derivatives into the gradient equations gives:

$$\frac{\partial S}{\partial b_j} = 2\sum_{i=1}^{m} \left(F_i - \sum_{k=1}^{n} A_{ik} b_k \right)(-A_{ij}) \qquad (j = 1, 2, \dots, n) \tag{4.26}$$

When b is minimized this becomes:

$$2\sum_{i=1}^{m} \left(F_i - \sum_{k=1}^{n} A_{ik} b_k \right)(-A_{ij}) = 0 \qquad (j = 1, 2, \dots, n) \tag{4.27}$$

When this is rearranged, the following matrix vector equation holds:

$$\left(\left[A\right]^T \left[A\right]\right)\left[b\right] = \left[A\right]^T \left[F\right] \tag{4.28}$$

The matrix $\left(\left[A\right]^T \left[A\right]\right)$ is known as the Gramian matrix of $\left[A\right]$. This is a positive semi-definite matrix. The matrix $\left(\left[A\right]^T \left[F\right]\right)$ is called the moment matrix. Finally the vector $\vec{b}$ is the coefficient vector of the least squares hyperplane. This provides the solution to the initial least squares estimation of the problem.

$$\left[b\right] = \left(\left[A\right]^T \left[A\right]\right)^{-1} \left[A\right]^T \left[F\right] \tag{4.29}$$

This is for the linearized system, which in practice is not the case. Friction and viscous damping terms are present, the actual equation of motion is:

$$(M_0 + A)\,(\ddot{x}) + b_{WRD}\dot{x} + b_{visc}\dot{x}^2 = F - F_{fric} \tag{4.30}$$

For now this is neglected and the linear equation of motion without friction is used.

Data Selection

The post processing method is based on the assumption that the frequency is *constant* and the same in $x(t)$ as in $F(t)$. Therefore the right point in time, where the actuator reaches its *constant* target frequency, needs to be determined. To determine this point, the output voltage of the frequency regulator is monitored. Assumed is that when this voltage becomes constant, the actuator is at constant frequency. Shown in figure 4.1 this is a clear point in the bottom volt signal.
From this point on the first zero-up-crossing point is located for the displacement signal. This point is then set to be the starting point of the data serie.

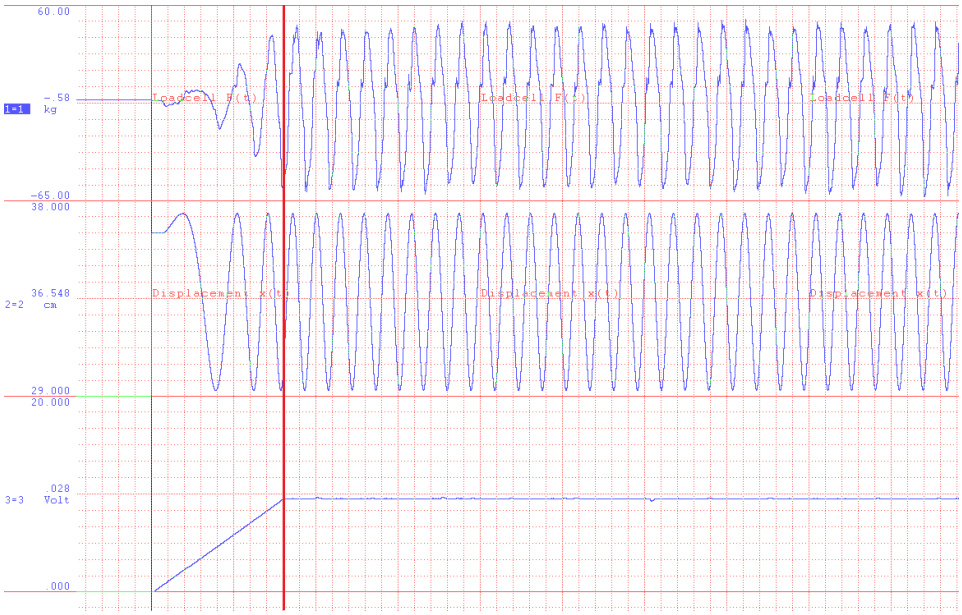

Figure 4.1: Moment Volt reaches required value, constant frequency for x(t). From top to bottom: Load-cell F(t), Displacement x(t), Voltage V(t)

Error and Uncertainties

Error and uncertainties are often present when doing experiments. But what is actually the difference between these two?

• *Error* is the actual difference between a result and the true value.
|Error| = | measured value – true value |

• *Uncertainty* is the expected error, based on calculations from statistics.

Uncertainty is the statistical representation of error. The problem is that the true value is often unknown, this is essentially why experiments are requested in the first place.

Bias and Precision Error

The general error can be separated into two types of error, the *Bias error* and the *Precision error*. The difference between these two types of error are explained here.

Precision error is the ”scatter” in the experimental results. This can be determined when identical measurements are repeated multiple times.

Examples Precision error:
• The physical potmeter. Due to human interaction with a physical potmeter it is hard to exactly repeat a certain setting by twisting a potmeter.
• Frequency response actuator, does the actuator gives the same RPM output at a fixed voltage number for each draft.

Bias error is a systematic error, these can *not* be found in repeated measurements
A way of determine the Bias error is testing only the test itself with known input and (expected) output, so called 'dry' tests. Also a new model and/or test set-up can be made to check if the results are identical. Check the set-up(s) in another tank.

Examples possible bias errors:
• Scaling effects. Scaling effects do not change with repeated experiments. An example of a scaling effect are viscous forces, viscous effects should be scaled with the Reynolds number. As explained earlier these experiments are scaled with the Froude number.
• No correct calibration of the sensors. The sensors keep giving the same incorrect values.
• Wave reflections. This can give both a bias and precision error.
• Geometrical inaccuracy of the model (for example deformation during experiments).
• Tank wall effects. Wave reflections can give both a bias and precision error. A standing wave in for example a tank is called 'Seicheing'. This did occur a few times in between experiments despite of the presence of a wave damper. This is why reflection times are required to be calculated. Generally wave reflections limit the duration of the tests, wave dampers at the ends of the tank are strongly advised. • Wave parameters and spectral shape. This is covered by later re-estimating the actual frequency and compare this to the initial frequency.

These bias errors can be reduced by careful calibration of all sensors and equipment. The scale model should be build carefully and accurate. Tank characteristics such as reflection times should be known before the experiments are executed.

4.5. Wave regimes

In 1987, Chakrabati described a set of regions in which structure-wave interactions can be divided (see figure 4.2)[6]. For this thesis the bucket diameter and wavelength are known. This provided the dimensionless $\frac{D\pi}{\lambda}$ range on the x-axis. Ranging from 0.05 to 0.17[-]. To estimate which regions are present in the hydrolab experiments, videos of the experiments are analyzed to determine the wave height H. Although these are diffracting waves, it gives an indication of what values on the y-axis can be expected in figure 4.2. The red square in the figure shows the region in which the experiments take place. As can be seen, this is an inertia dominated region. This is what was aimed for initially, because with not much damping the inertia term (added mass) can be determined more accurately [6].

Reflection times
The wave reflection times in the tank are calculated with the theory shown earlier, the reflection times are shown in table 4.1. As can be seen for low frequencies the reflection times are short, while for higher frequencies the reflection time goes up to almost half a minute. Initially was chosen to pick the 30[s] as the fixed test duration for all frequencies. When wave reflections are influencing the experiment this could be shortened. In the end this was not the case, due to the fact that a wave damper at the end of the tank was present, no influences have been detected.

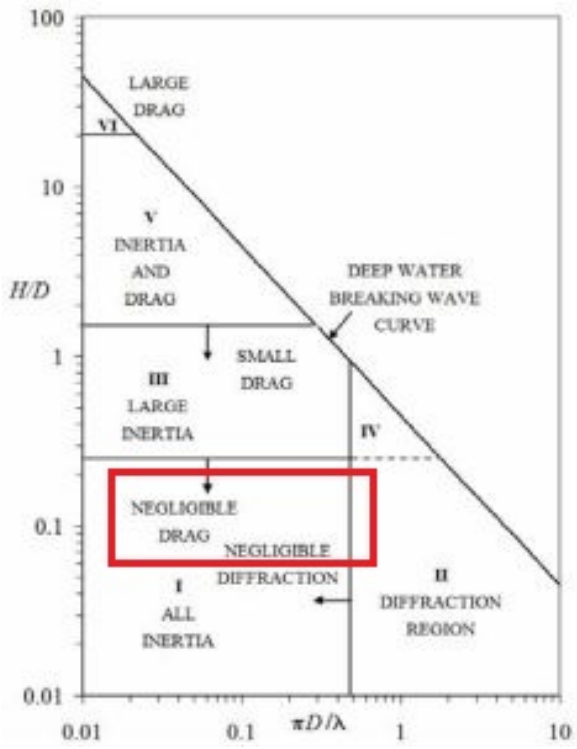

Figure 4.2: Wave regimes according to Chakrabati (1987), red shows studied ranges

Initial frequency [Hz]	0.41	0.45	0.50	0.56	0.64	0.75	0.89	1.12
Actual frequency [Hz]	0.41	0.52	0.64	0.76	0.88	1.00	1.13	1.15
λ_0 [m]	9.4484	7.8340	6.3078	5.0026	3.8485	2.8035	1.9585	1.2367
$k_0 d$ [-]	0.6650	0.8020	0.9961	1.2560	1.6326	2.2412	3.2082	5.0805
n [-]	0.6891	0.6681	0.6384	0.6025	0.5624	0.5253	0.5052	0.5002
c_g [m/s]	2.0186	1.9056	1.7466	1.5525	1.3270	1.0867	0.8821	0.6950
$t_{refl}[s]$	**9.9078**	**10.4956**	**11.4507**	**12.8825**	**15.0717**	**18.4036**	**22.6742**	**28.7758**

Table 4.1: Wave reflection times

Initial frequency versus actual frequency

The regular wave periods for the forced oscillation signals are determined. This is a known input variable, but checked afterwards to make sure frequencies are known and correct.

This is done using the zero up crossing method. It was the preferable method over measuring the period between maxima or minima, because the signal tends to be more noisy at the extremes (because relative more dominant friction effects are present there). While at the zero crossings the signal is cleaner and more steep, this makes it more accurate to determine the exact zero crossing point in time.

It turned out that the measured frequency did not exactly meet the intended initial frequency. This can be seen in table 4.1. This does not have a large impact on the experiments, the results still have a clear trend over the measured frequency range.

Sloshing

Sloshing is a non-linear effect. Because all analysis is based on linear theories, aimed is to stay out of the sloshing domain. Nevertheless, when the experiments were carried out, sloshing took place for almost all drafts at the higher tested frequencies. For real scale (10[m]) the sloshing periods were around 4-5[s].

Draft 1: no sloshing at all
Draft 2: T=4s
Draft 3: T=5s and shorter
Draft 4: T=5s and shorter
Draft 5: T=5s and shorter

Sloshing starts at more or less the same frequency for each draft.
Draft 1, when the bucket is just touching the water obviously does not experience any sloshing at all.
Draft 2, where the draft is equal to one fourth of the diameter starts to experience sloshing at a slightly higher frequency.
This could be because water can flow out easier, the average water particle is on average closer to the bottom of the bucket. This could reduces the sensitiveness to sloshing.
Faltinsen stated that when $\frac{h}{R_0} > 1.0$, the resonance period differs by less than 2.5% from the infinite depth value, for $\frac{h}{R_0} > 1.5$ this diverges to less than 1%.
In the case of an infinite depth cylinder, assumed is that there is no way of distinguish whether the bucket is closed or open at the bottom. The sloshing characteristics merge into the same period for both cases. During the experiments the relation $\frac{h}{R_0} > 1.0$ is never reached, but its sloshing period gives a good first estimate.

5

Results

In this chapter the results of the experiments will be presented: what variables are studied and what are the relations found between *added mass versus wave frequency* and *added mass versus draft*. The data is analyzed and relations are defined here. A more in depth discussion is presented and conclusions are drawn, in the next chapter *Discussion & Conclusions*.

5.1. Variables

In this thesis the following two relations are studied:

- The change in the inertia term, representing the added mass, related to changing wave frequency.
- The change in the inertia term, representing the added mass, related to changing bucket draft.

Due to the method in which the added mass is extracted from the data, it is also possible to determine the damping for the same draft and frequency relations. The frequency dependency and the draft dependency of the damping is determined likewise.

- The change in the damping term related to changing wave frequency.
- The change in the damping term related to changing bucket draft.

The damping results are also presented in this chapter. The damping shown in this chapter is the complete damping, this includes (mechanical) friction $\left(\vec{F}_{friction} \propto \mu \cdot \vec{F}_{normal}\right)$, wave radiation damping $\left(\vec{F}_{WRD} \propto B \cdot \vec{v}\right)$ and viscous damping $\left(\vec{F}_{viscous} \propto B \cdot \vec{v}^2\right)$.
The most dominant damping term is expected to be the wave radiation damping (WRD). Due to the forced oscillation of the bucket, waves are generated, dissipating energy from the system, this is acting as a damping term.
More information on how to exclude the mechanical friction can be found in the chapter Recommendations. In the next chapter an estimate is made for the dominance of the viscous damping.

Accuracy load-cell F(t) fit

For each dataset the norm function (Euclidean distance), explained in the chapter Post Processing (equation 4.22), is determined. The norm values do not have a physical meaning in the sense that they can only be used as a reference compared to other measurements. The norm value changes with the accuracy of the fit, but also depends on the duration of the signal. As not all signals are of equal length (but do not change much either), they can only be used for relative comparison. Low norm values (probably) indicate accurate fits.

Frequencies	Draft 1	Draft 2	Draft 3 1.0e+03 *	Draft 4 1.0e+03 *	Draft 5 1.0e+03 *
f_1	348.09	355.57	0.4457	0.4879	0.5759
f_2	499.94	513.08	0.6012	0.5974	0.7378
f_3	508.47	594.73	0.7172	1.1741	1.0334
f_4	512.14	572.21	0.7363	0.9928	1.1619
f_5	522.46	592.8	0.8096	1.0308	1.5335
f_6	517.81	648.17	0.9505	1.1669	1.5650
f_7	498.97	661.64	3.7492	1.7934	2.0572
f_8	491.59	645.11	4.5146	2.0802	2.3792

Table 5.1: Average norm in [N] between fitted signal F(t) and raw data from load-cell

Accuracy displacement x(t) fit

For the displacement signal x(t) the norm function is again determined for each dataset. The same properties hold regarding the physical meaning of the values. They are only used for comparison within table 5.2.

Frequencies	Draft 1	Draft 2	Draft 3	Draft 4	Draft 5
f_1	0.0886	0.0433	0.0570	0.0498	0.0479
f_2	0.0381	0.0407	0.0341	0.0365	0.0385
f_3	0.0415	0.0416	0.0362	0.0496	0.0363
f_4	0.0374	0.0446	0.0381	0.0454	0.0423
f_5	0.0394	0.0380	0.0412	0.0416	0.0403
f_6	0.0372	0.0332	0.0394	0.0450	0.0474
f_7	0.0455	0.0409	0.0498	0.0340	0.0355
f_8	0.0424	0.0336	0.0507	0.0436	0.0347

Table 5.2: Average amplitude in [m] fitted signal x(t) and raw data from LBT-sensor

The forced oscillation displacement turned out to be a very clean signal. This makes sense due to the fact that this is exactly the controlled variable. The pipe is what was forced to oscillate with a clean sinusoidal displacement. Physical stiffness of the system (e.g. rigid crankshaft) resulted in a clean oscillatory displacement signal. It is easy to see the accuracy of the fit by eye, the fit and the original signal are almost identical to each other, see the figure 5.1 for one of the fitted signals. Overall, the same argument goes for the build up time, increasing frequencies need more ramp up time. Hence the signal is shorter and the norm likely to turn out lower. In addition, this is confirmed looking at table 5.2.

Displacement amplitude

The amplitude of the displacement fit *does* have a physical meaning. The amplitude of the displacement represents the stroke the crankshaft is making in time. The fit of this displacement signal should be equal to the physical stroke the crankshaft is making. In table 5.3 the average amplitude is shown.
The full stroke is a physical limited and constant value of 8.3[cm]. The amplitude of the fit should be approximately half of this, being 4.15[cm] (note: this *has* to be frequency independent, which is the case). These values are within a range of 2% of the physical measured crankshaft stroke. Therefore this is considered sufficient accurate and reliable.

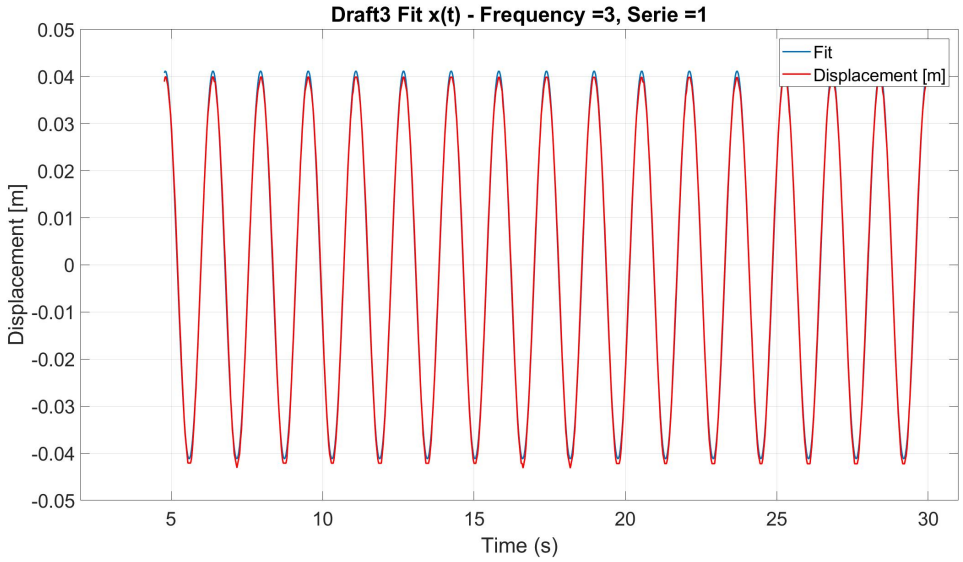

Figure 5.1: Example of a displacement signal x(t) and its fit function.

	Draft 1	Draft 2	Draft 3	Draft 4	Draft 5
Amplitude fit [m]	0.0413	0.0413	0.0405	0.0407	0.0408

Table 5.3: Average amplitude in [m] displacement fit

Phase difference between Force and displacement

The phase difference changes generally with increasing draft *and* frequency. This indicates that the relation added mass and damping is changing. In the next chapter is explained more in depth on what the physical interpretation of this trend is.

Frequencies [Hz]	Draft 1	Draft 2	Draft 3	Draft 4	Draft 5
0.41	104.97	112.11	124.48	135.38	138.51
0.52	99.54	109.40	124.04	137.05	144.84
0.64	106.04	118.02	136.46	151.75	154.66
0.76	113.05	126.83	140.05	145.62	143.76
0.88	120.76	132.27	140.36	145.15	140.42
1.00	127.72	135.46	140.737	144.70	144.78
1.13	135.43	137.25	113.46	132.37	136.14
1.15	142.31	135.48	109.37	128.84	133.01

Table 5.4: Average phase difference in degree per draft and frequency

5.2. Raw data

Data from low frequencies show more irregular behavior. This can be seen in the plots 5.2 in the attachments. It is likely that this (static/dynamic) friction occupies a larger percentage of the total measured force, resulting in a (relative) more distorted, noisy signal. Notice that the friction force from equation 6.1 is frequency *independent*, But that the damping term B itself can be frequency dependent. Noisy signals introduce linear fitting errors and are harder to fit properly in the first order. The data can become less reliable when the noise becomes a large part of the overall signal.

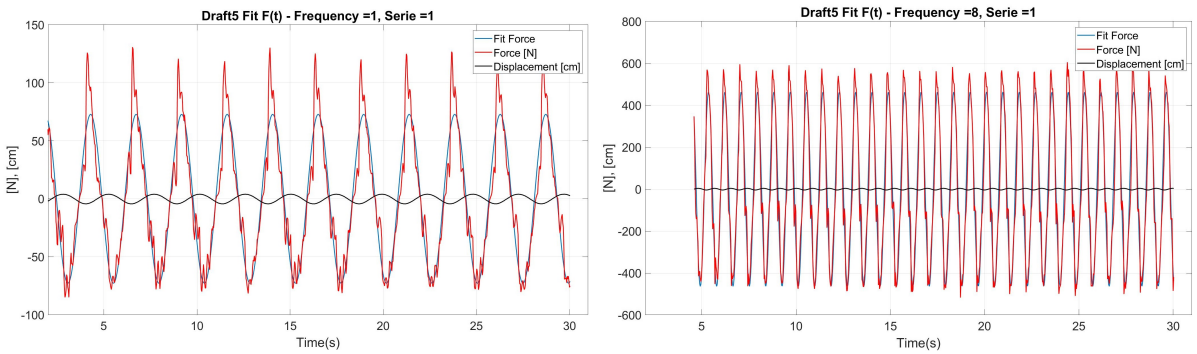

Figure 5.2: Low frequency force signals tend to be more noisy due to non-linear effects.

5.2.1. Force frequency spectrum

When the FFT operation is applied to the force signal of the load-cell, a lot of information about the system can be unveiled. The frequency domain shows the dominant frequencies present in the force signal. Expected is that the forced oscillation will be the most dominant frequency, but other harmonics or system resonances might become visible. Two plots are presented here, more graphs can be found in Appendix C.11.

The FFT spectrum of draft 3 frequency 8 showed some irregular behavior. As can be seen in the graph, the forced oscillation frequency (1.15 [Hz]) shows up as the dominant frequency, exactly as expected. But, multiple harmonics show up as well, with different non-negligible amplitudes.

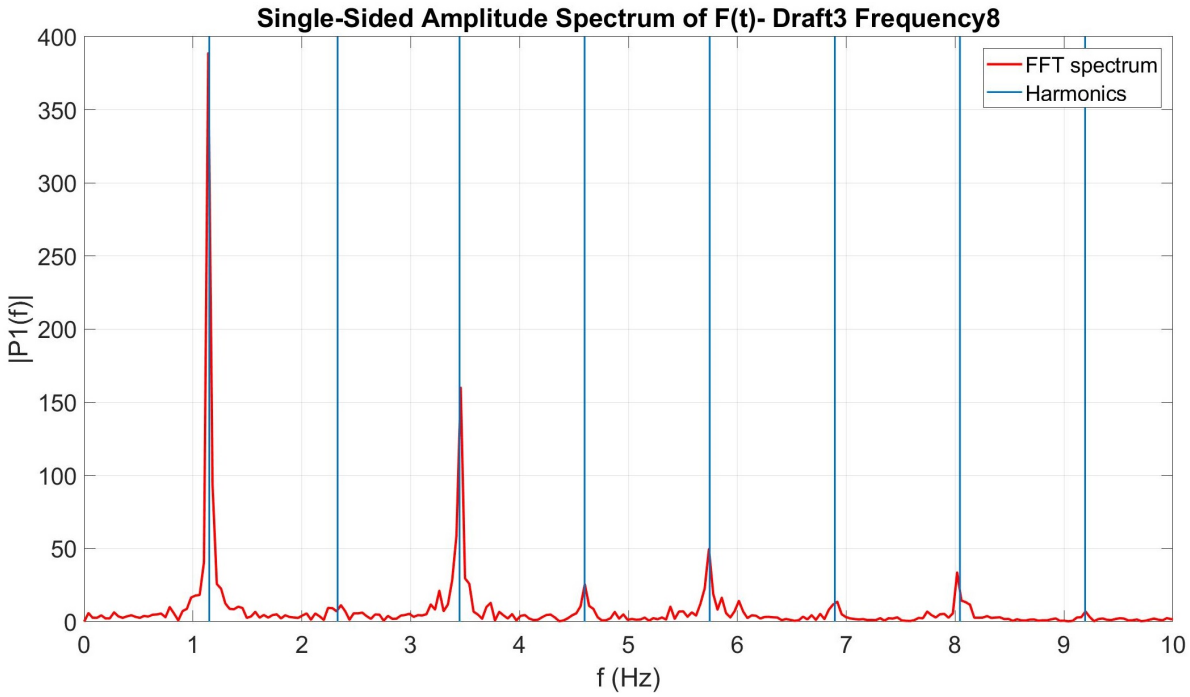

Figure 5.3: Single-Sided Amplitude Spectrum of F(t) for draft 3, frequency 8.

For draft 3, the same FFT is plotted in figure 5.4, this time for frequency 1 .

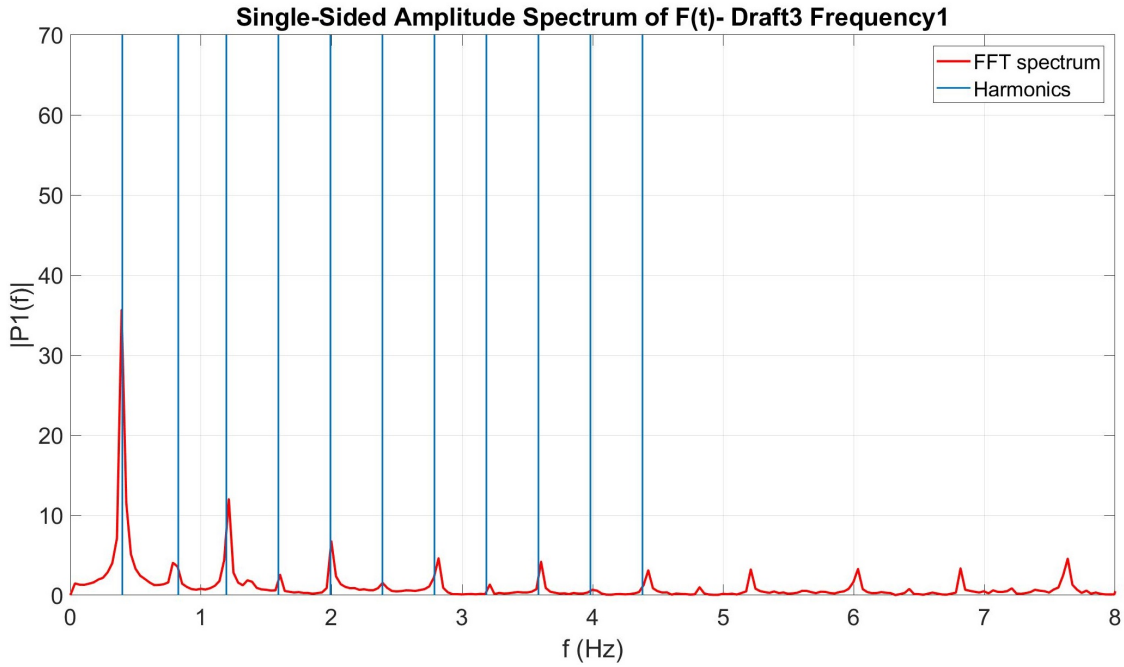

Figure 5.4: Single-Sided Amplitude Spectrum of F(t) for draft 3, frequency 1.

As can be seen again, the dominant frequency is the forced oscillation frequency of 0.41 [Hz]. This time the peak is even harper with a higher amplitude compared to its higher harmonics. Here can be concluded that friction and viscous damping are less dominant that for lower drafts and/or frequencies. More discussion about these two spectra in the chapter *Discussion*.

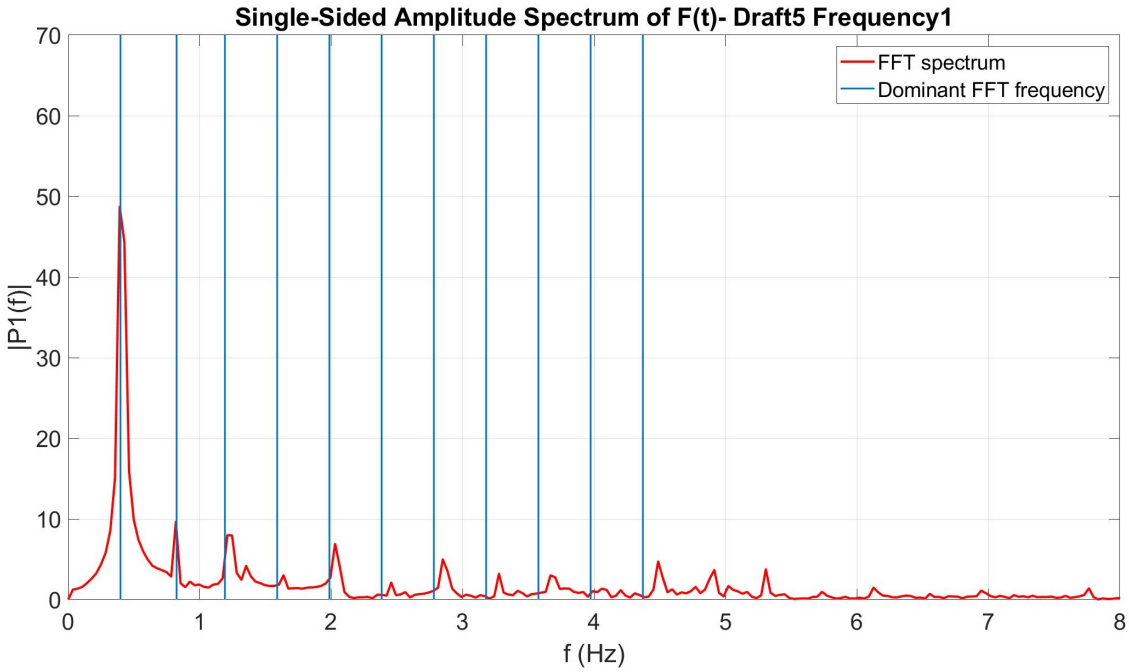

Figure 5.5: Single-Sided Amplitude Spectrum of F(t) for draft 5, frequency 8.

5.3. Added mass

In this section the found added mas - frequency relation is plotted for each draft. The individual series are plotted in the same graph, together with error bars showing the accuracy of the experiments. Additionally the numerical values of the added mass from the computational program AQWA are plotted in the same graph. The AQWA model uses the same dimensions, frequencies and drafts as in the experiments. A small trick is applied to include viscous damping in the model. A small lid is placed inside the model to suppress the added mass at resonance. A lid can have a value between 0 (no lid) and 1 (fully closed), generally such applied lids have low values, in this model the lid has a value of 0.04.

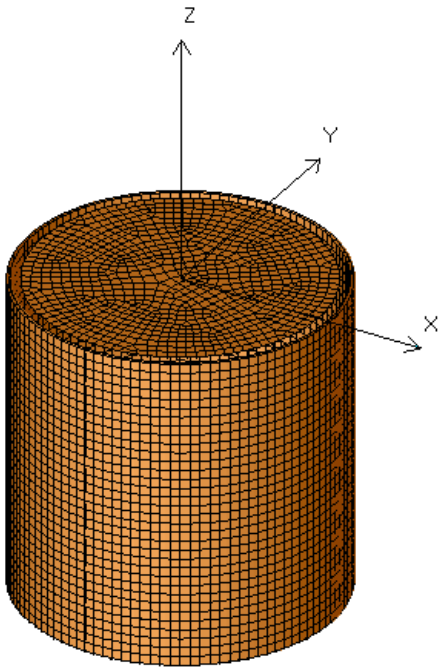

Figure 5.6: Ansys AQWA model to determine added mass and damping from potential theory.

Draft1 = 0[m]
Draft 1 has no wetted surface, therefore it has virtually no interaction with the water. The added mass term should be non-existent by definition here, only intrinsic mass is measured here in the inertia term (the added mass due to air is assumed negligible here). The intrinsic mass is removed in the post processing process. That is why the added mass specific term is close to zero and negligible.

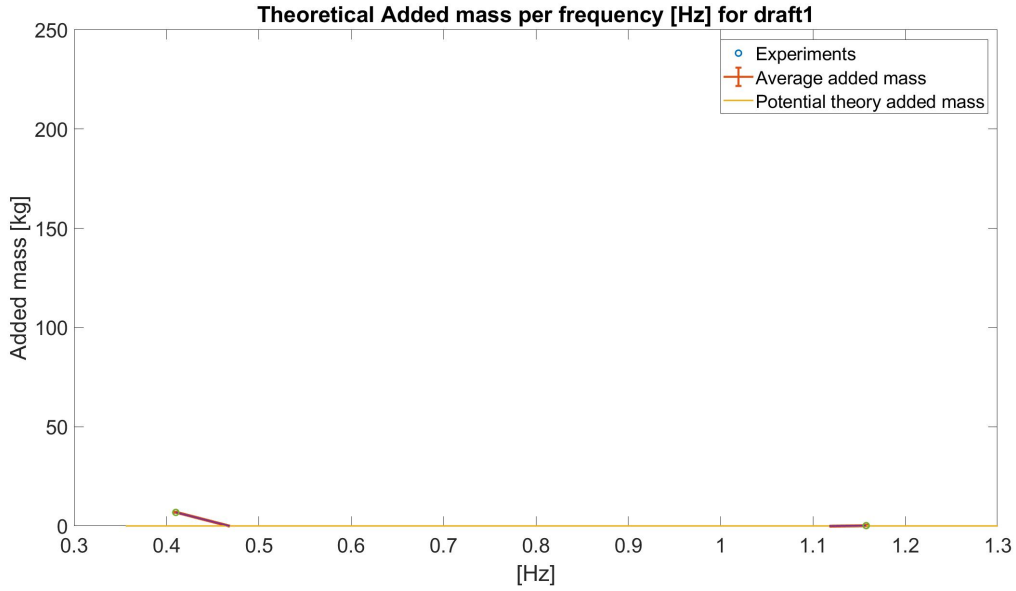

Figure 5.7: Draft 1. Experimental versus numerical added mass

Draft2 = 0.125[m]
Draft 2 consists of 12.5[cm] wetted surface. The added mass term stays more or less constant over the frequency range, from 20 to 30[kg]. Even in the sloshing domain (>1.1[Hz]) the added mass stays more or less constant. The added mass is close to the added mass determined by the potential theory. Compared to the potential theory is slightly increasing with increasing frequency.

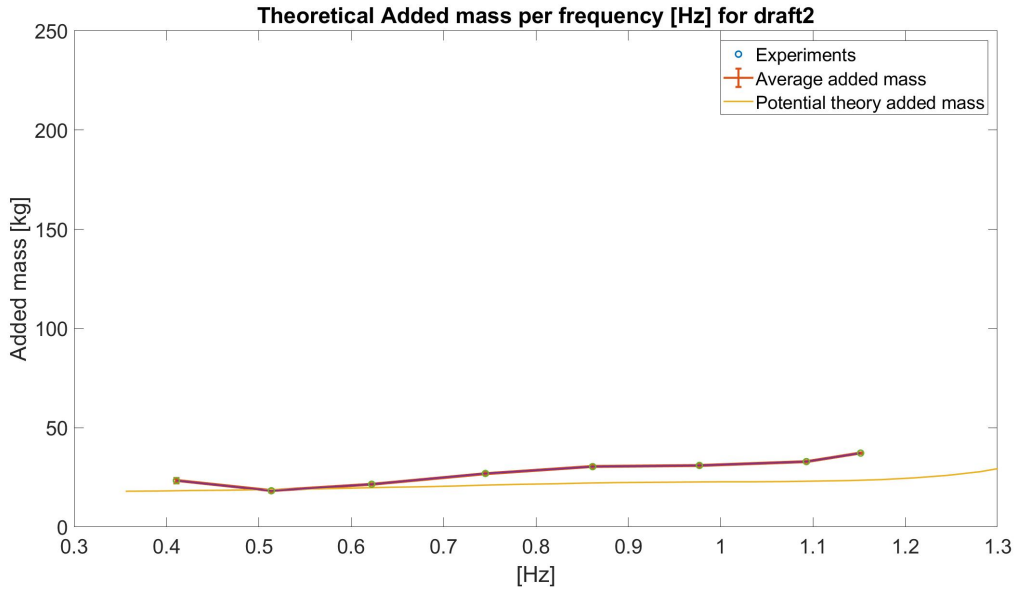

Figure 5.8: Draft 2. Experimental versus numerical added mass

Draft3 = 0.25[m]
The added mass for draft 3 keeps more or less constant (slightly increasing) till sloshing occurs, at this time the added mass drops rapidly, proportionally the most of all drafts. When the damping is checked, it turns out that the damping increases the most of all drafts at the same frequency. This indicates a change in phase shift between the force and the displacement. In table 5.4 this presumption is confirmed. Fairly low deviation between separate repeated measurements is observed over the entire frequency range. The measurements are (just) slightly over estimated to the predicted added mass from the potential theory. At sloshing the added mass gets underestimated. Overall the added mass increases from 65[kg] to 80[kg] to then decrease rapidly to 40[kg]. This is a 50% decrease in added mass due to sloshing.

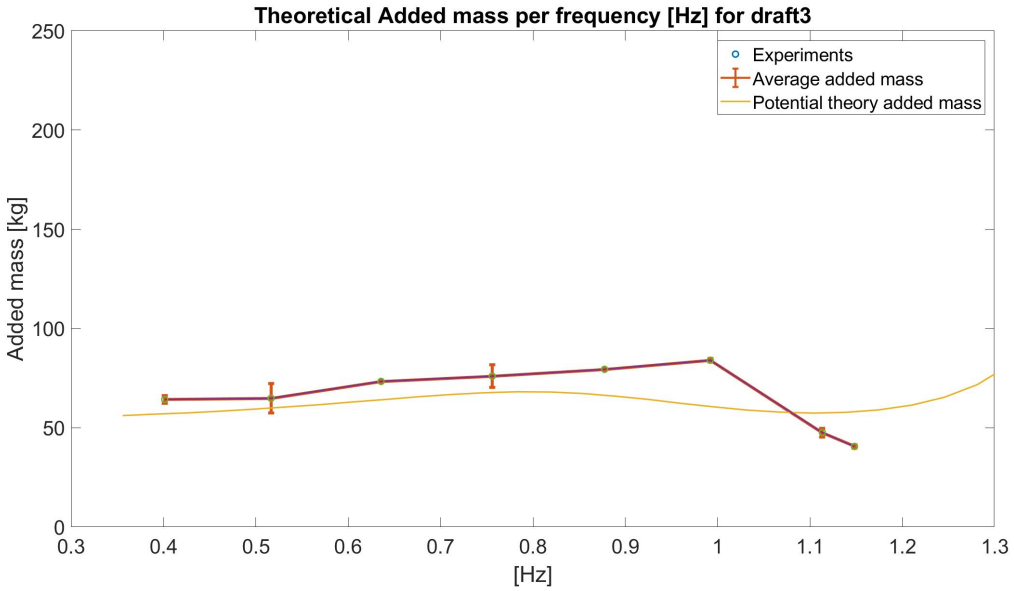

Figure 5.9: Draft 3. Experimental versus numerical added mass

Draft4 = 0.375[m]
Draft 4 represents a draft of 37.5[cm], these test series have some inaccuracies as can be seen in this graph. This can also be seen in the graph for the damping for the same draft. Again the added mass is dependent on the draft, but is further fairly constant over the frequency range. The added mass in the experiments keeps its value while the potential theory predicts a decline. At higher frequencies when sloshing is observed this decline eventually takes place. This decline can be observed in the other drafts as well.

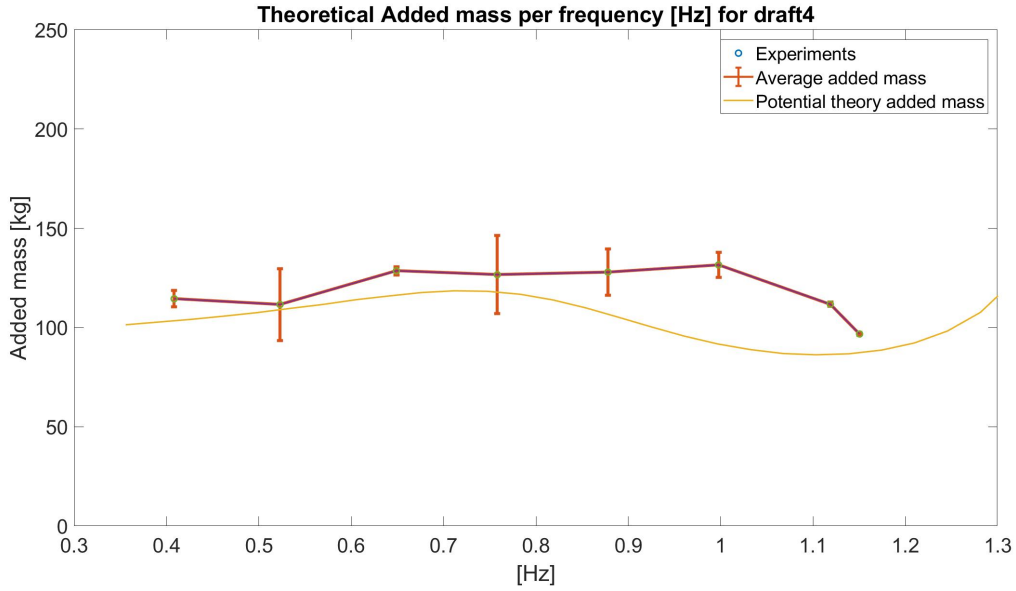

Figure 5.10: Draft 4. Experimental versus numerical added mass

Draft5 = 0.5 [m]

For the final draft, draft 5, the added mass is again increased with draft. The lower frequencies have a higher uncertainty than higher frequencies (up to 20%), probably because high frequencies result in higher reaction forces and thus relative lower (non-lineair)damping/friction terms. Frequency independent factors such as friction, which might introducing inaccuracies which become less dominant with increasing frequency. Although, at shallow drafts the reaction forces are low in general, but the results do not show large uncertainties. The damping values for draft 5 at low frequencies don't show any unlikely high uncertainties. Again, the average experiment results match the predicted added mass graph as expected, only a small frequency delay in the moment of decrease can be noticed.

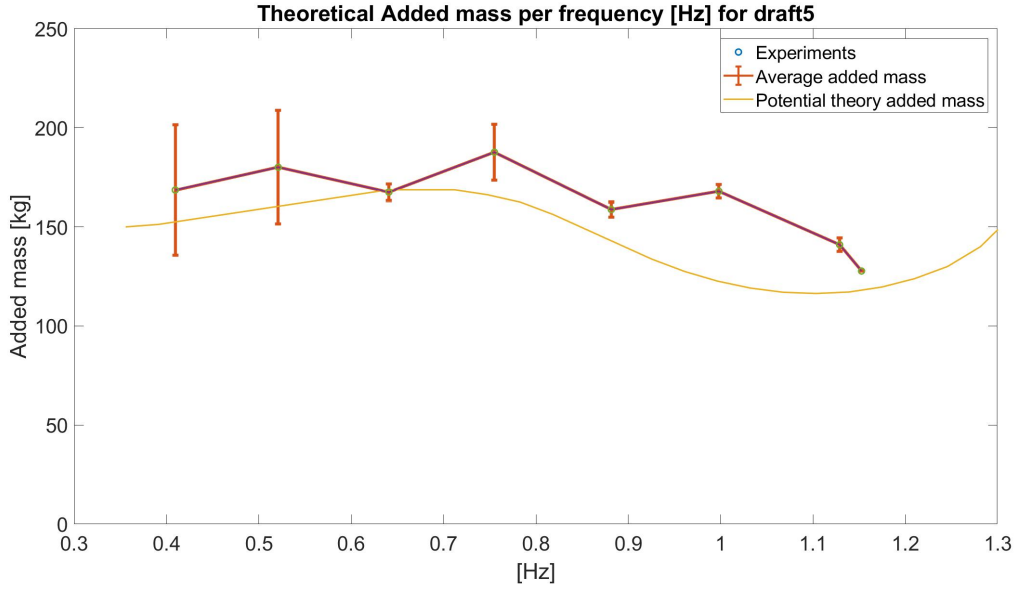

Figure 5.11: Draft 5. Experimental versus numerical added mass

The following graph shows a single graph where the added masses for each draft are plotted. Again with its error bars to show the accuracy of the tests. The individual tests are removed, only the average added mass and the uncertainty are plotted.

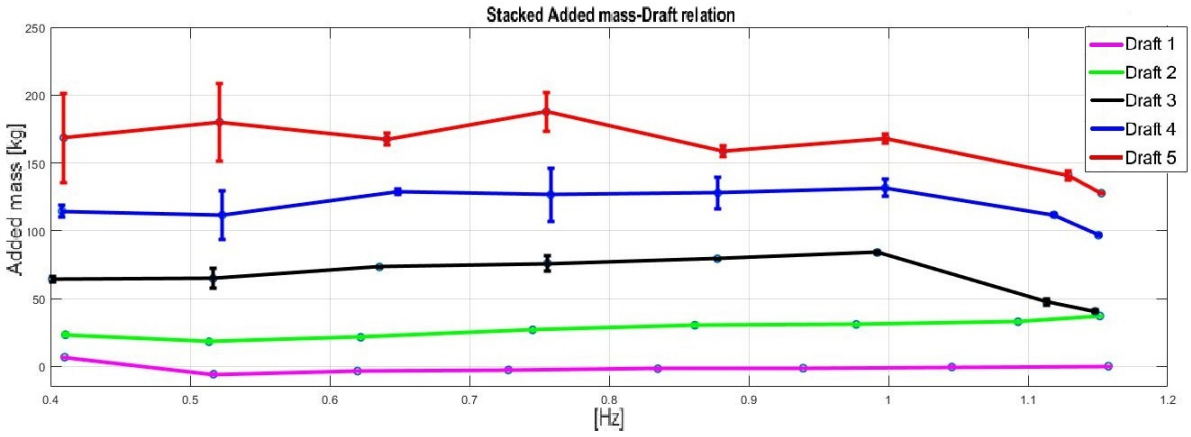

Figure 5.12: Stacked graphs of added mass versus frequency)

5.4. Damping

While the added mass dependency is the initial goal of this thesis, the damping is also determined. By applying basic mathematics (see section 2.8) the damping is determined. Damping plays an important role during any type of installation operation. When the damping of the system is high, reaction motions (or forces) (Response Amplitude Operators (RAO's)) gets reduced, which will be beneficial for the overall performance of the installation operation.
The same structure is used here to present the damping behavior while draft and frequency are changed.

Draft1 = 0[m]
Draft 1 has no wetted surface, therefore it can not produce any waves. The wave radiation damping and viscous damping should be non-existent by definition here, only frictional damping is measured here. A clear friction dominant factor can be seen in this graph, introducing a non-zero damping.
The damping decreases with increasing frequency. Low uncertainties are encountered in this set-up. Again damping due to aerial effects are considered negligible.
Overall, the damping decreases with almost 60% from 35[kg/s] to 15[kg/s].

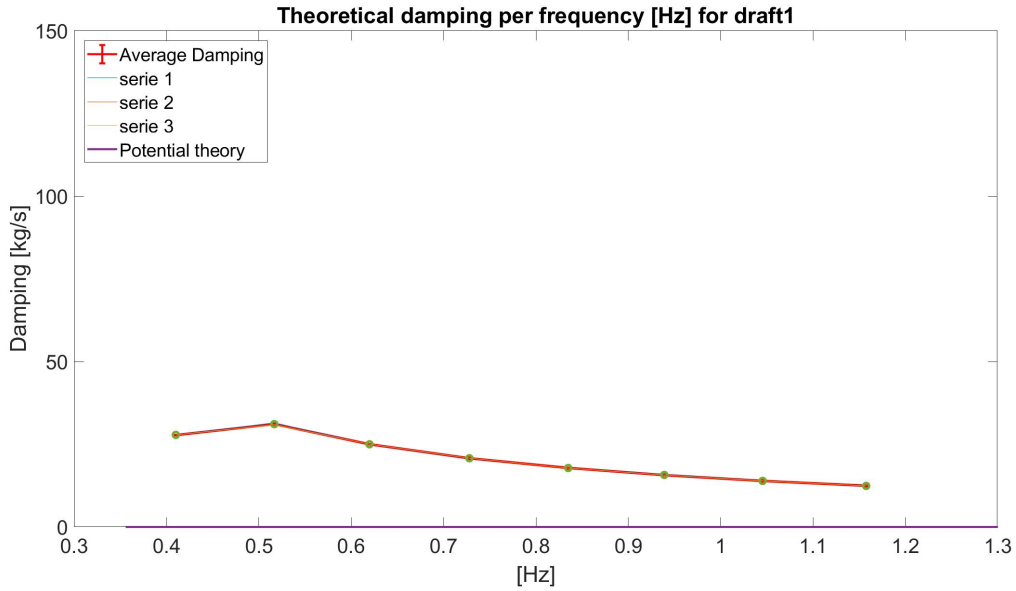

Figure 5.13: Draft 1. Experimental versus numerical wave radiation damping

Draft2 = 0.125[m]
Draft 2 consists of 12.5[cm] wetted surface. The damping stays more or less constant over the frequency range, although in sloshing region the damping increases lightly, albeit that no intense sloshing is observed at this draft. When the potential damping from draft 2 is added to the determined damping from draft 1 ('dry' test) it becomes close to identical to the determined damping in draft 2. This can be seen as a cross-check of the experiment series.
Overall, the damping increases lightly with about 30%, from 35[kg/s] to 45[kg/s].

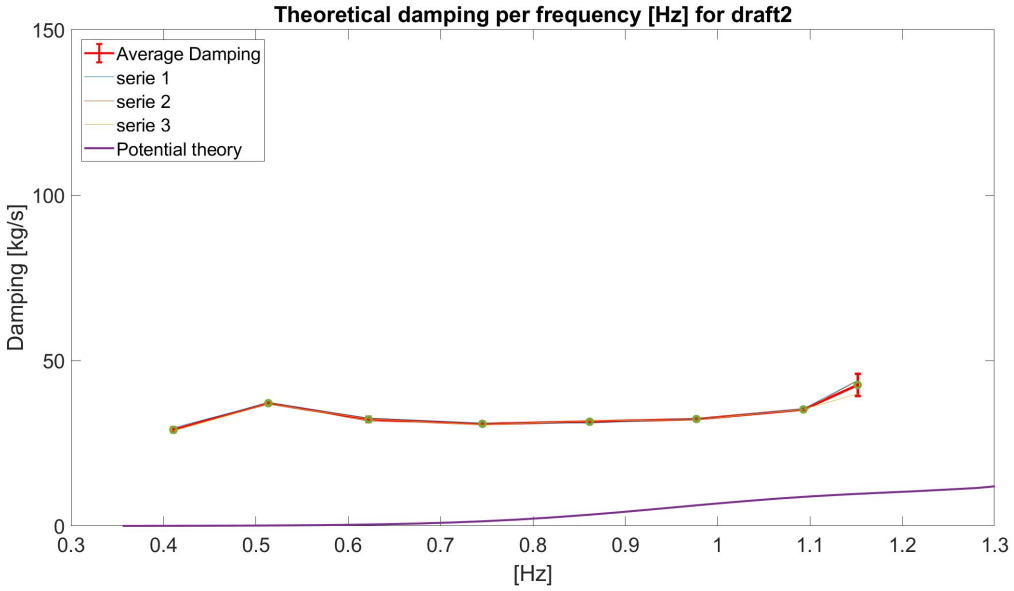

Figure 5.14: Draft 2. Experimental versus numerical wave radiation damping

Draft3 = 0.25[m]

Draft 3 is when the bucket is halfway submerged (37.3[cm]). This setting provides significant wetted area to radiate waves, waves are mainly radiated near the water-air interface, but it also provides enough volume inside the bucket for waves to break when sloshing takes place. Both effects contribute in the damping, but for draft 3 the biggest increase in damping is identified when sloshing started. Low uncertainties are encountered in these test series. Note that the potential theory does not include sloshing, hence this effect is excluded from the computed damping.

Overall, the damping increases the most of all drafts with about 300% from 35[kg/s] to 140[kg/s] in the sloshing domain.

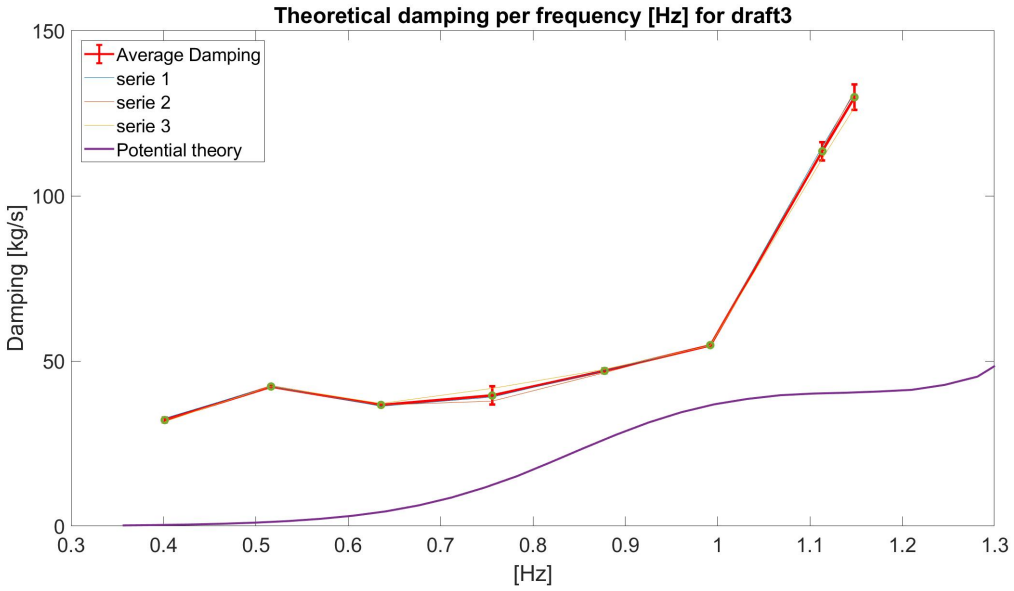

Figure 5.15: Draft 3. Experimental versus numerical wave radiation damping

Draft4 = 0.375[m]
For draft 4 the determined damping more or less increases linearly. Uncertainty between test series has increased, especially for frequencies 2 and 4 ($\pm$ 20%). At frequencies just before sloshing domain the determined damping almost matches the computed damping.
Derived from this could be that in theory wave radiation damping increases compared to the previous draft, while in practice the determined damping is less influenced its change in draft. Concluded from this can be stated that another damping term compensates for this effect.
Overall, the damping increases with about 175% from 35[kg/s] to 140[kg/s].

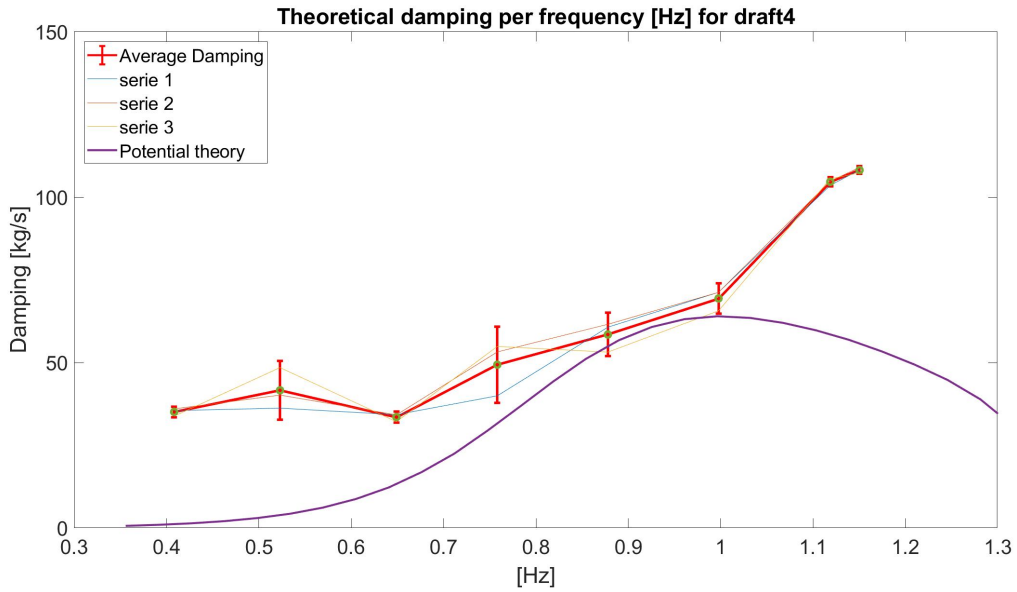

Figure 5.16: Draft 4. Experimental versus numerical wave radiation damping

Draft5 = 0.5 [m]
For draft 5 the shape of the determined damping has not changed much from the previous draft. This confirms that wave radiation damping is a dominant effect and is mainly taking place at the water-air interface. Uncertainties have decreased compared to draft 4.
The last two measured frequencies are again in sloshing region, introducing a large additional damping term which is not (fully) covered in the potential theory. Overall, the damping increases with about 200% from 40[kg/s] to 120[kg/s].

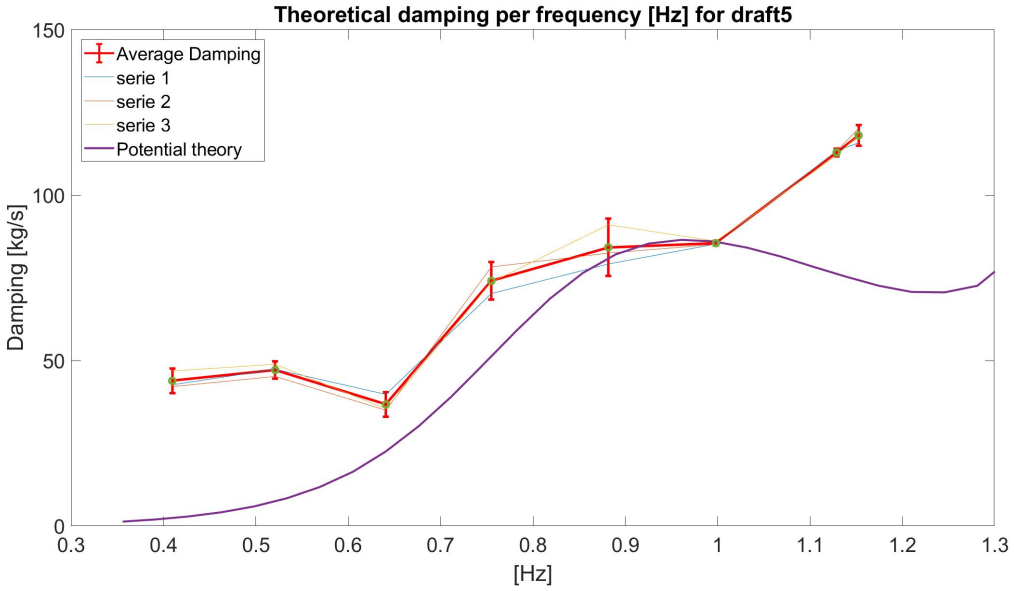

Figure 5.17: Draft 5. Experimental versus numerical wave radiation damping

As can be seen in the graphs below, the damping seems fairly constant for each draft at low frequencies, this is concluded to be a dominant friction term, introducing a non-zero damping. At a certain frequency the damping starts to increase rapidly. Known is that the last two tested frequencies for each draft showed sloshing behavior, therefore the initial increase in damping is not because of sloshing but because of another effect. This same increase is observed in the potential theory, identifying this as wave radiation damping. More on this in the next chapter *Discussion*.

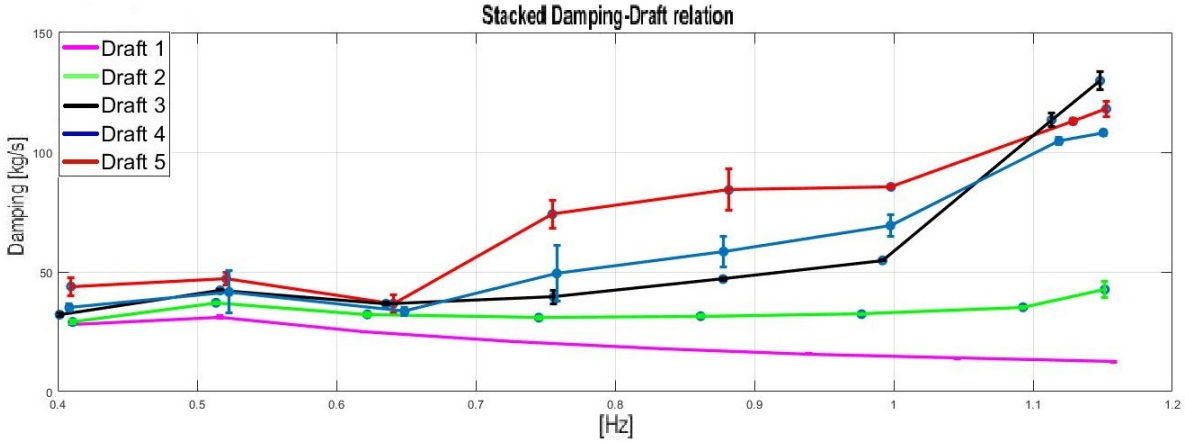

Figure 5.18: Stacked graphs of Damping versus frequency)

Dimensionless Added Mass

The added mass can be made dimensionless[2] by dividing the outcome by the mass of its enclosed volume as been done in equation 2.10:

$$Added\ mass[-] = \frac{Added\ mass}{\rho \cdot Volume\ pipe} = \frac{A}{\rho \cdot \frac{\pi}{4} D^2 T} = [-] \tag{5.1}$$

For each draft the enclosed mass is:

Draft 1 = 0[m] mass enclosed volume $=\rho\frac{\pi}{4}D^2h = 0[kg]$
Draft 2 = 0.125[m] mass enclosed volume $=\rho\frac{\pi}{4}D^2h = 24.54[kg]$
Draft 3 = 0.25[m] mass enclosed volume $=\rho\frac{\pi}{4}D^2h = 49.09[kg]$
Draft 4 = 0.375[m] mass enclosed volume $=\rho\frac{\pi}{4}D^2h = 73.63[kg]$
Draft 5 = 0.5[m] mass enclosed volume $=\rho\frac{\pi}{4}D^2h = 98.17[kg]$

The dimensionless added mass makes it possible to compare results from different drafts, or even other experiments found in literature.

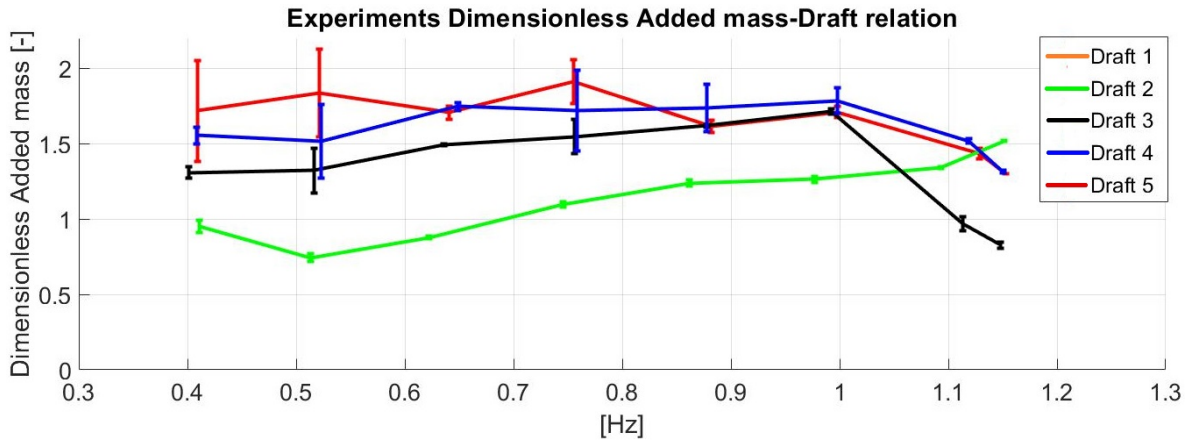

Figure 5.19: Dimensionless added mass for all drafts

5.5. Dimensionless Damping

Just like the added mass the damping can be made dimensionless. This can be done according to the following relation from equation 2.11:

$$D_{dimless} = \frac{Damping}{\rho V \sqrt{\frac{g}{D}}} = \frac{Damping}{\rho \frac{\pi}{4} D^2 \sqrt{\frac{g}{D}}} = \frac{Damping}{\rho \frac{\pi}{4} D^{\frac{3}{2}} \sqrt{g}} = [-] \tag{5.2}$$

The dimensionless damping is convenient when comparing damping from the experiments to other experiments or to the literature.
The dimensionless damping for all drafts is plotted in a single graph below. Here is presented how the damping evolved versus draft and versus frequency.

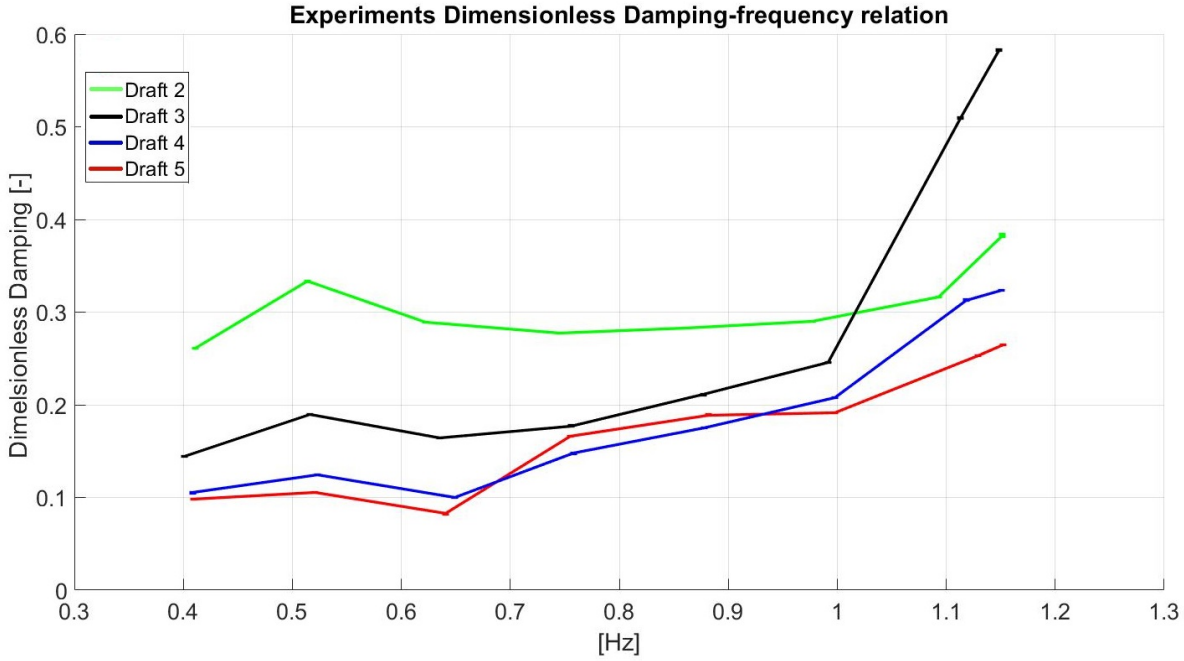

Figure 5.20: Dimensionless damping for all drafts

Summary Results

A condensed summary of the observed results for damping and added mass is listed here, in the next chapter *Discussion* the relations are discussed in more depth.

Added mass:

• In general the test results matched the predicted added mass well, in the linear region (before sloshing) it stayed well within a 10% deviation, which is considered acceptable.
• The added mass is dependent on the bucket draft, this tends to be a linear-like relation, increasing draft increasing added mass accordingly. Although in the dimensionless added mass the graphs deviate from each other, therefore it is *not exactly* a linear relation.
• Added mass does not depend heavily on the frequency, it stays nearly constant in the linear range.
• In the sloshing domain the added mass decreases significantly, tests have shown a decrease in the range of 20-50%. Potential theory shows a similar decrease.
• Sloshing occurred slightly at higher frequencies than Ansys AQWA predicted.

Damping:

• Test results show similar shape as predicted by the potential theory. This indicates WRD is the dominant damping factor.
• Damping measured in the low frequency range is almost constant for all drafts, indicating friction being the dominant factor.
• At Draft 1 (draft =0[cm]) no WRD nor viscous damping is measured since this is a dry test. draft 1 shows pure friction.
• Sloshing increases the damping significantly.
- Effect biggest in mid draft (draft3 = 0.375[cm])
- Trend of effect decreases for increasing draft. Indicating it being surface effects (WRD/sloshing).

Other observations

• FFT spectrum of load-cell shows clear dominant (forced) frequency for all draft and frequencies.
• FFT of load-cell signal shows multiple harmonics.
• FFT of load-cell signal shows increased presence of 3ω frequencies for several tests.

6

Discussion & Conclusions

6.1. Discussion

Observations of the results are discussed in this chapter. Odd behavior of certain signals are explained here, expected characteristics are confirmed when present. Reflections are made on the entire research in the last section Reflection.

6.1.1. Force frequency spectrum

As can be seen in figure 5.3 only odd number of harmonics are present. This can be explained when the Fourier series of the signal are studied. Some Fourier series are represented in figure 6.1. The force signal ideally is a clear cosine function and then a clear single peak at the forced frequency would then be expected. But odd harmonics show up as well, in figure 6.1 this corresponds to a square wave. A friction force typically gives a square wave for a harmonic oscillation. The friction force is not frequency related but acts always counter directed to the motion according to the relation:

$$\vec{F}_{friction} = -\mu \cdot F_N \cdot \frac{\vec{v}}{|\vec{v}|} \tag{6.1}$$

Note that this friction force is only dependent on the normal force F_N and the friction coefficient μ which both are assumed to be constant during the experiments.

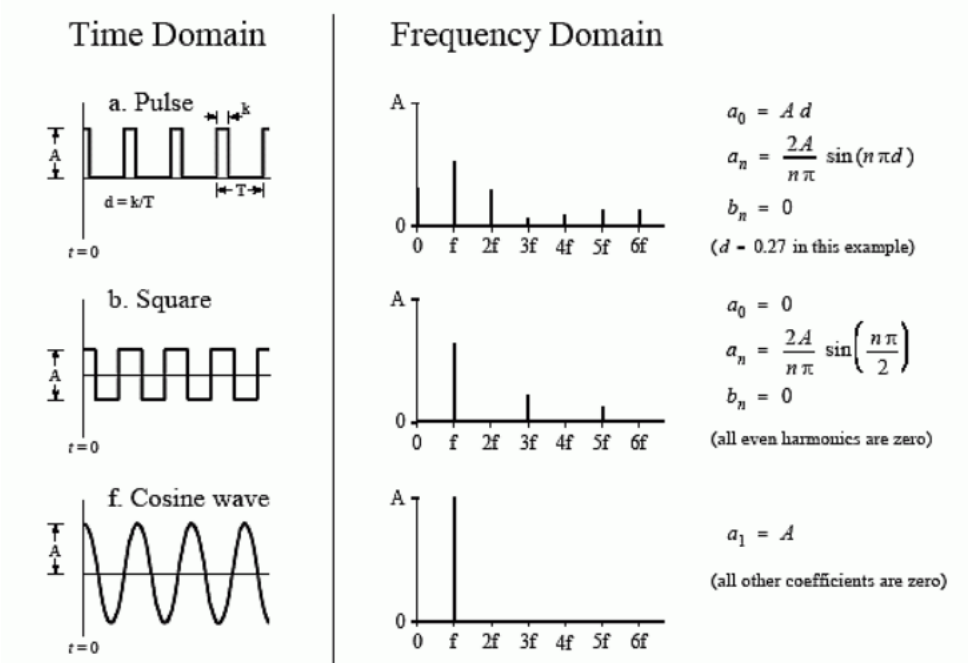

Figure 6.1: Fourier series for certain type of waves.

Uncertainties

Unfortunately it is impossible to execute experiments without introducing uncertainties in any way. Some sources of uncertainty are described and discussed here.

6.1.2. Test set-up

• Manual input frequency regulator

A manual pod-meter was used to give the input value for the voltage c.q. output frequency of the frequency regulator. The ideal Volt values were determined through interpolation. Although the display showed up to four digits in accuracy, it was hard to reach these exact values with the physical pod-meter. Small errors were introduced here (see attachments for initial and final Volt values).
A digital input can be used to avoid this kind of errors.

• Conversion frequency regulator to actuator output frequency

The frequency regulator only gives a relative value in Volts. Frequencies are calibrated by adjusting the display volt value till the right RPM value is reached. This is done for all minimum and maximum values for minimum and maximum draft, all values in between are linear interpolated.
Finally it turned out that the actual actuator output frequencies are not that evenly distributed (see table 6.1). This is represented by the data points on the frequency axis, they are not evenly distributed on the x-axis. This is not considered a big problem because of the following reasons; there is not a major concentration of data points in a small frequency range. Therefore the trend is still visible with a decent, evenly spread, set of data point. Note: this was what the initial goal, the frequency relation for the added mass given a certain frequency range.
Avoid conversion uncertainties by making use of an actuator with a known conversion factor, or at least its individual conversion properties.

• Non-linear regions

High frequencies have shown sloshing effects, while the post processing is based on linearity.
As discussed in the previous chapter and can be seen in figure 5.12 and figure 5.19, the added mass decreases for higher frequencies (sloshing regions). Force in phase with the displacement is decreasing here. This effect can in theory be extrapolated till negative added mass terms when sloshing is perfectly in anti-phase with the displacement (in phase with the applied force). It is impossible to exe-

cute hydro mechanic experiments excluding viscous effects, this is a non-linear effect.
This experiments and the post processing methods are based up on linear properties, this can introduce uncertainties when non-linear effects come into play.

• Non-ideal set up
Loose parts and connections.
Uncertainties are introduced due to non-infinite stiff connections. In the case of the crank shaft there can be some slack on the connections of crank shaft to the actuator or in the swivel to the load-cell. Tension and compression will in this case lead to spike loads at the points of reversal motion. More non-ideal parts might be present in the set-up introducing inaccuracies.
A trade-off has to be made between costs and effort and perfectioning the test set-up.

• Alignment guiding system
Mis-alignment of the set-up.
Because the trolleys and the rails are aligned by hand and eye, there might be some misalignment introduced by practical imperfections. For example drilling the holes for the attachment of the rails to the frame. However, this might be not perfectly in line with the force applied by the actuator. The fact that the rails consists of two separate pieces is not increasing the alignment either. Although this effect over all is assumed small.
Again this is a trade-off between costs and effort and perfectioning the test set-up, adviced is to use a single rail for both trolleys instead of two separate pieces and make sure the trolleys are properly aligned to reduce friction.

• Stiffness of the set-up
Although the hammer tests shows that the natural frequencies of the system are not in the range of the forced frequency and that the response in range of the studied frequency range is small, it *does* have a non-zero effect on the measured force and displacement. This is because the frame is not infinitely stiff.
Due to the fact that the response is small, this indicates that the frame is sufficiently stiff, is assumed this is not a problem for the experiments.

• Wave reflections
Generated waves from the bucket can propagate to the finite walls of the tank, reflect there and come back to interfere with the set-up. This limits the duration of the test duration. Some time between tests is reserved for waves to damp out until the water level is flat again before starting new experiments. Even though there still could be some wave-bucket interaction. Still water level is checked by eye through the window with a marked scale drawn on it to compare the wave amplitude. Together with measuring the excitation force of the load-cell while the bucket is submerged in the tank and supposed to be stationary with no forces acting up on it. Reflected waves may keep on interfering with the bucket before they damp out, even when the experiment is already stopped.
Lower frequency waves have longer wavelengths and higher wave velocities. Hence, reflection times are shorter for low frequencies.
The importance of a tank of sufficient dimensions or decent wave dampers is emphasized here. Wave reflections should be avoided as much as possible. No significant wave reflections were measured, probably due to the presence of wave dampers.

• Water depth
Because deep water is assumed during the calculations some inaccuracies may be introduced for low frequencies. Here the wavelength compared to the water depth would suggest intermediate water depth (n values up to 0.68). While this is still not interpreted as shallow water, it is neither considered as deep water anymore. Bottom influences might possibly not be negligible, even though the studied direction (surge) is parallel to the bottom of the tank.
Advised is to stay within the linear domain, this includes 'deep water' properties. Influences of the tank bottom should be avoided.

6.1.3. Post processing methods

• Accuracy of the cut off time

The method of removing the build up time is considered sufficient, but is based on the assumption that if V_{max} is reached the actuator is at its maximum and constant frequency. When post processing the data the cut-off time is chosen to be 97.3% of this maximum voltage. This due to possible inconsistencies in the voltage. Although this is not the exact point at which V reaches its maximum value, the first zero up crossing after this point is taken as a starting point of the dataset. The exact starting point is not that big of an issue, at least the frequency should be constant and if possible to be as early as possible since then the signal lasts longer and fitting a longer function becomes usually more accurate.

• Fast Fourier Transform

Possible reflected wave interactions are limiting the allowable duration of the experiments. The resolution of the FFT in the frequency domain is dependent on the length of the signal in the time domain. Because this is a relative short duration for all records, less than 30[s]. The resolution of the FFT is not that accurate. This is about 0.05[Hz], which as a reference, is hard to distinguish two neighboring frequencies in the low test frequency range. It can cause inaccuracies in determination of the actual forced oscillation frequency. A sharp peak should be observed in the frequency spectrum. When the signal is coarse, it is hard to determine the exact location of the peak.
A sufficient duration of the experiments is required to improve the resolution of the FFT signal, the longer the better, but avoid wave reflection interactions.

• Damping factors

Software programs such as Ansys Aqwa are based on linear damping. These programs neglect other types of damping, for example viscous damping due to produced vortices around the edges of the bucket bottom.
Sloshing inside the bucket will also dissipate energy due to breaking waves (splashing and bubble formations) and thus will introduce a (viscous) damping term, this will also not be taken into account.

Draft	**f1**	**f2**	**f3**	**f4**	**f5**	**f6**	**f7**	**f8**
$f_{initial}$	0.4100	0.4500	0.5000	0.5600	0.6400	0.7500	0.8900	1.1200
Draft 1	0.4101	0.5167	0.6198	0.7279	0.8349	0.9390	1.0454	1.1575
Draft 2	0.4108	0.5136	0.6222	0.7453	0.8614	0.9769	1.0928	1.1515
Draft 3	0.4014	0.5165	0.6356	0.7559	0.8775	0.9920	1.1133	1.1480
Draft 4	0.4083	0.5230	0.6489	0.7582	0.8779	0.9977	1.1186	1.1504
Draft 5	0.4096	0.5210	0.6408	0.7550	0.8816	0.9981	1.1287	1.1525

Table 6.1: Initial frequency and the actrual frequency achieved per draft

6.2. Post Processing

In this thesis the linear least squares method is used to post process the data. This is, as described in chapter Post Processing, assumed to be more accurate than the Morison approach. The Fast Fourier Transform (FFT) is considered to be a good estimate to see the overall system impulse response. Due to possible wave reflections the tests are limited in duration, this has as a result that the frequency domain is coarse. The studied frequencies are in the 0.41-1.12[Hz] range, this requires a fine resolution and therefore longer duration of the tests. This was initially not possible due to possible wave reflections.
The least squares method is used to analyze the data.

6.3. Added mass versus Frequency

The added mass turns out to be more or less constant per draft for each frequency.
This is what was expected with the estimated numerical added mass, although, some things can be mentioned;

• For deeper drafts the added mass decreases at higher frequencies.
Sloshing will dissipate energy into other excitation modes as described later in this chapter in section *sloshing*. From mid draft on more sloshing takes place. This introduces a phase difference in the experienced force. The decomposition of this sloshing effect contributes to damping, but also a reduction in the added mass component. Reducing the retrieved added mass in the post processing.

• The uncertainty bars decrease with increasing frequency.
The uncertainty bars are decreasing with frequency because larger forces are measured and the relative error decreases. Frequency independent factors such as mechanical friction do not scale with the increasing applied force to the bucket. Therefore reducing the relative error.

• The added mass in the experiments is higher than the numerical values from Ansys AQWA.
This has to be the case because the numerical values *purely* describe the added mass, while in the experiments other effects that are in phase with the force can contribute to the added mass. One thing to mention here is that the amount of added mass found is a multiple of the numerical value, which is clearly way too much. This is the case for all studied frequencies and drafts, indicating that there is a systematic error.

6.4. Added mass versus Draft

• Added mass increases with increasing draft.
This makes sense, more surface of the pipe is able to interact with the water.
Although, there is **no linear relation** between increasing draft and the corresponding added mass. The added mass for the linear region (for low frequencies) does not change accordingly to the change in draft. This becomes better visible when the dimensionless added mass is used. In the next section is explained in more detail about the dimensionless added mass and its relation to the different drafts.

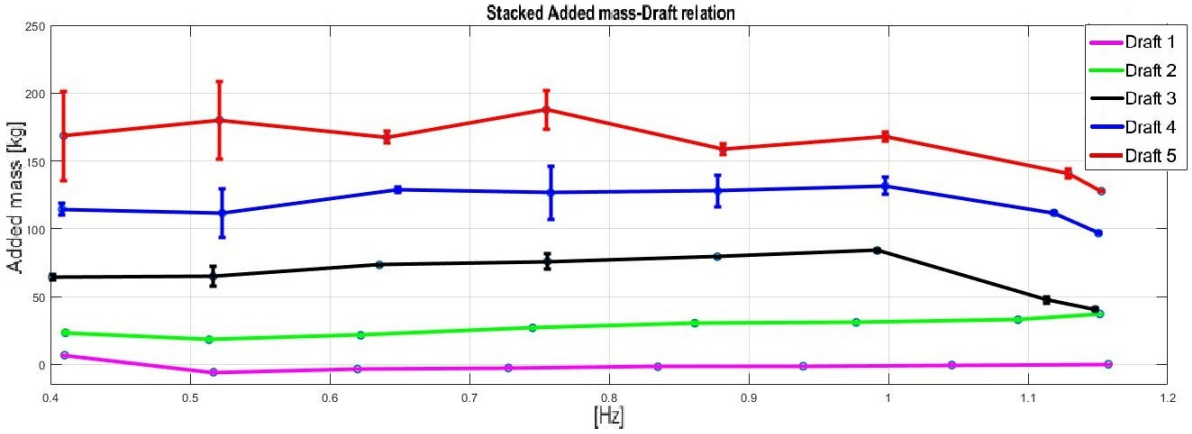

Figure 6.2: Added mass for all drafts

6.5. Dimensionless Added Mass

The added mass can be made dimensionless by dividing it by the mass of its enclosed volume, as can be seen in graph 5.19. In this graph the added mass per draft is divided by its enclosed volume times the water density. This gives the dimensionless added mass. If there was a linear relation between draft and added mass, this dimensionless added mass would project all graphs on top of each other. This is clearly not the case, increasing draft results in relative more added mass. This effect though does decrease with increasing draft.
The theorem that the average water particle becomes more remote from the bucket bottom and therefore is more restricted to flow in and out of the bucket supports this conclusion.
When the frequency reaches 1[Hz], draft 3, 4 and 5 (mid draft towards almost fully submerged) tend to have the same dimensionless added mass, they all approach a dimensionless added mass of about 1.75.

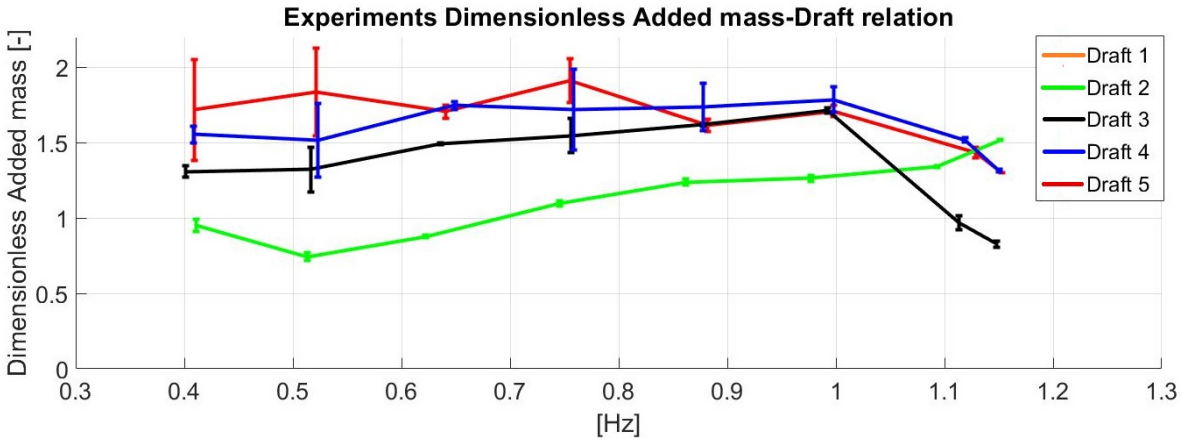

Figure 6.3: Dimensionless added mass for all drafts

The mass of the water inside the bucket for each draft is presented below.

Draft 1	0[cm]	0[kg]
Draft 2	12.5[cm]	24.54[kg]
Draft 3	25[cm]	49.09[kg]
Draft 4	37.5[cm]	73.63[kg]
Draft 5	50[cm]	98.17[kg]

Detailed analysis - Draft 3

Draft 3 is chosen to shed some extra light on, it represents mid-draft of the bucket. Enough water to initiate sloshing effects, but enough space inside to leave room for sloshing effects. On top of that draft 3 showed some irregular behavior in the added mass and damping graphs.
As can be seen in graphs the third harmonic is more dominant in frequency 8 than in frequency 1. This can be explained by the fact that viscous damping plays a more dominant role in the higher frequency range. The drag force consists of friction and viscous damping. The viscous damping is proportional to the velocity squared in the form $v|v|$. According to G. Clauss in Offshore Structures [8] the Fourier series for the drag force become:

$$dF_d \approx \left[\frac{8}{3\pi}\cos(\omega t) + \frac{8}{15\pi}\cos(3\omega t)\right] C_d \frac{\rho}{2} v_a^2 \, dA \tag{6.2}$$

The first term describes the *linear* drag, while the second term describes the *non-linear* viscous damping(see figure 6.4). As can be seen a 3ω term pops up in the equation, with an amplitude of $\frac{1}{5}$ of the forced oscillation frequency.

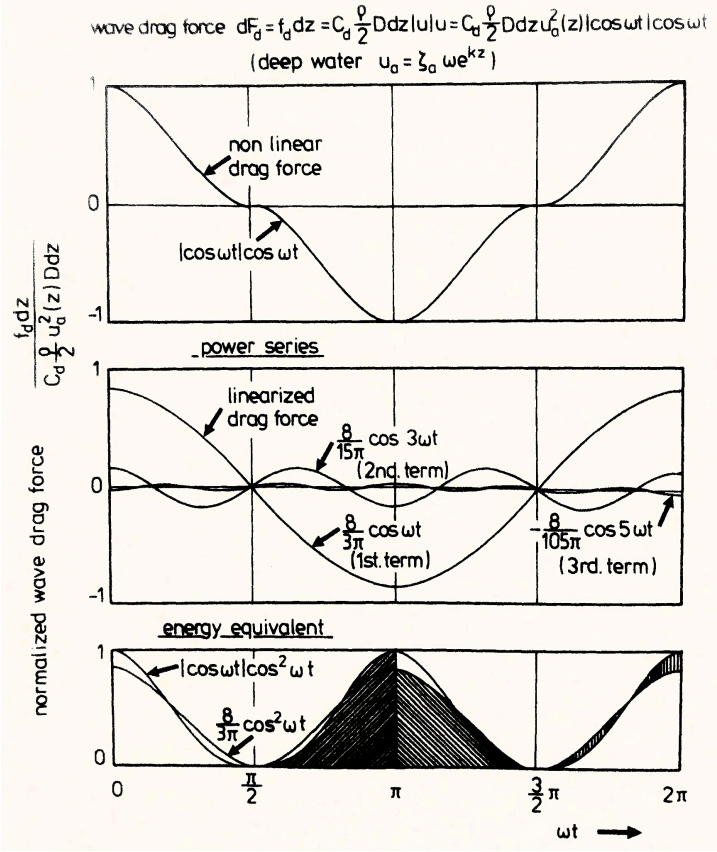

Figure 6.4: Linearization of drag force.[13]

While the forced oscillation load-cell signal ideally should be a clear harmonic oscillation, the non-linear viscous forces distort the signal. See figure 6.5 for an (exaggerated) theoretical example on how the non-linear viscous effect influence the drag term.

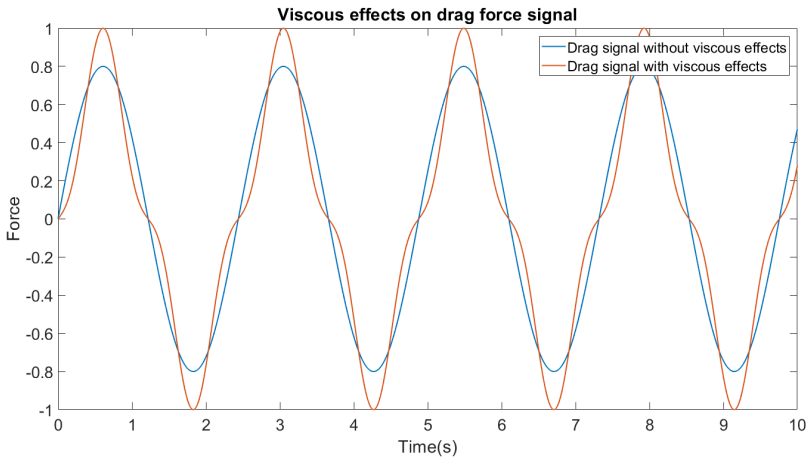

Figure 6.5: Influence of viscous effects on the force signal

This effect can clearly be seen at the FFT spectrum for draft 3 frequency 8.
Note: frequency 8 is sloshing domain, non-linear damping (viscous effects) increase in dominance when sloshing is present.

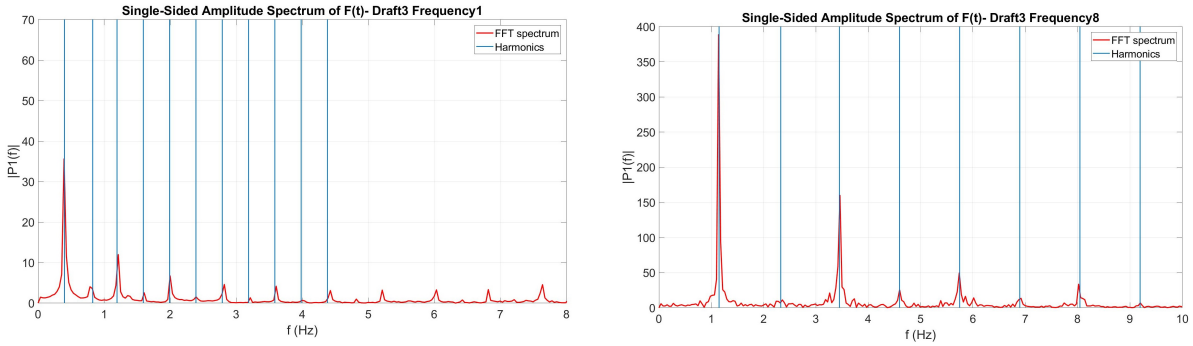

Figure 6.6: Single-Sided Amplitude Spectrum of F(t) for draft 3, frequency 1 and frequency 8.

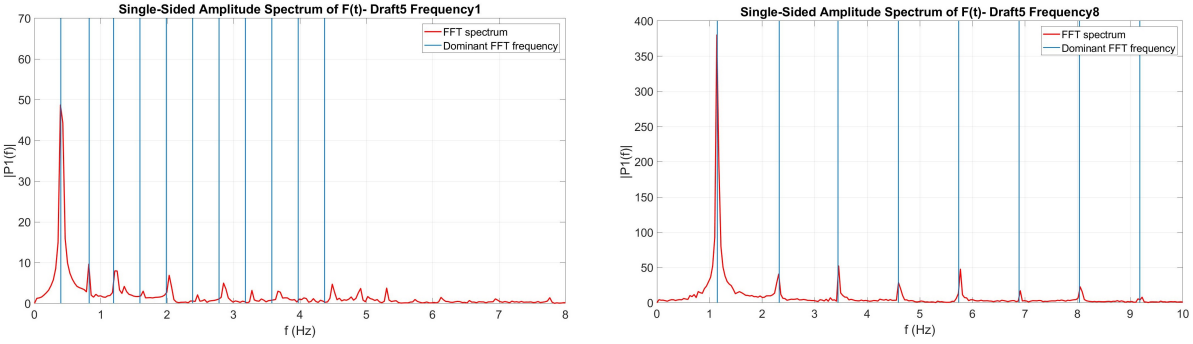

Figure 6.7: Single-Sided Amplitude Spectrum of F(t) for draft 3, frequency 1 and frequency 8.

According to Faltinsen [13] the first harmonic represents the linear component of the viscous drag, while the second term evidences the presence on non-linear terms. The amplitudes of the first and

third harmonic can be determined from the FFT spectrum. The following relation for the amplitude of the third harmonic A_3 holds:

$$A_3 = A_{friction}\left(\frac{2}{\pi}\right) + A_{viscous}\left(\frac{8}{15\pi}\right) \tag{6.3}$$

This first harmonic includes contributions of the linear effects added mass and WRD.

6.6. Verification dimensionless added mass with literature

The non-dimensional values have the advantage that they can be directly compared to other experiments or literature.
Simultaneously, T.Balkema executed experiments, including added mass tests, at the TU Delft. A forced oscillation was done with a vertical pipe of 30[cm] (9[m] full scale), full scale periods of 5 to 11 seconds were tested at a draft of 1.5 times the diameter. T.Balkema also did a verification with the 3D panel method in the computational program called WAMIT [3]. The results of the panel method calculation for the dimensionless added mass are shown below.

Note that the x-axis here shows wave *periods* instead of wave *frequency*, but the studied wave periods both cover the (full scale) 4-11[s] range. The values found for the added mass are comparable to the experiments done at Boskalis.
The change in the trend both take place at about the same wave period. In the WAMIT model the decrease in added mass takes place at about 6[s]. In the experiments this is at the third last test serie, this represents a full scale 6[s] wave as well. The WAMIT 2.5[m] draft ($\frac{\phi}{D} \approx 0.28$) shows a trend that does not decrease over frequency.
At draft 2 ($\frac{\phi}{D} \approx 0.0.25$) in the experiments the trend shows a similar trend (except for the first frequency).

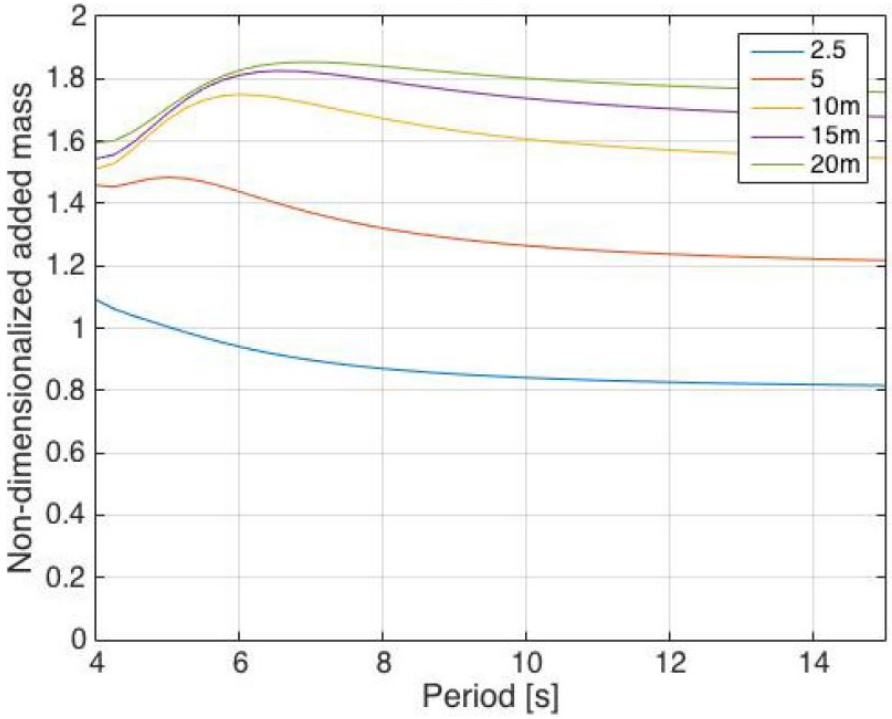

Figure 6.8: WAMIT Dimensionless added mass for several drafts [3]. (Note: periods instead of frequency)

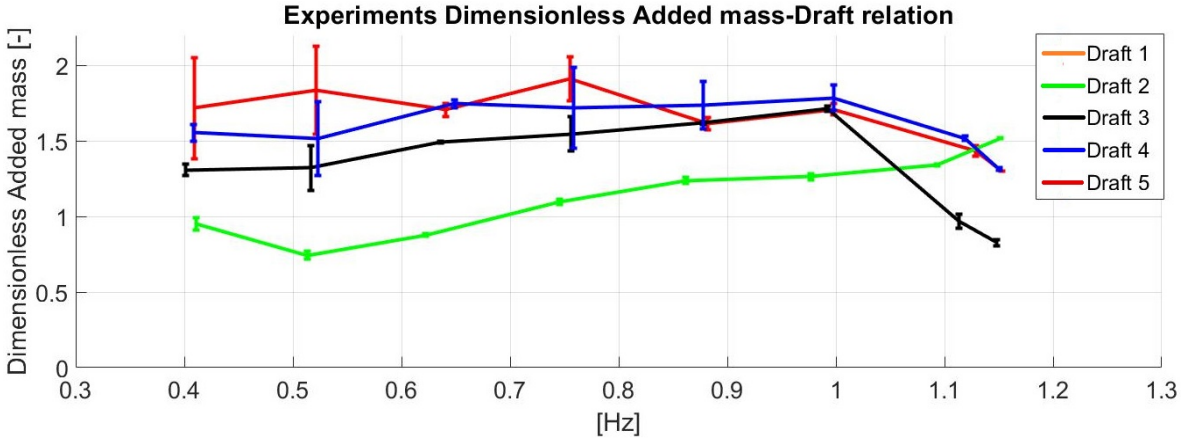

Figure 6.9: Dimensionless added mass for several drafts.

The potential theory is applied to determine the dimensionless added mass and dimensionless damping in ANSYS AQWA. The following graphs show the dimensionless added mass and damping terms versus oscillation frequency in model dimensions. As can be seen the WAMIT model gives slightly higher dimensionless added mass terms. But when the 10,15 and 20[m] are not taken into consideration, since the AQWA model does not consider drafts larger than the diameter, the results are comparable. For the dimensionless damping the results are checked with the Ansys AQWA model of a hollow cylinder.

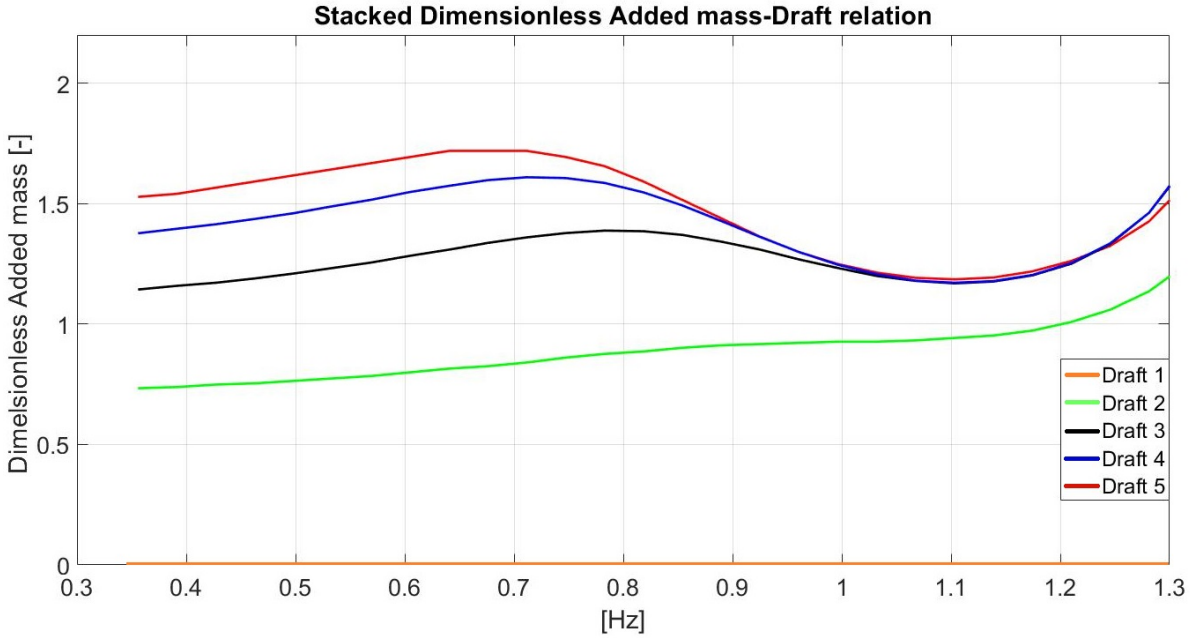

Figure 6.10: Dimensionless added mass from potential theory.

For the dimensionless damping the results are checked with the Ansys AQWA model of a hollow cylinder.

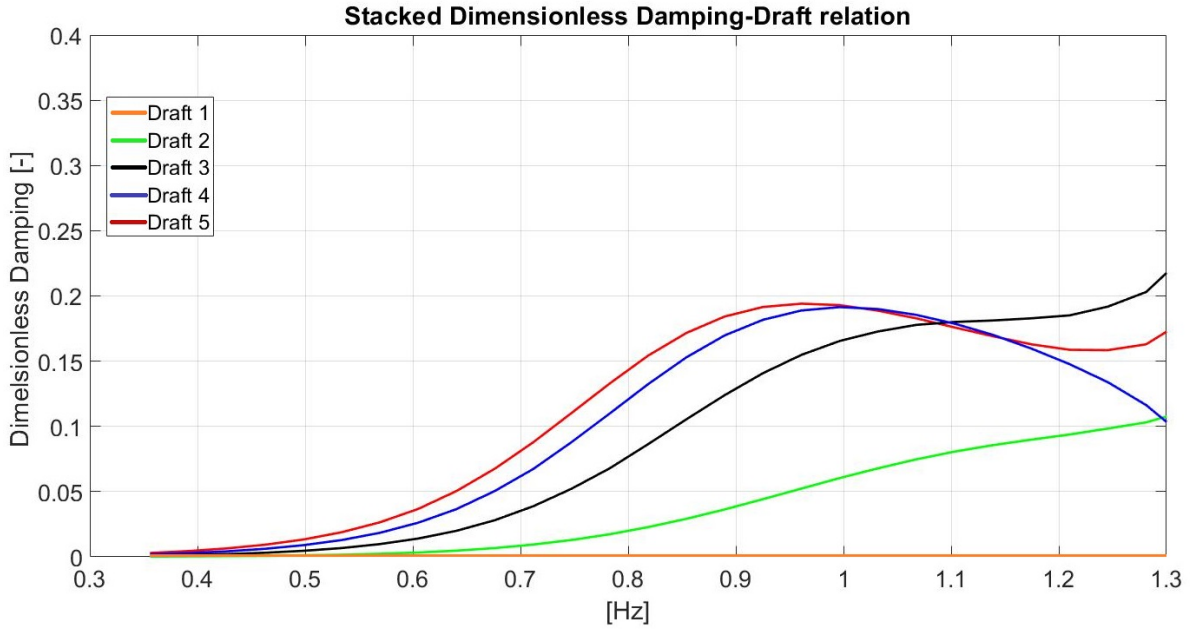

Figure 6.11: Dimensionless damping from potential theory.

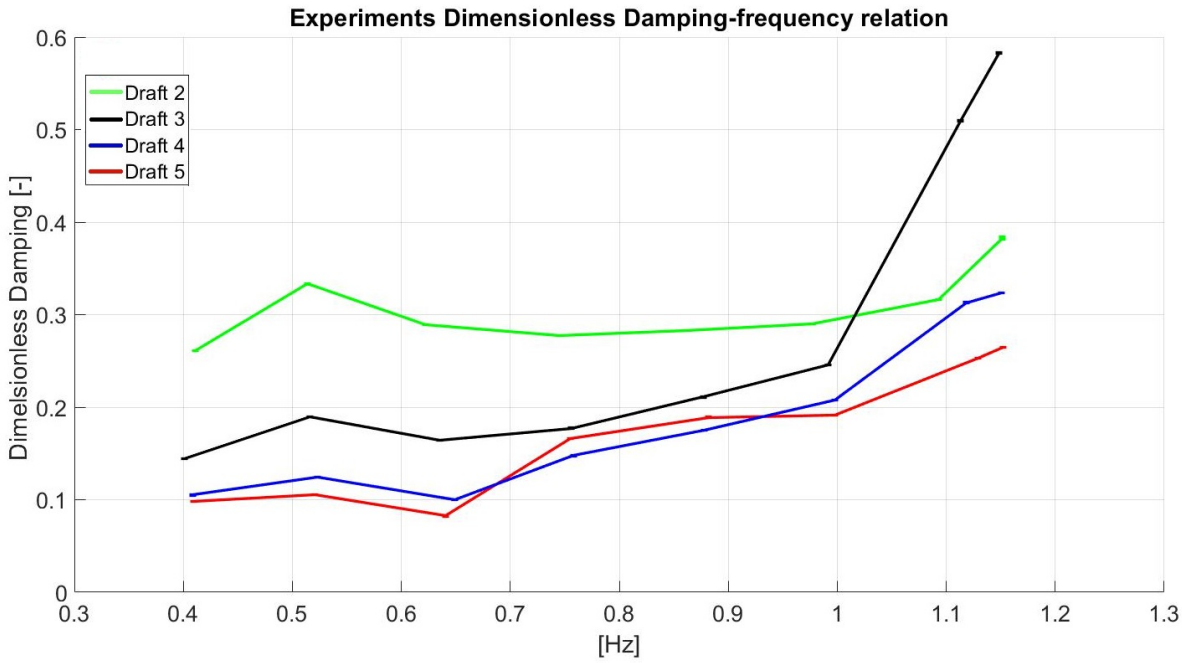

Figure 6.12: Dimensionless added mass from the experiments.

6.7. Sloshing

Sloshing starts to occur at frequencies f_7 and f_8. When looking at the radiated wavelengths present in these situations (see table 4.1) it shows wavelengths of 1.95[m] resp. 1.24[m].
While the bucket being 50[cm] in diameter, it is likely that this is the first excitation mode described in Sloshing by Faltinsen [14]. Faltinsen derives the spectral problem of natural modes analytically in cylindrical coordinates. Bessel functions of the first and second kind satisfy the differential equation. Finally the equations can be solved for the first natural period.

$$T = T_{1,1} \approx \frac{2\pi}{\sqrt{g l_{1,1} \tanh\left(\frac{l_{1,1} h}{R_0}\right)/R_0}}$$

The radiated wave length is one fourth of the bucket diameter. This results in the first standing wave inside the bucket, which is at the first odd natural mode.

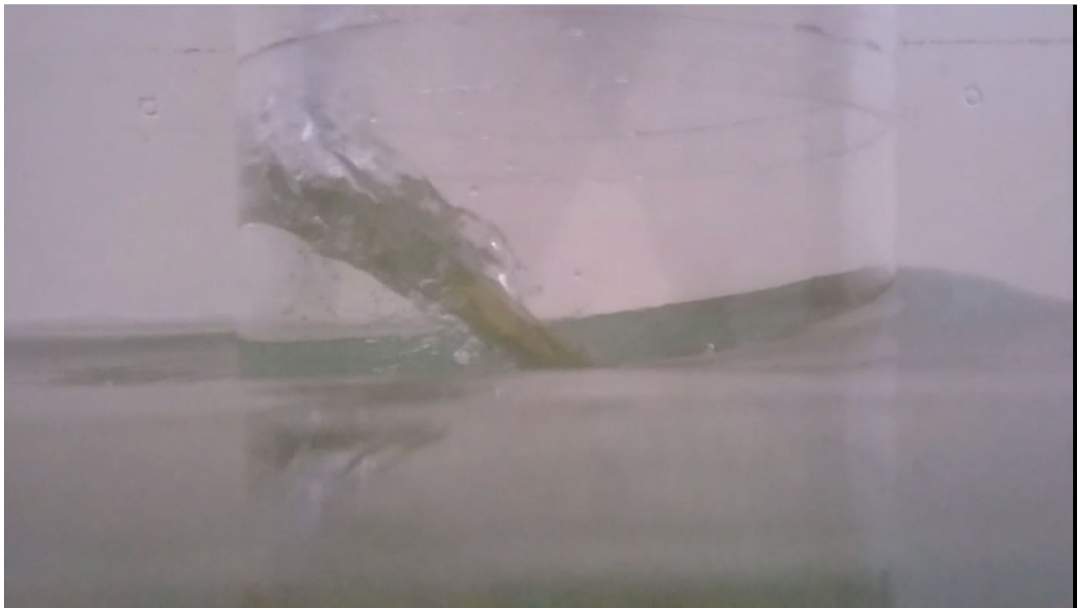

Figure 6.13: Start of sloshing in bucket during experiments.

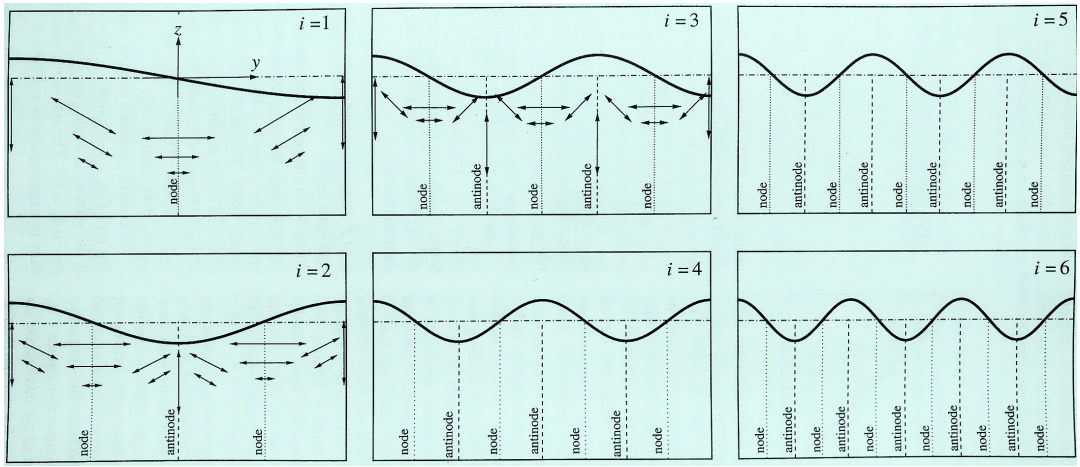

Figure 6.14: Eigen modes of standing waves in a tank.

From this can be derived that the wavelength inside the bucket is not equal to the wavelength outside

of the bucket. The wave inside the bucket has the same excitation period, but it experiences other boundary conditions. For a standing wave, rigid boundaries are required, anti-nodes are solutions to the potential function at the boundary conditions. Each multiple of $\frac{n \cdot \lambda}{2}$ $(n = 1, 2, 3, \ldots)$ waves are higher order harmonics for standing waves inside an enclosed volume. For a cylindrical volume the solutions are a bit more complex, but the boundary conditions still hold. When sloshing takes place the energy from this first excitation mode transfers to a set of higher modes, the higher modes can be resonantly excited due to secondary resonances [14]. Because the experiments include forced oscillations, energy builds up inside the bucket. Due to this increasing energy over time, the wave amplitude grows till the wave steepness outruns the critical value. At this point waves break and the earlier discussed wave dissipation is taking place. This effect is called sloshing.

Electron in a potential well analogy
For readers with an interest in quantum physics, this is the good analogy to an electron in an infinite potential well (except that an electron in the well *only* can exist at certain energy levels). The electron can be described as a wave according to D. Griffiths in Introduction to Quantum Mechanics [15].When this electron is put in an infinite deep potential well with square walls, it has certain eigenstates and certain energy levels. The wave-function is restricted here and has to go to zero here due to the infinite potential wall, hence the wave-function (energy) goes to zero here. This results in no anti-nodes as boundary conditions but nodes. Resulting in the set of $\frac{n \cdot \lambda}{2}$ (n=1,2,3..) possible waves fit into the well with increasing energy levels proportional to n^2.
Where the first, or so called ground,-state represents the wave-function $\Psi(x, t)$ fitting in the well with $\frac{n \cdot \lambda}{2}$ $(n = 1, 2, 3, \ldots)$. This ground state represents the lowest energy (longest wavelength) that fits the requirements for the well [15].
In the case of water waves, no nodes are required at the edges but anti-nodes. Just like the eigen-modes of electrons, for waves this also results in the 'ground-state' of $\frac{\lambda}{2}$.

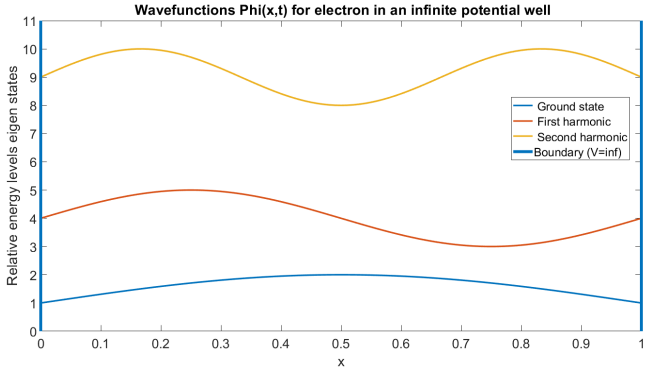

Figure 6.15: Analog to Eigen-modes of electrons in an infinite square potential well.

Verification with literature

Faltinsen wrote in his book 'Sloshing' about many phenomenons of sloshing in multiple situations, including the filling level dependency of sloshing periods for a vertical cylindrical tank [14].

6.8. Full size predictions

Sloshing is experienced in the range that Faltinsen predicted for closed vertical cylinders. To determine the exact sloshing period a finer time resolution should be taken. For all drafts sloshing started about 5[s] (real scale), while the draft (denoted as *h* in figure 6.16) ranges from 0-10[m]. According to figure 6.16 this results in a sloshing period increasing with draft from 8-3[s].
In the experiments sloshing was more or less constant at 5[s] for every draft. because only drafts (filling

levels)

$$\frac{n \cdot \lambda}{2} \quad (n = 1, 2, 3, \ldots)$$

Faltinsen predicts sloshing for tanks with certain filling factors, in this experiment suction buckets with open bottoms are studied. This can be the reason why sloshing is experienced at lower frequencies. The periods are more than 2.5% deviated from the deep water limit in the closed bucket case which was mentioned earlier.
If the test results are reliable, the fact that the bucket is open at the bottom must then have an influence on the sloshing period. The fact that the bottom is open during the experiments and water is allowed to flow in and out of the bucket can lead to a changing sloshing period. Energy can radiate outside the bucket instead of building up inside the bucket and initiate sloshing.
Only the first sloshing mode is observed, waves with multiple wavelengths inside the bucket were out of the studied frequency range. Simultaneously, higher order effects (e.i. harmonics) are decreasing in amplitude and therefore decrease in dominance in the overall effect.

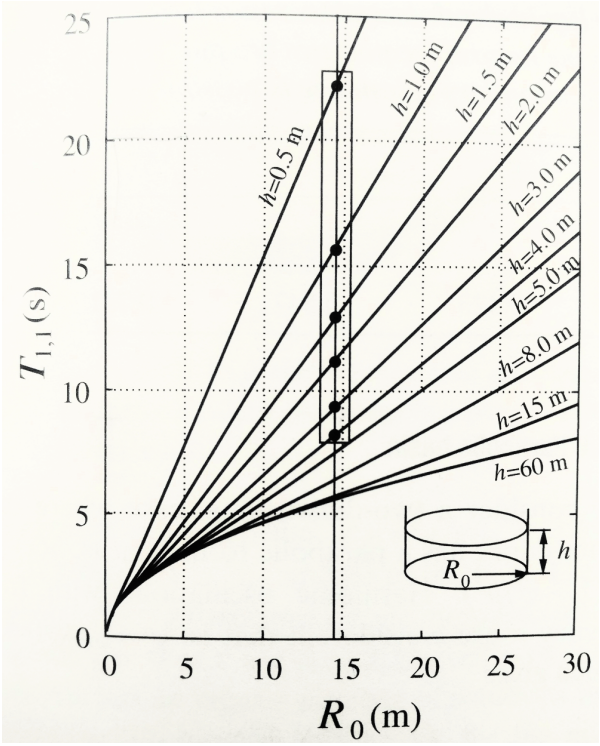

Figure 6.16: First excited modes inside a vertical cylinder of diameter R_0 and liquid depth h [14]

6.9. Influence of air vent on top of bucket

Assumed is that the air vent, which is present on the suction bucket, does not have any influence on the horizontal added mass of the buckets. It is very unlikely that this is also the case for the vertical direction, but this is discussed in the chapter Recommendations.
For the horizontal added mass experiments the buckets are 'closed' on top. Which means the bucket was made watertight, but then a very small hole, about 4[mm], was drilled through the top plate. This was done to be able to let air escape/flow in when the draft was changed. The hole is assumed to be small enough to not influence any hydro-mechanic effects during the experiments in surge direction.

6.10. Conclusions

6.10.1. Added Mass

Frequency

The dependency of the added mass related to the frequency turned out to be almost constant in the linear range. Draft 3, 4 and 5 ended up at a dimensionless added mass of 1.75[-] just before sloshing takes place. Draft 1 and 2 have no to insufficient volume of water to properly initiate sloshing inside the bucket. At sloshing frequency the added mass decreases rapidly with 25% to 50%.

Draft

The dependency of the added mass related to the draft turned out to have a powerfactor just above 1. As can be seen in the stacked dimensionless added mass figure 5.19, increasing draft results in increasing dimensionless added mass. Albeit that the drafts larger than half the bucket diameter go to a dimensionless added mass of 1.75[-]. The sloshing at draft 3 showed proportionally the biggest decrease in added mass and the biggest increase in damping. Mid draft is concluded to have the optimal relation of enclosed volume of water to initiate sloshing and enough volume of air inside the bucket for waves to break.

6.10.2. Damping

Frequency

The dependency of the test results related to the frequency turned out to be of great importance. In lower tested frequencies the determined damping was about constant for each draft. This indicates non-linear behavior, expected is that friction is dominant here because the friction force is independent on frequency.

Once a full scale frequency of 9[s] is reached the damping increases, this is still in the linear domain. When sloshing takes place at about 6[s] full scale, non-linearities are introduced. Sloshing increases the damping significantly, up to 150% from before sloshing, or even 300% compared to the 11[s] damping.

Draft

The dependency of the damping related to the draft turned out to be inverse related. Increasing draft turned out to have a less dimensional damping (see figure5.20). This indicates that most of the damping takes place at the surface near the water-air interface, this confirms the earlier hypothesis.

This also implies that viscous damping is the dominant damping factor in sloshing domain. The friction force is independent of the frequency, while the damping factor itself (B) is proportional to $\frac{1}{\omega}$.

6.10.3. Current Analysis method

Currently the suction buckets are modeled in Ansys AQWA with the water inside the bucket considered as 'trapped. According to the experiments the hollow cylinder model matches the test results more accurately. Despite the probable numerical errors in the diffraction solution, for example due to non-linear sloshing effects, this model gives an accurate representation of the real situation. Advised is to use the hollow cylinder model in Ansys AQWA for future SBJ (or monopile) installation projects.

6.10.4. General remarks

The found relations for added mass and damping give insight in the to be expected reaction forces of a suction bucket going through the splash-zone. Damping is increasing when sloshing starts, at this moment the added mass decreases simultaneously. At this moment the energy dissipation is increasing. For the case of the installation of a suction bucket jacket this is a favorable event, this means energy is taken out of the system instead of stored in the eigen-modes of the structure, hence reducing the amplitudes of the system.
The curerct AQWA model consisting of a hollow cylinder predicts the added mass term well, while the damping is underestimated in the sloshing domain. This is underestimated because AQWA does not include viscous effects, while as stated earlier this is the dominant effect when sloshing occurs. Sloshing creates a significant increase in the damping.
Because the damping is underestimated the current approach by Boskalis turned out to be a conservative approach, while the added mass (and hence the eigen-frequencies) of the system are predicted accurately.

RAO and resonance

It is hard to say if the decrease in added mass is favorable, this can change for each situation. The combination of a certain excitation frequency spectrum (for example a Pierson-Moskowitz or a JONSWAP spectrum) and the Response Amplitude operator (RAO) determine the final excitations of the complete system. The RAO is what determines what the dynamic response of the system is due to incoming waves. This RAO usually has a certain resonance peak at a certain resonance frequency. Depending on the frequency of this resonance peak and the excitation frequency on the system it can be beneficial to decrease the added mass and increasing the eigen-frequency to stay away from this resonance peak. This can be done in the low frequency limit where the RAO usually is one, or in the high frequency limit where the RAO tends to go to zero.
For now, in the general case without any RAO or excitation spectrum definitions, it is impossible to tell if a change in added mass will be favorable, or maybe even make the response even worse. What can be concluded is that additional damping will have a positive effect (as long as no equipment is damaged) on the behavior of the system due to incoming waves near the RAO resonance peak. This because damping *always* takes energy out of the system and reducing the dynamics.

6.11. Reflection

In this section is reflected on the way of working, the methodology used and other choices that have been made during the thesis. In hindsight with the gained knowledge during the research, were choices made the right ones, or were there better alternatives possible? Why are they better than the applied theories or choices made?

6.11.1. Actuator and its frequency regulator

For future research it is good to determine the actual frequency output or find a more reliable, calibrated, frequency regulator. In case this is not available, check (post process) the output frequency while doing the experiments to make sure the controlled input variable gives the right values which were aimed for initially.

6.11.2. Railing system

To reduce possible friction in the trolley cars on the rails, use a single rail piece. Now two pieces are used, each trolley had its own rails. Practical imperfections due to lack of skills/inaccurate work can cause misalignment, which in the end might introduce extra (non-linear) friction. This can (in theory) be compensated for, see chapter *Recommendations* for details. This is not done in this thesis.

6.11.3. Closed bucket

Extra experiments could have been done to check if there is an influence of a lid at the bottom of the bucket. Does this restriction of water flowing in and out of the bucket have influence on the found damping and the added mass?
This can be studied by doing the exact same experiments all over again, but this time with a closing lid at the bottom. Of course the water inside the bucket should match with the SWL outside the bucket.
By doing these experiments the results can be compared with the case the bucket is open at the bottom. If the inertia results match the inertia results of the open bucket, it can be thought of that the idea of a water flow underneath the bucket that flows slightly inside the bucket and is reducing the amount of 'trapped' water is actually absent.
This can only be compared to the non-dimensional added mass. The found added mass is then divided by the mass of the 'enclosed' volume inside the bucket. If the found added mass is the same for open and closed cases nothing can be concluded on water flows around/inside the bottom of the bucket.
Currently an Ansys AQWA model is present to determine the added mass and damping from the potential theory, these results differ significantly from the hollow cylinder, added mass is roughly one third of the hollow cylinder model. Experiments can distinguish if this will also be the case in reality.
This is definitely a recommendation for future research. (see *Recommendations*)

6.11.4. Sloshing

Extra experiments could have been done around the moment sloshing takes place. The studied wave period interval is wide (1[s]), this is not accurate enough to study the exact moment sloshing starts to occur. For the open bottom the results matches the predicted sloshing periods by Faltinsen for closed buckets. Because of the relative big interval periods all drafts seemed to experience roughly the same sloshing period of about 5[s]. In theory there will be a deviation from this for different drafts.

7

Recommendations

In this chapter the choices that were made are re-evaluated and that in hindsight maybe might be reviewed for other choices or methods. After doing the experiments and the corresponding studies, what are interesting topics to dig into even further. What doors were opened to new research fields with the gained knowledge during the thesis.

7.1. Horizontal versus Vertical added mass

It is recommended to study vertical loads as well. Vertical loads can during installation become more critical than horizontal loads. Vertical loads can result in slam loads at the ceiling of the buckets Which in their turn can result in snap loads in the crane wires, this could ultimately result in a damage to the crane itself [20].
Vertical added mass (e.i. slam loads) are highly correlated to the vent present at the top of the suction bucket. The diameter of the vent determines the (maximum) air flow, which determines the air pressure built up inside the bucket [25] [30] . This dynamic pressure can compress the effect of slam loads, this effect is known as the '*Air cushioning effect*'.
Besides an additional dynamic air pressure inside the buckets it is also possible when a wave trough is passing the bucket an under pressure is created inside the bucket. Air is then sucked through the vent inside the bucket, but more importantly, the crane does then experience an *additional* weight in its hook. It can become dangerous when this effect is not accounted for.
Of course the horizontal added mass and the vertical added mass are not necessarily uncoupled, so additionally there is room for investigation of both coupled effects as well (in all DOF).

7.2. Degrees of Freedom

No coupling between surge motion and any other direction is assumed in the entire thesis. In practice this might not be the case. Motions in any directions might influence the motion in any other direction, dissipating energy, or more important, could accumulate energy in a certain state.
Imagine: If a forced motion in direction A is applied and its reaction force is measured. Assume now that motion A is coupled with motion B. If for any reason, the forces excitation in motion A coincides with the eigen-mode of direction B, motion B will be excited the most. While the overall response, with the aim of retracing the motion of A, is measured. This can cause inaccuracies in the researched motion of A.

7.3. Bucket interactions

Responses of different buckets could interact with each other. This is dependent on the orientation of the buckets with respect to the incoming waves.

Excitation phases

A special case that deserves more investigation is the situation where the incoming wave excites different buckets (vertically) in anti-phase. This will lead to large pitching moment of the suction bucket jacket, which again will lead to side- or off-lead forces in the crane, reducing the workability of the crane vessel or jack-up.

Footprint SBJ

The distance between the legs (and thus the suction buckets) can play a role on the added mass. When the SBJ has a small footprint the suction buckets are closer to each other. The volume between separate buckets can (for longer waves) also become a spot where added mass effects could be experienced. As a result, the amount of added mass, not only inside the buckets but also between separate buckets, can increase significantly.

7.4. Mechanical friction

The mechanical friction is measured as a check to see if there is any exceptional friction present. This information can be further analyzed, although it is not chosen to do in this thesis. The approach to use this information is as follows. The (dynamic) friction component can be described as;

$$\vec{F}_{friction} = -\mu_{kinetic} \cdot F_{normal} \cdot \frac{\vec{v}}{|\vec{v}|}$$

This friction force in the equation of motion (equation 4.6) appears at the damping term B.

$$F_{damping} = B \cdot v = \mu_{kinetic} \cdot F_{normal} = F_{friction}$$

Where the friction component in the equation of motion can be put to the force side of the equation. This way the mechanical damping (friction) can be removed from the time domain measured force. This is shown in equation 4.30. This will slightly improve the accuracy of the studied properties Added mass and Damping *due to hydrodynamic effects*.

7.5. Closed bucket

To study the water flow behavior at the bottom of the bucket extra test can be done. By doing the same test over again, but this time with a closing lid at the bottom of the bucket. The results then can be compared to the open bucket results. It is important that the water inside the closed bucket is identical to the SWL outside the bucket.
When the results for added mass are the same as for the open bucket case, the idea of considering all the water inside the bucket trapped might be correct. The theory of a water flow inside the cavity of the bucket reducing the amount of trapped water can then possibly be rejected.
While this is a way of studying the amount of trapped water inside the bucket, this does not necessarily provide extra information about damping. Vortex shedding about the bucket draft might slightly reduce due to the closing lid (no sharp edges inside the bucket are present anymore), but shear friction along the lid introduces a small amount of extra friction. It is therefore hard to tell what in the changed experienced damping originated for the reduction of vortices's and what originated in the increase of shear friction.

7.6. Increasing the accuracy of the experiments

The accuracy of the experiments can possibly be increased by several points. All of them have a trade off whether it is worth the extra effort and/or money. Several possible points of interest are mentioned below.

• Increased resolution
Decrease the frequency step in which the experiments are done, now steps of 1[s] full scale are done. Especially the sloshing range could use more tests around the period when sloshing starts to occur.
• Change to more accurate transducers
This will be more expensive, but they will provide a more sensitive dataset.
• Re-design test set-up
For example using a larger model in a larger and deeper tank. Redesign the frame where the bucket, all sensors and the actuator are attached to. Make this frame even stiffer to suppress possible vibrations. A deeper tank will reduce bottom influences, for most frequencies the tank is assumed deep, but for a few frequencies it was in intermediate region (although still near deep water limit ($n \approx 0.6$)). A deeper tank will take away any possible bottom interactions
• More careful test execution
For instance even longer waiting periods between runs, let waves damp out even further even when not visible anymore. Also improve the wave dampers at the end of the tank.
• Repeated measurements
Accuracy increases with $\sqrt{N}$, now three test series are done (N=3). When more test series are done the accuracy increases.
• Improve calibration procedures
More careful calibration, include more of the test set-up in the calibration and not only the sensor itself. Study non-linear calibration relations as well.

7.6.1. Viscous and friction damping

The load-cell signal can be decomposed by using Fourier series, some examples are shown in figure 6.1. Viscous effects add an extra contribution to the 3ω frequency in the frequency spectrum. While the friction show a contribution to all odd harmonics (see figure 6.1). By analyzing the amplitudes of all contributions and compare them to the Fourier series, the contribution of each factor, viscous and friction, can be determined.
From this can be determined which non-linear damping is dominant after the wave radiation damping.

Over all, this research can be taken as a first iterative step. Future studies could incorporate vertical added mass/slam-loads and air cushioning effects. Sloshing can be an interesting topic to study in more depth since it does align with the periods suggested for closed buckets by Faltinsen [14], but the period interval was too course to exactly determine at what period sloshing took place for each draft. Therefore all drafts experienced sloshing at the same frequency, no draft dependence could be studied. Faltinsen predict that for closed cylinders there is a liquid level (draft) dependency regarding the sloshing period.

A

Appendix

A.1. Drawings test-set-up

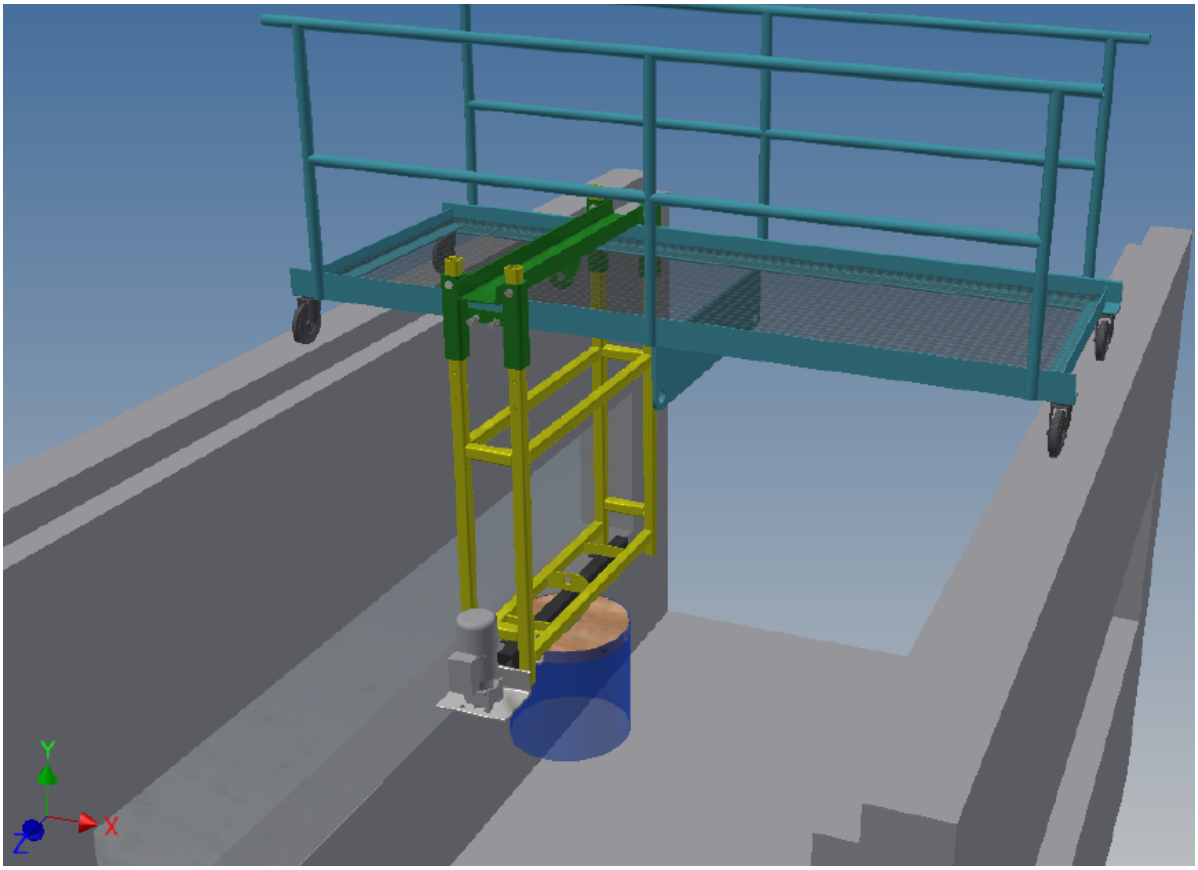

Figure A.1: Bridge with set-up attached

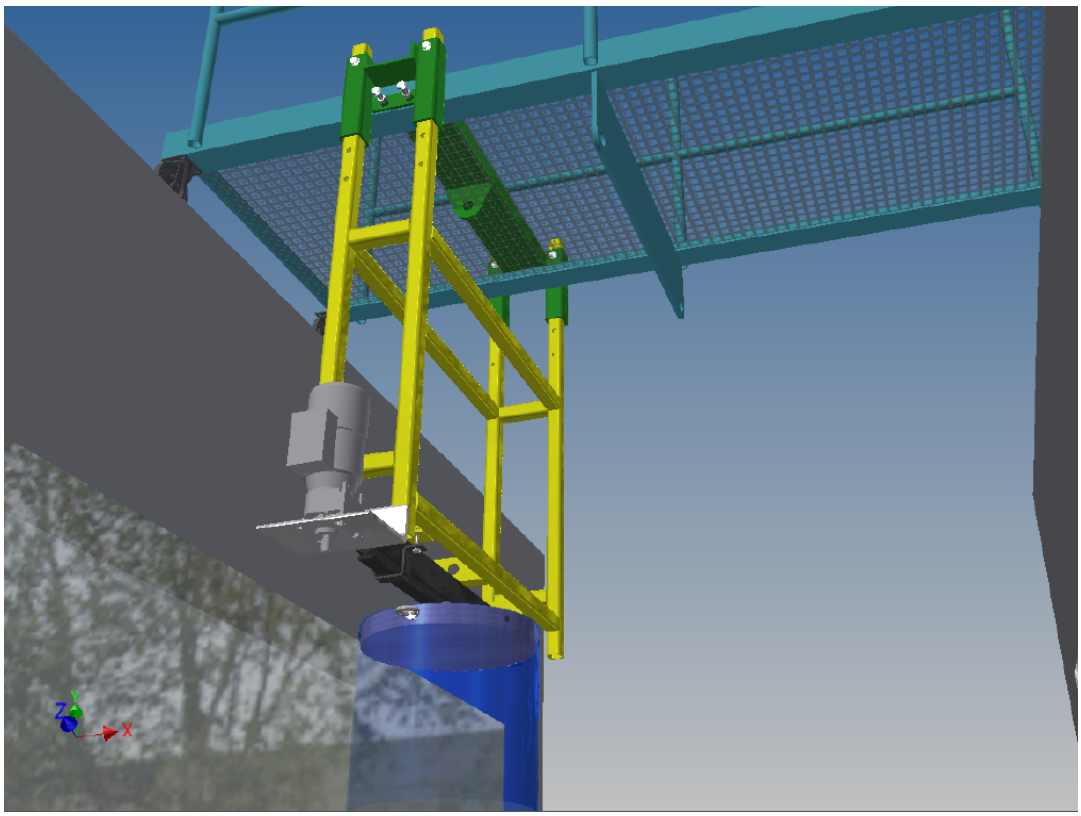

Figure A.2: Bridge with set-up attached

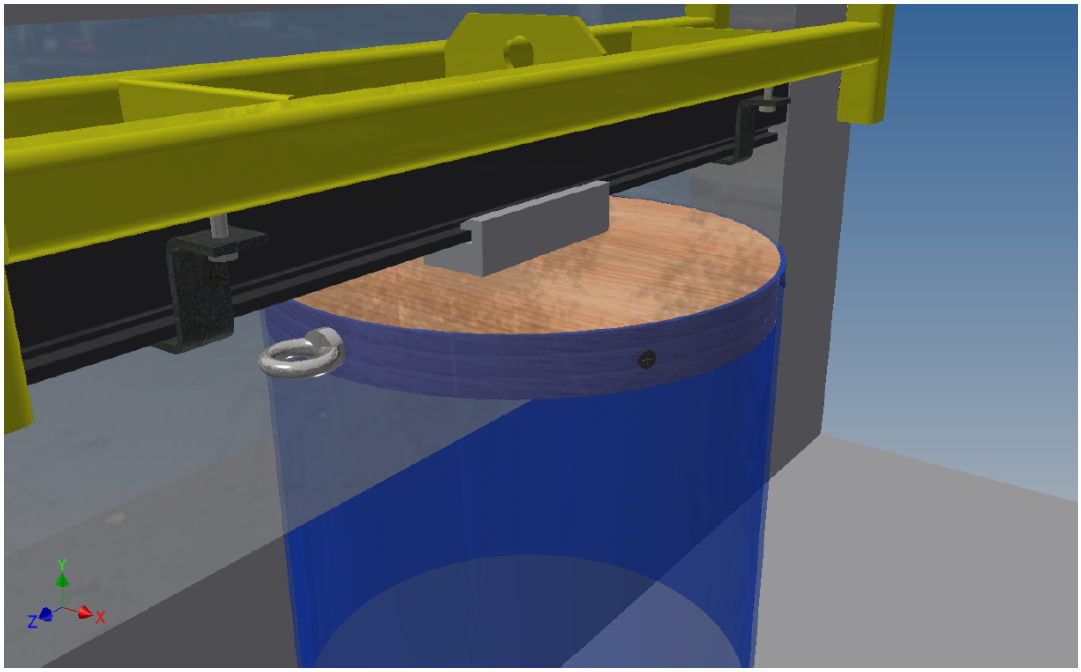

Figure A.3: Bridge with set-up attached

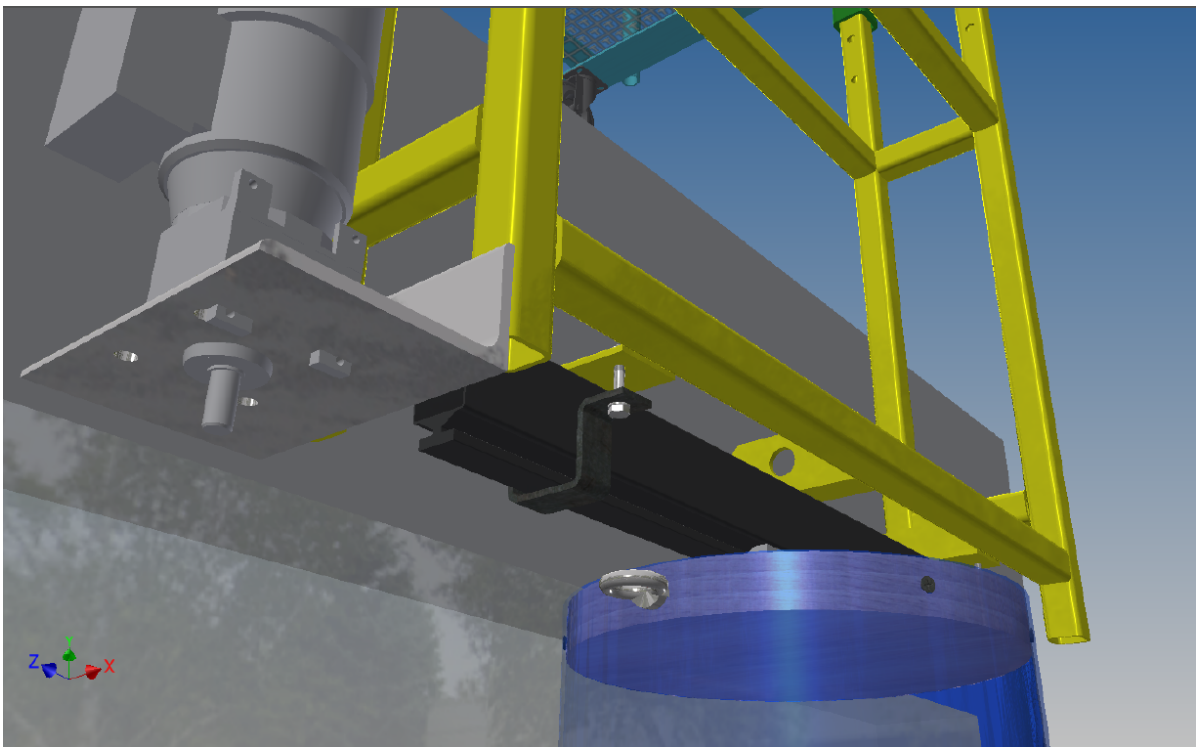

Figure A.4: Bridge with set-up attached, close-up on guiding system.

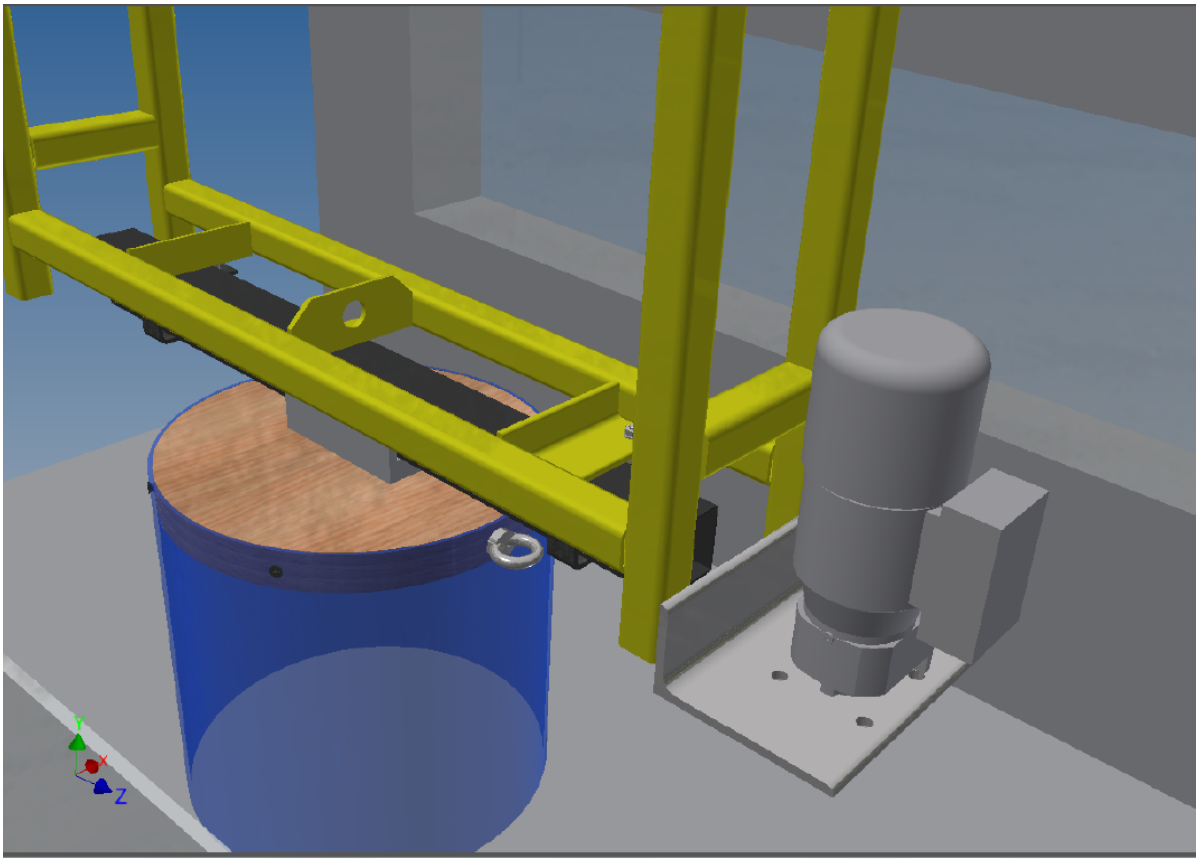

Figure A.5: Bridge with set-up attached

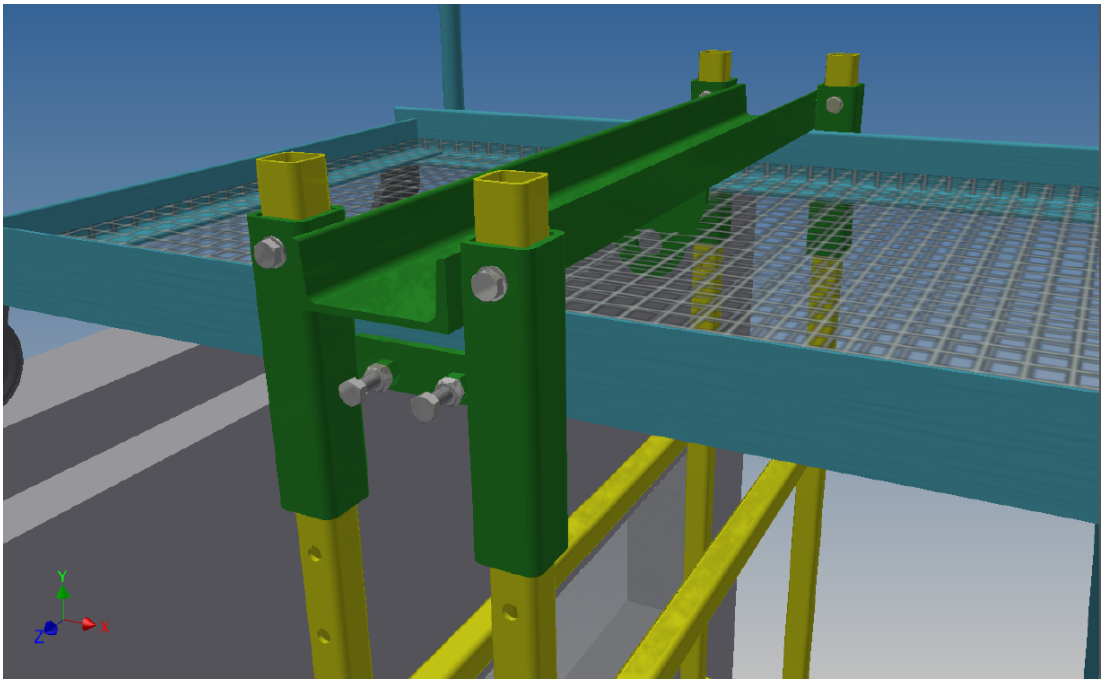

Figure A.6: Bridge with set-up attached

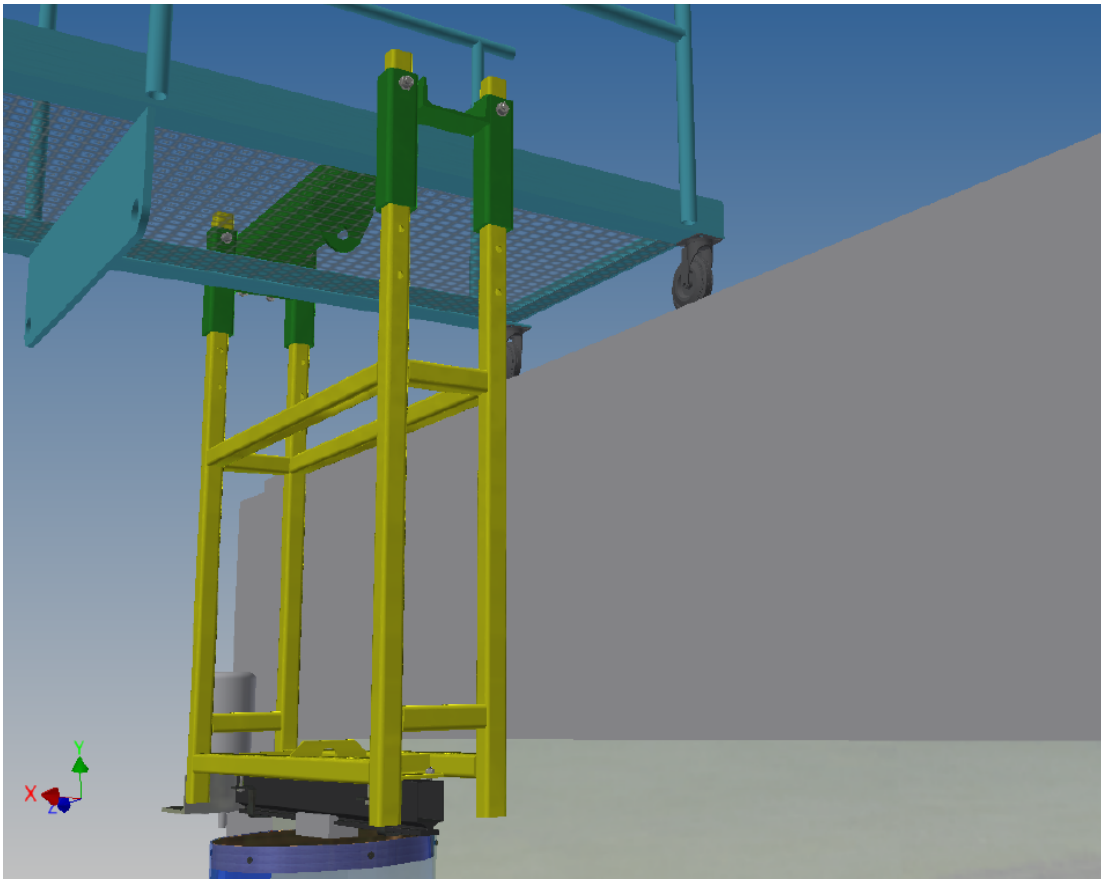

Figure A.7: Bridge with set-up attached

Figure A.8: The actual frame set-up, filling of the tank

A.2. Welding & Assembly drawings

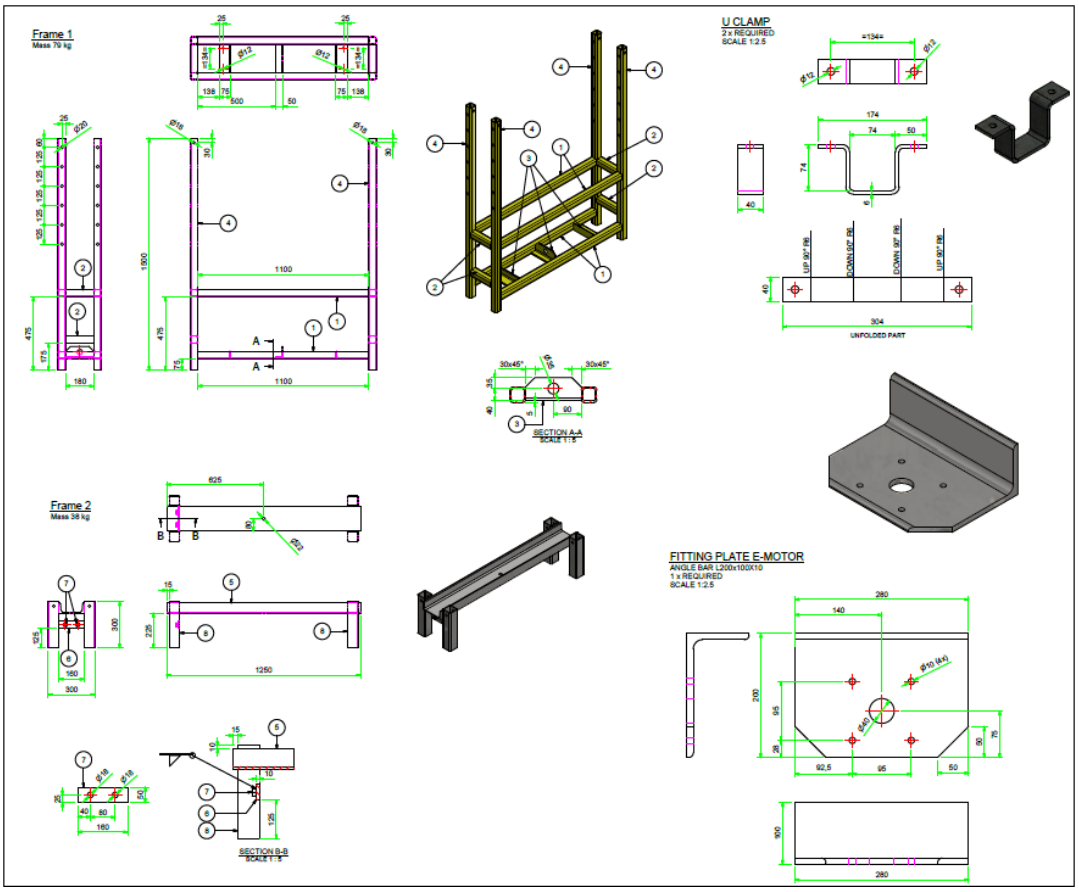

Figure A.9: Welding plan test frame.

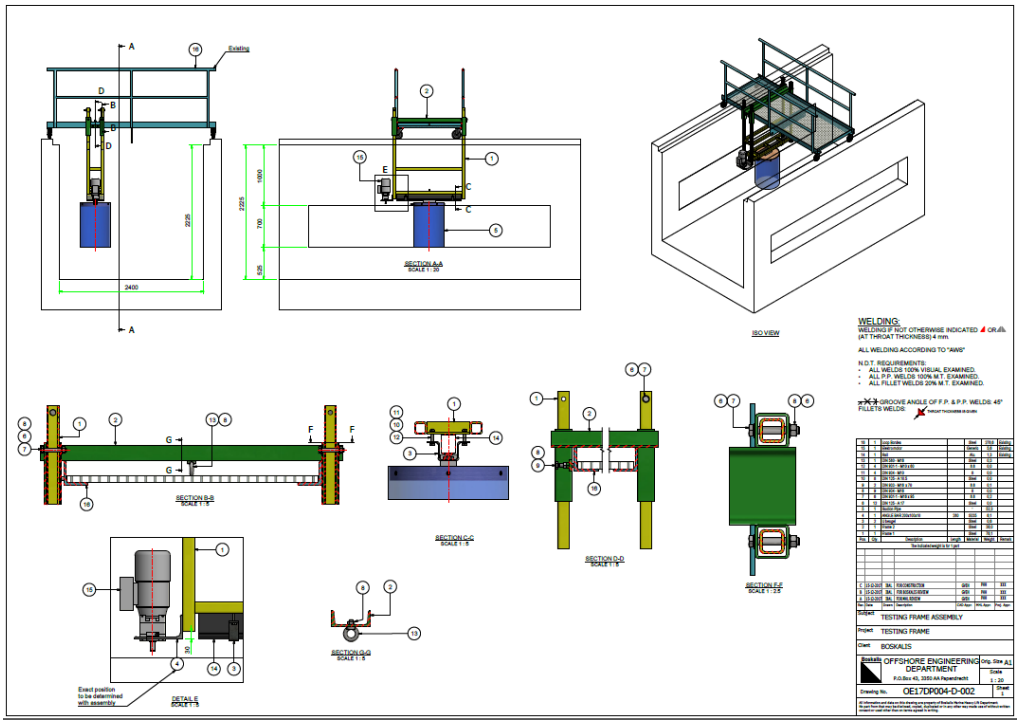

Figure A.10: Assembly scheme test frame.

Experiment Checklist

Task	Check
Calibrate **Displacement sensor** (BTL sensor)	
Calibrate **Load-cell**	
Check logging **Accelerometers**	
Calibrate **Frequency regulator**	
Measure water temperature	
Data logging works correct, universal time	
Install Gopro	
Free movement of bucket	
Rails lubricated	

Test Matrix and Settings set-up

Series	Configuration	Frequency [Hz]							
Real size [s]	**.**	**11**	**10**	**9**	**8**	**7**	**6**	**5**	**4**
D_1	Draft= 0	0.41	0.45	0.50	0.56	0.64	0.75	0.89	1.12
D_2	Draft= $\phi/4$	0.41	0.45	0.50	0.56	0.64	0.75	0.89	1.12
D_3	Draft= $\phi/2$	0.41	0.45	0.50	0.56	0.64	0.75	0.89	1.12
D_4	Draft= $3\phi/4$	0.41	0.45	0.50	0.56	0.64	0.75	0.89	1.12
D_5	Draft= ϕ	0.41	0.45	0.50	0.56	0.64	0.75	0.89	1.12

Series	Configuration	Periods[s]							
Real size [s]	.	**11**	**10**	**9**	**8**	**7**	**6**	**5**	**4**
D_1	Draft= 0	2.46	2.24	2.01	1.79	1.57	1.34	1.12	0.89
D_2	Draft= $\phi/4$	2.46	2.24	2.01	1.79	1.57	1.34	1.12	0.89
D_3	Draft= $\phi/2$	2.46	2.24	2.01	1.79	1.57	1.34	1.12	0.89
D_4	Draft= $3\phi/4$	2.46	2.24	2.01	1.79	1.57	1.34	1.12	0.89
D_5	Draft= ϕ	2.46	2.24	2.01	1.79	1.57	1.34	1.12	0.89

Frame and water properties

Topic		
Temperature water		$6C°$
Natural frequency (Hammer test)	Draft=0	0.10sec
Natural frequency (Hammer test)	Draft= $\phi/4$	0.12sec
Natural frequency (Hammer test)	Draft= $\phi/2$	0.12sec
Natural frequency (Hammer test)	Draft= $3\phi/4$	0.12sec
Natural frequency (Hammer test)	Draft= ϕ	0.12sec
Natural frequency (Hammer test)	Draft= $5\phi/4$	0.14sec

Initial and actual voltages frequency regulator

Initial Voltage	f1	f2	f3	f4	f5	f6	f7	f8
D1	3.400	4.277	5.154	6.031	6.909	7.786	8.663	9.540
D2	3.417	4.291	5.166	6.146	7.125	8.105	9.034	9.540
D3	3.433	4.305	5.292	6.279	7.267	8.254	9.241	9.540
D4	3.450	4.320	5.315	6.309	7.303	8.298	9.292	9.540
D5	3.466	4.334	5.345	6.356	7.367	8.378	9.389	9.540
Actual Voltage	**f1**	**f2**	**f3**	**f4**	**f5**	**f6**	**f7**	**f8**
D1	3.422	4.293	5.165	6.031	6.899	7.767	8.662	9.541
D2	3.422	4.292	5.165	6.161	7.115	8.112	9.063	9.581
D3	3.423	4.292	5.292	6.289	7.286	8.241	9.268	9.569
D4	3.423	4.295	5.334	6.288	7.286	8.281	9.271	9.579
D5	3.425	4.294	5.334	6.333	7.373	8.368	9.403	9.579

B

Fitted data

Fit Displacement x(t), Draft 1, serie 1

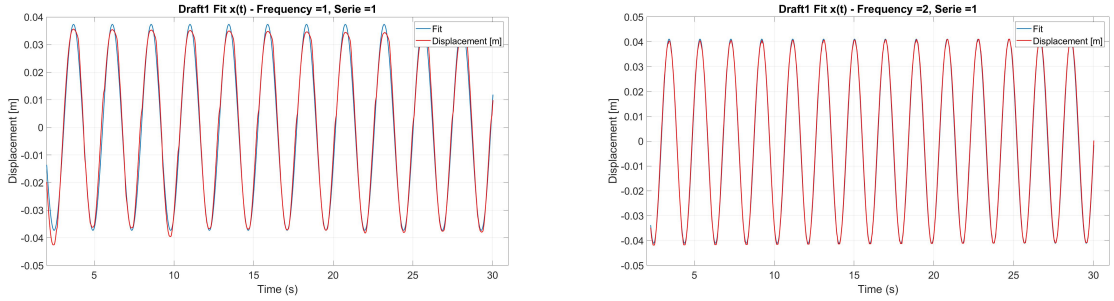

Figure B.1: Fitted displacement Draft 1, frequency 1 and frequency 3.

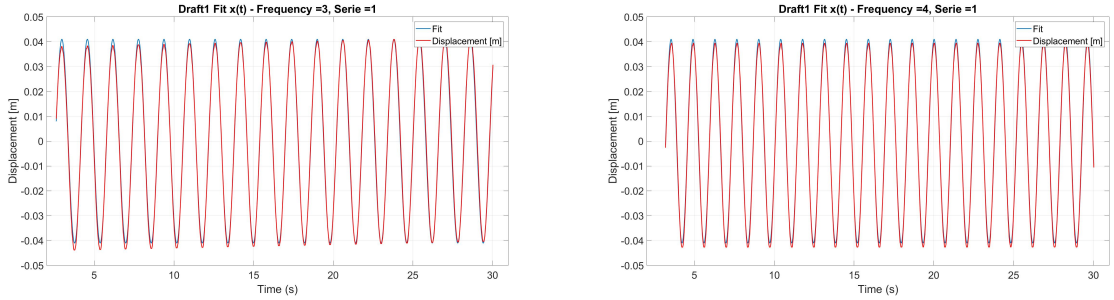

Figure B.2: Fitted displacement Draft 1, frequency 3 and frequency 4.

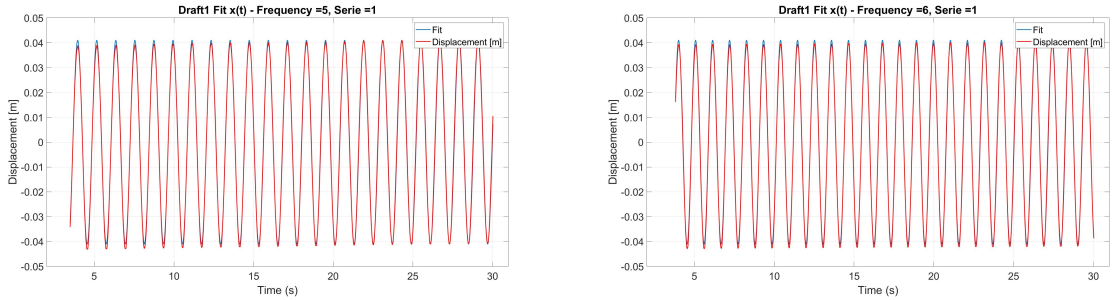

Figure B.3: Fitted displacement Draft 1, frequency 5 and frequency 6.

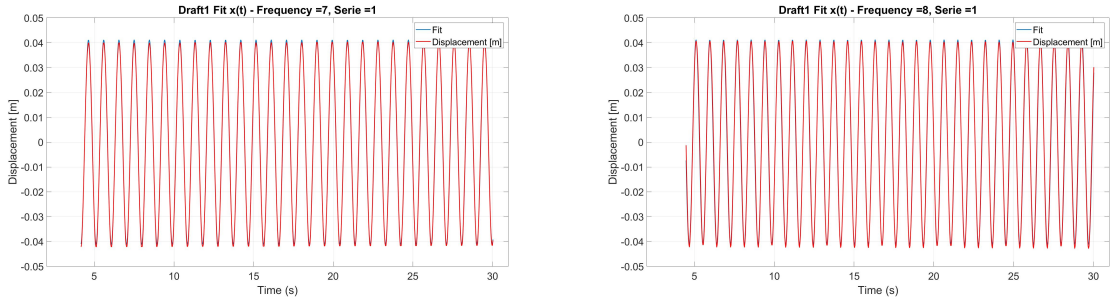

Figure B.4: Fitted displacement Draft 1, frequency 7 and frequency 8.

Fit Displacement x(t), Draft 3, serie 1

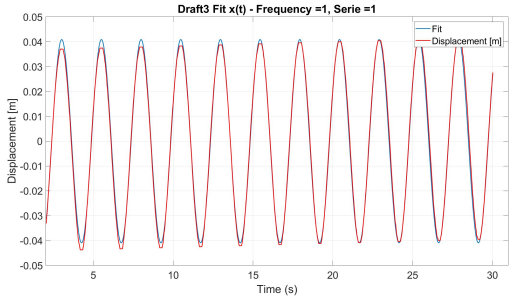

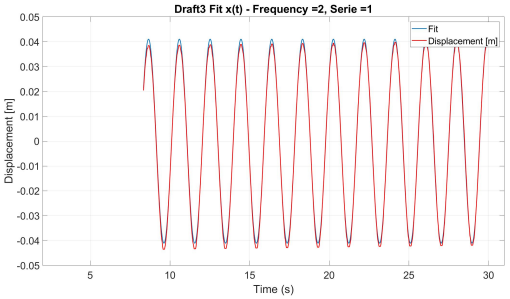

Figure B.5: Fitted displacement Draft 3, frequency 1 and frequency 2.

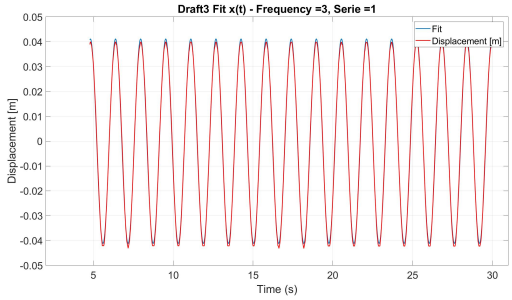

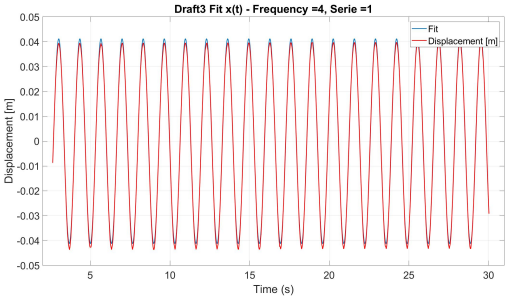

Figure B.6: Fitted displacement Draft 3, frequency 3 and frequency 4.

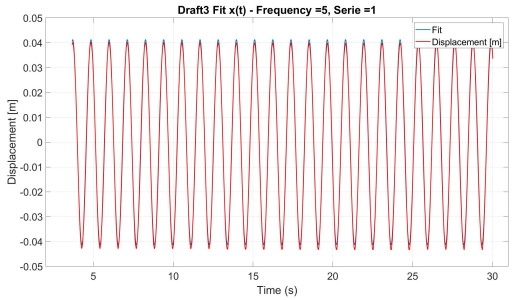

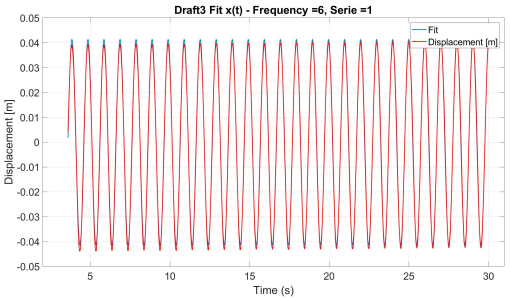

Figure B.7: Fitted displacement Draft 3, frequency 5 and frequency 6.

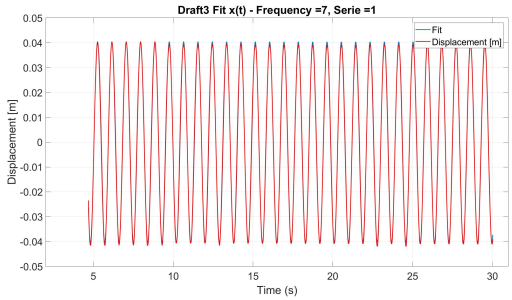

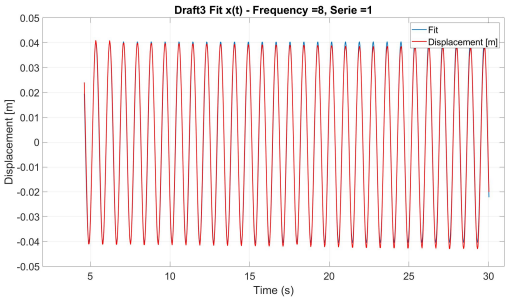

Figure B.8: Fitted displacement Draft 3, frequency 7 and frequency 8.

Fit Displacement x(t), Draft 5, serie 1

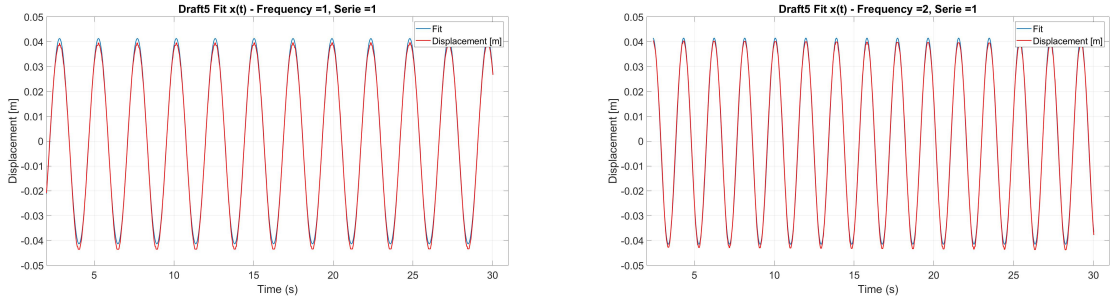

Figure B.9: Fitted displacement Draft 5, frequency 1 and frequency 2.

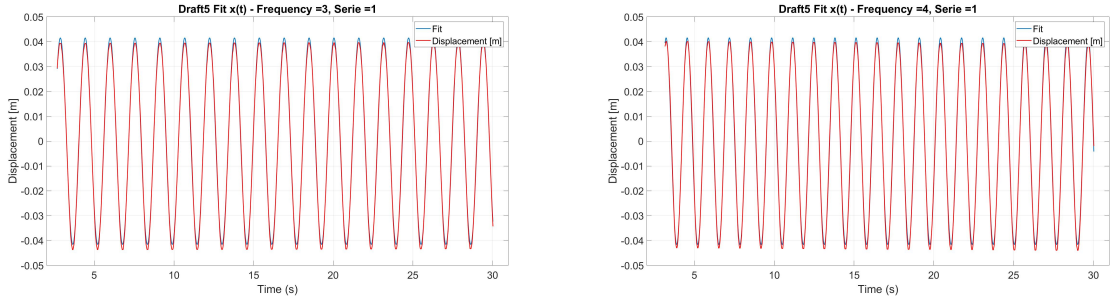

Figure B.10: Fitted displacement Draft 5, frequency 3 and frequency 4.

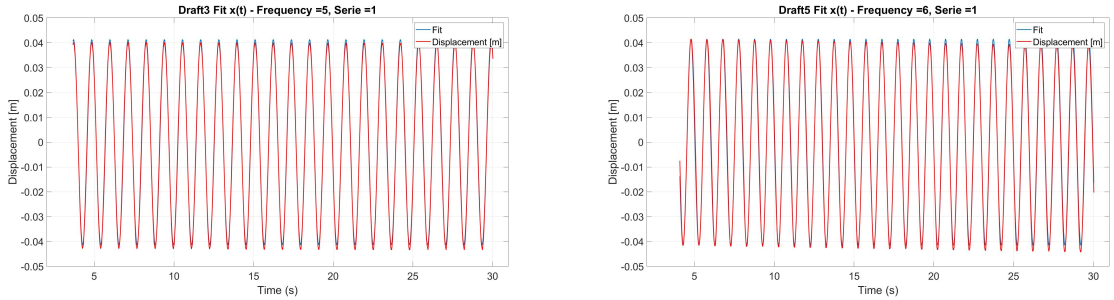

Figure B.11: Fitted displacement Draft 5, frequency 5 and frequency 6.

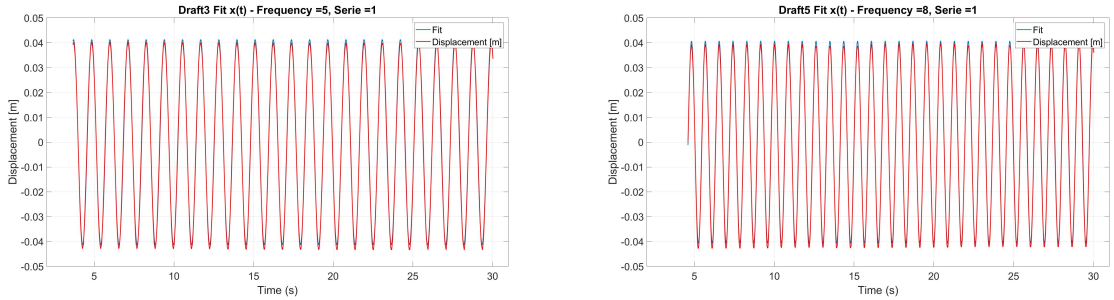

Figure B.12: Fitted displacement Draft 5, frequency 7 and frequency 8.

Fit Force F(t), Draft 1, serie 1

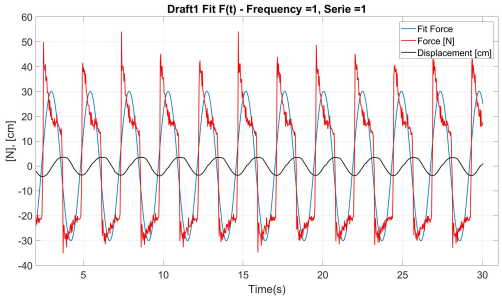

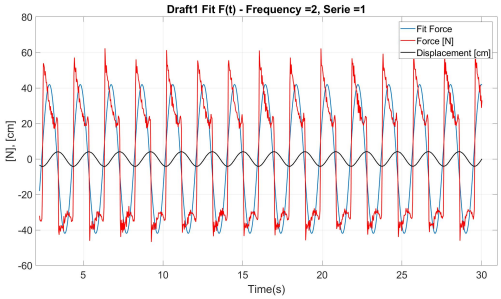

Figure B.13: Fitted force Draft 1, frequency 1 and frequency 2.

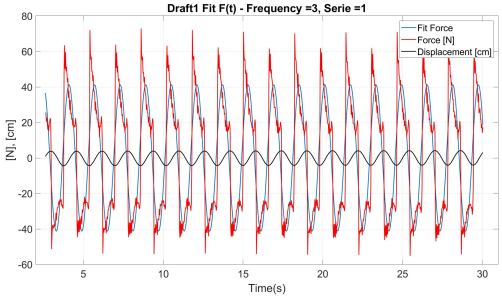

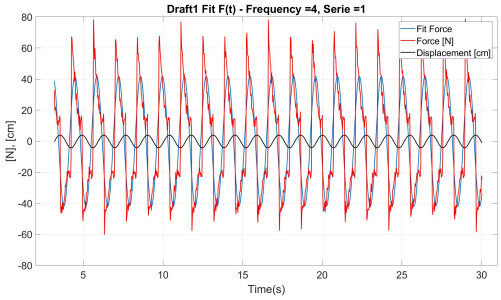

Figure B.14: Fitted force Draft 1, frequency 3 and frequency 4.

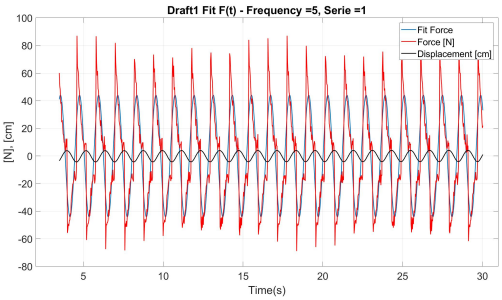

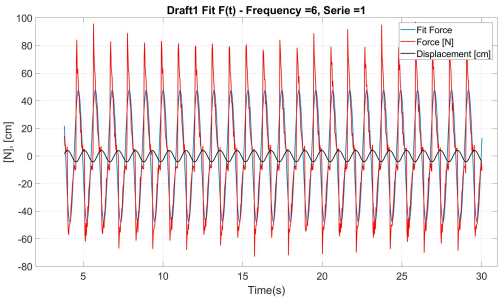

Figure B.15: Fitted force Draft 1, frequency 5 and frequency 6.

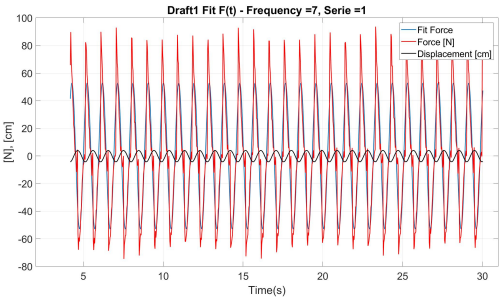

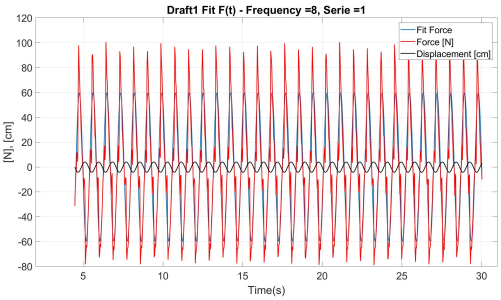

Figure B.16: Fitted force Draft 1, frequency 7 and frequency 8.

Fit Force F(t), Draft 3, serie 1

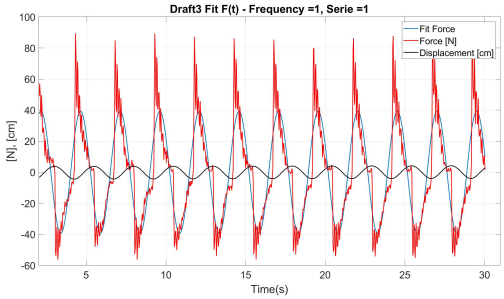

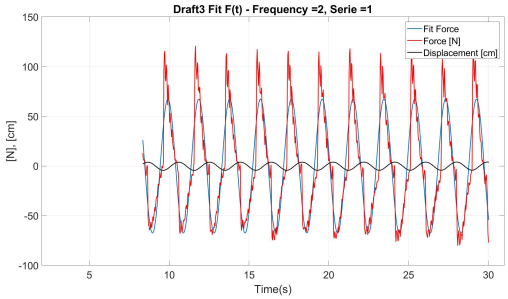

Figure B.17: Fitted force Draft 3, frequency 1 and frequency 2.

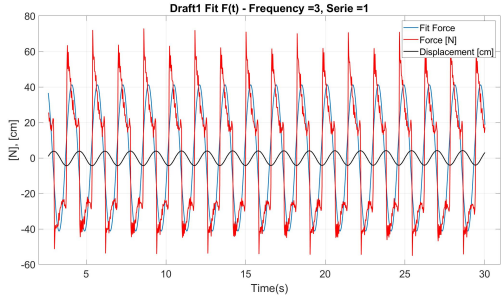

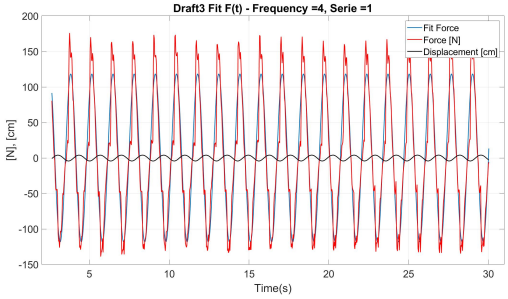

Figure B.18: Fitted force Draft 3, frequency 3 and frequency 4.

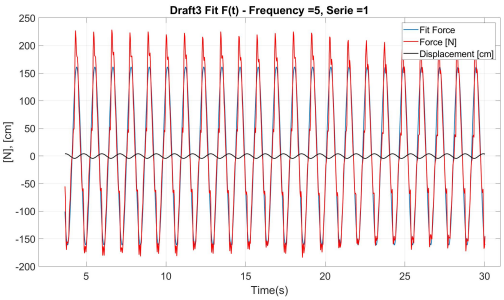

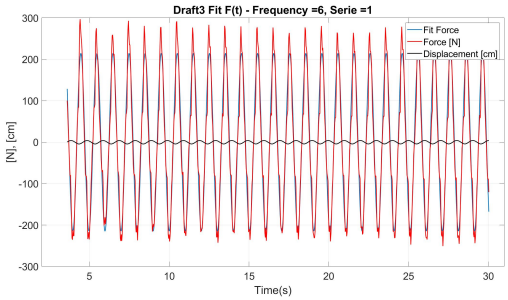

Figure B.19: Fitted force Draft 3, frequency 5 and frequency 6.

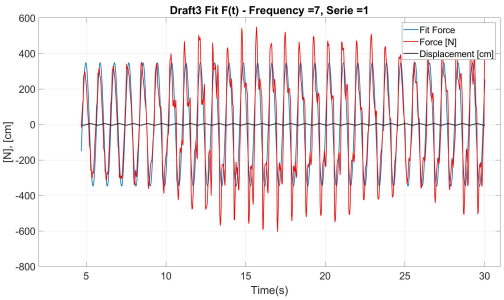

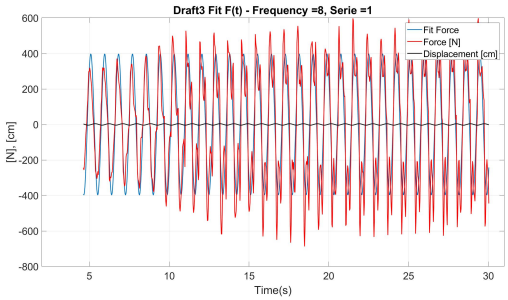

Figure B.20: Fitted force Draft 3, frequency 7 and frequency 8.

Fit Force F(t), Draft 5, serie 1

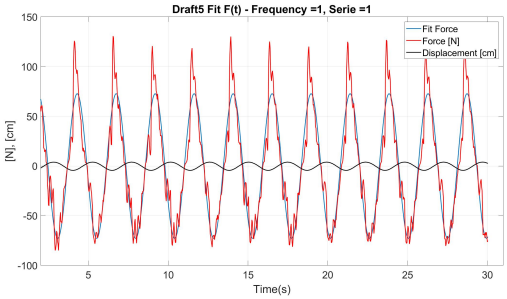

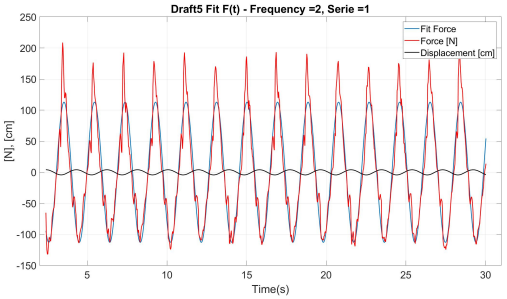

Figure B.21: Fitted force Draft 5, frequency 1 and frequency 2.

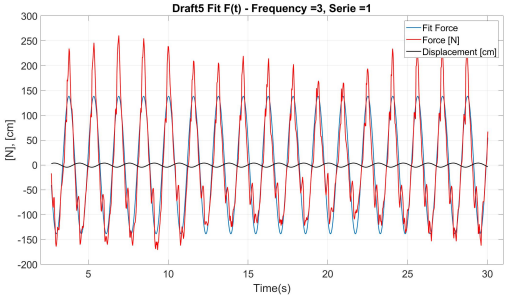

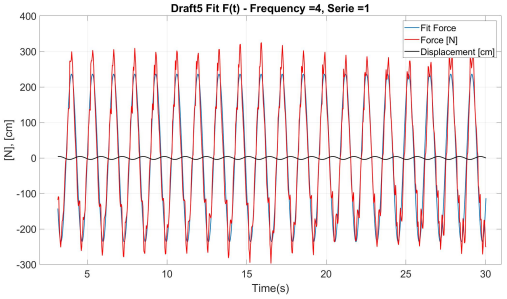

Figure B.22: Fitted force Draft 5, frequency 3 and frequency 4.

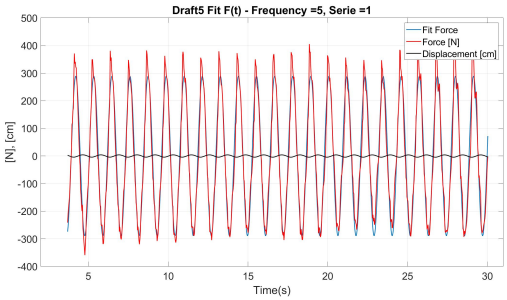

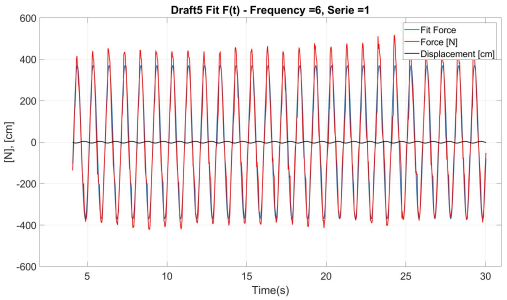

Figure B.23: Fitted force Draft 5, frequency 5 and frequency 6.

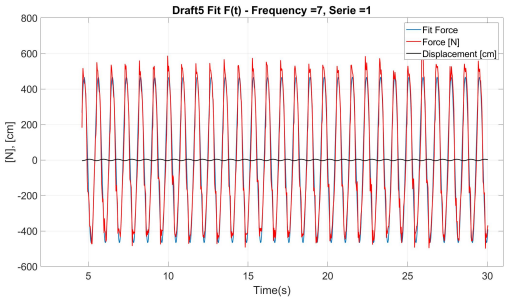

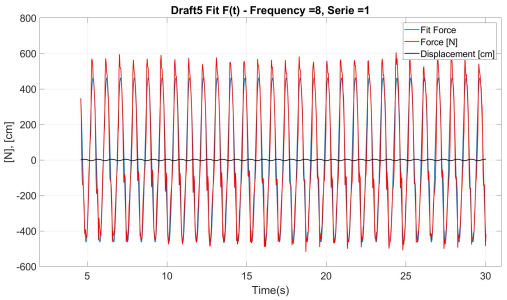

Figure B.24: Fitted force Draft 5, frequency 7 and frequency 8.

C

Appendix

Friction test

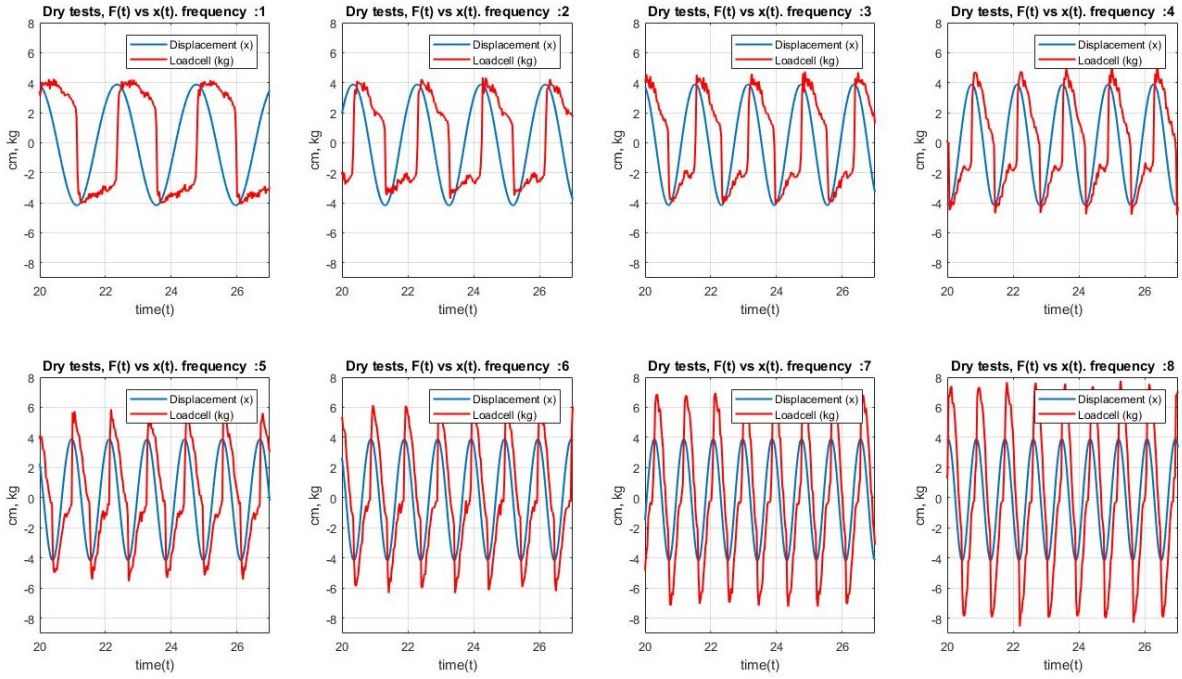

Figure C.1: Dry tests, Force [N] and displacement [cm] versus time

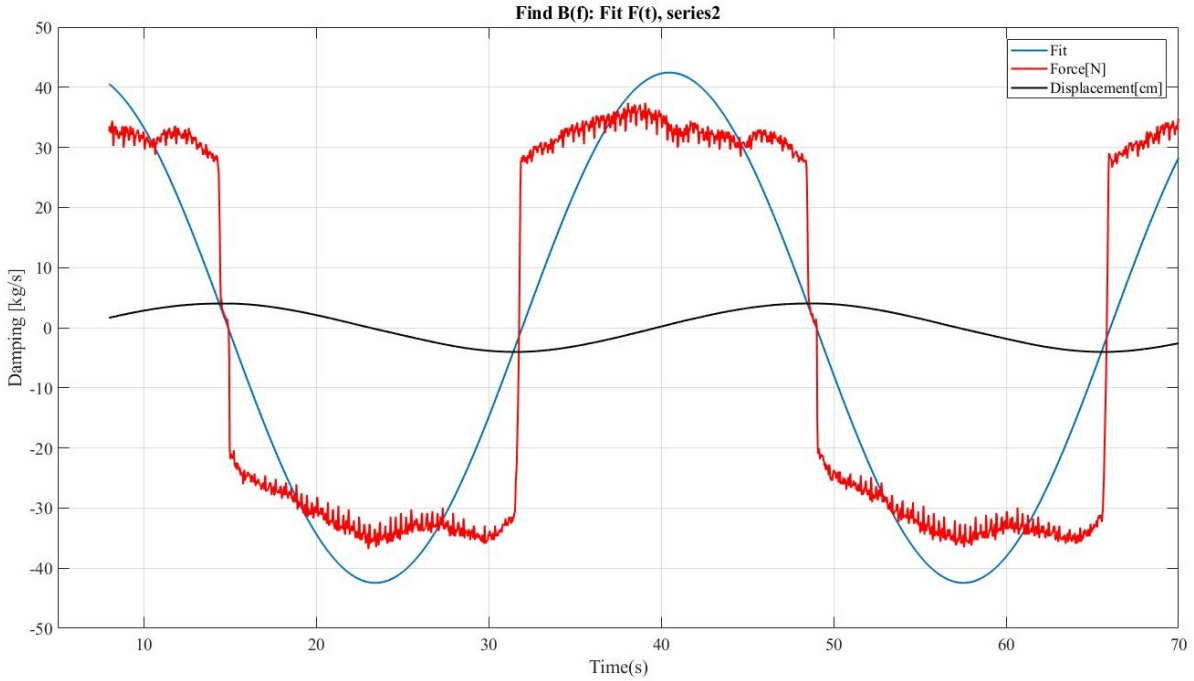

Figure C.2: Slowest possible dry test, just out of stick-slip region, test 1.

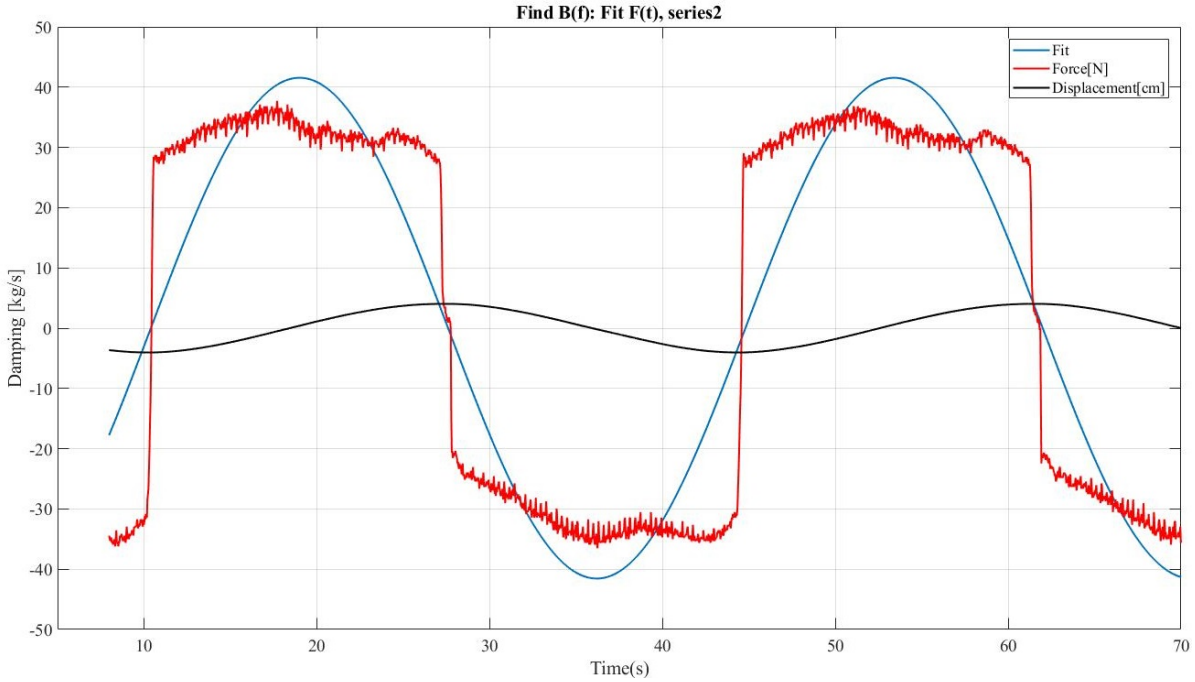

Figure C.3: Slowest possible dry test, just out of stick-slip region, test 2.

C.1. Hammer test

Each hammer test is executed three times and final results are compared

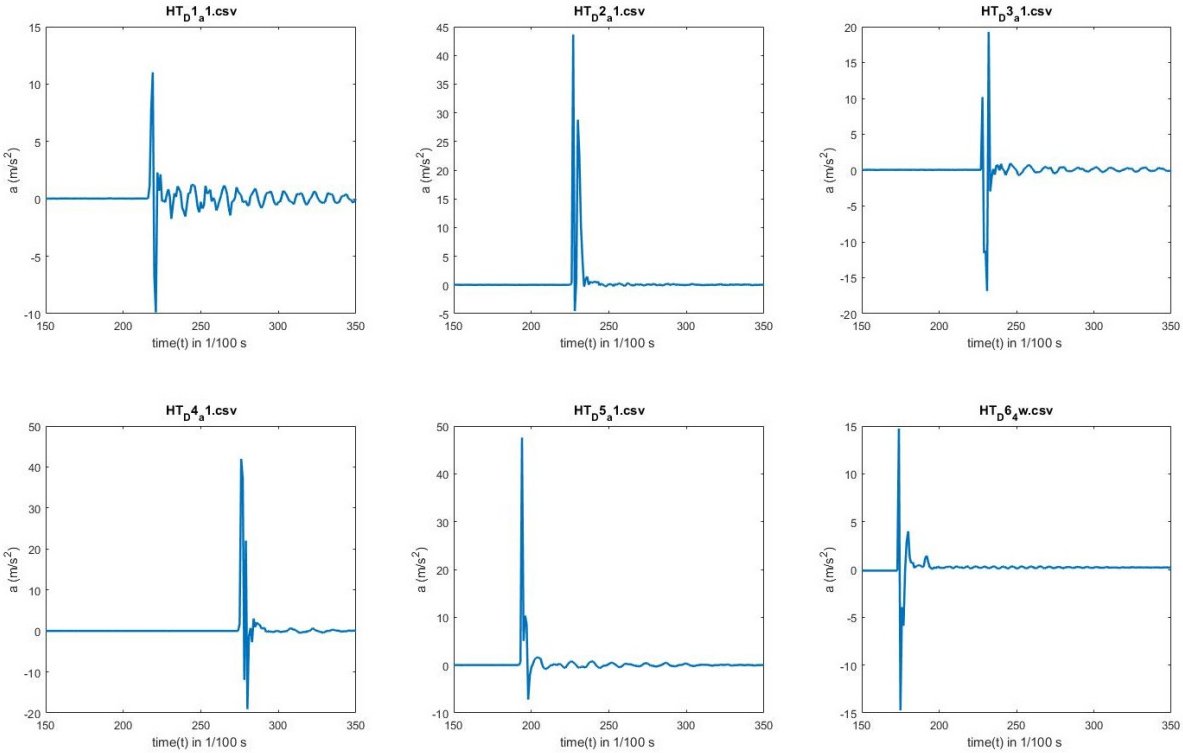

Figure C.4: Hammer test serie 1, Force in time domain.

FFT Hammer test for draft 1-6

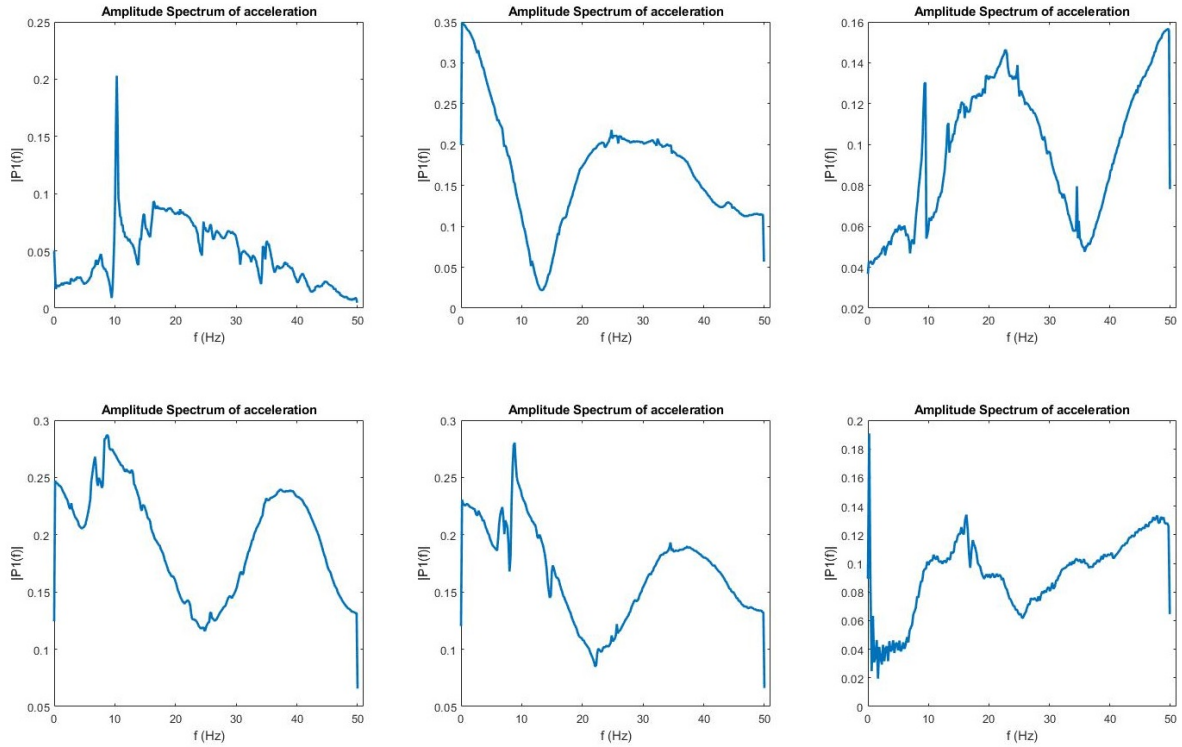

Figure C.5: Hammer test serie 1, frequency domain 0-50 [Hz]

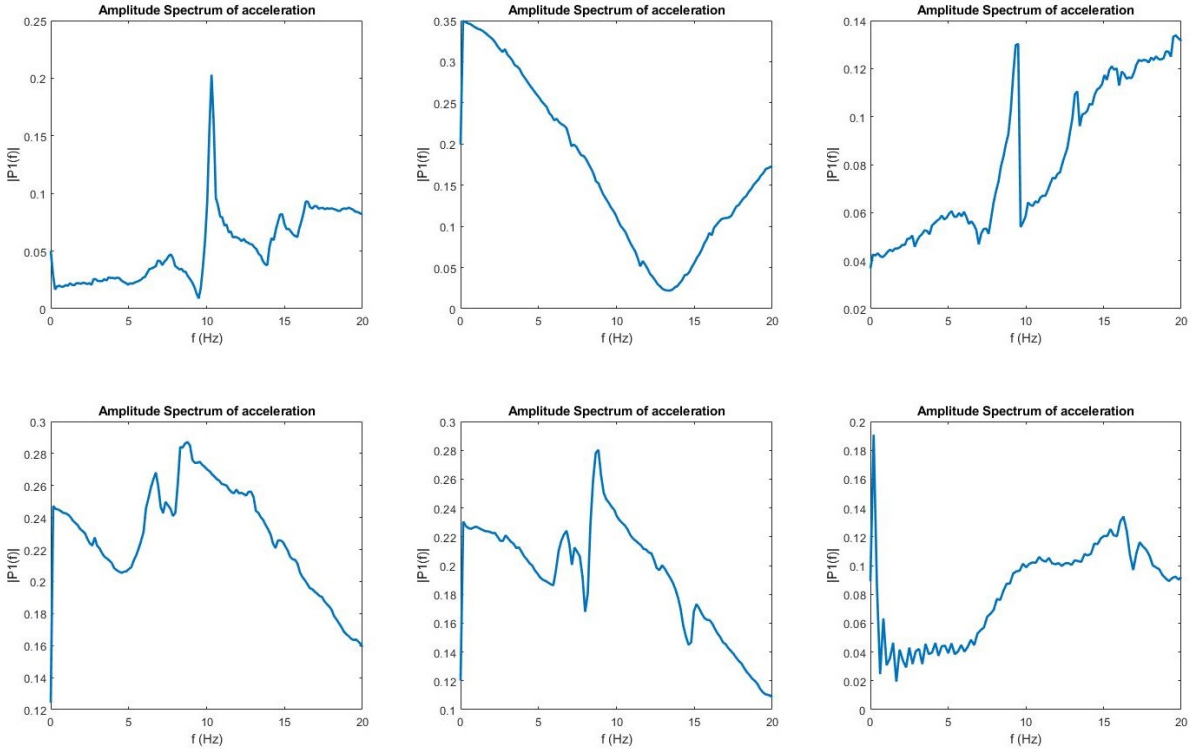

Figure C.6: Hammer test serie 1, frequency domain 0-20 [Hz]

C.2. Force FFT spectra

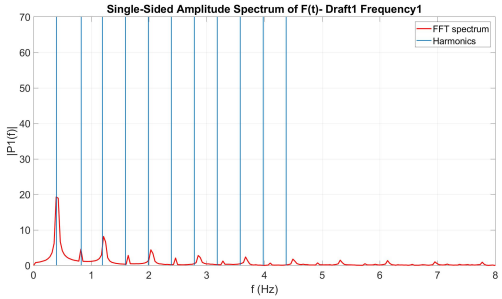

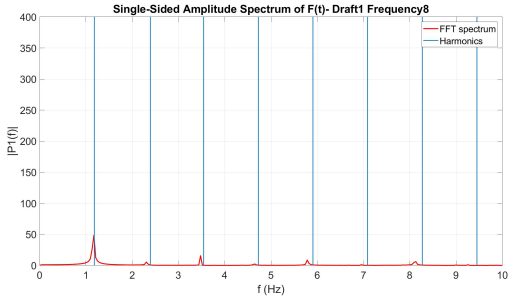

Figure C.7: Draft 1 FFT spectrum frequency 1 and frequency 8.

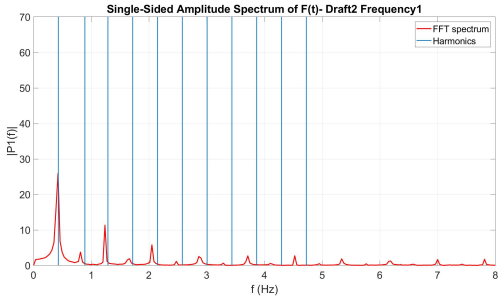

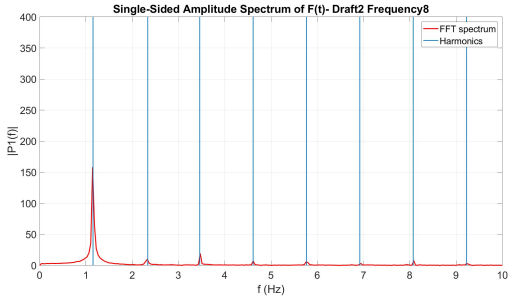

Figure C.8: Draft 2 FFT spectrum frequency 1 and frequency 8.

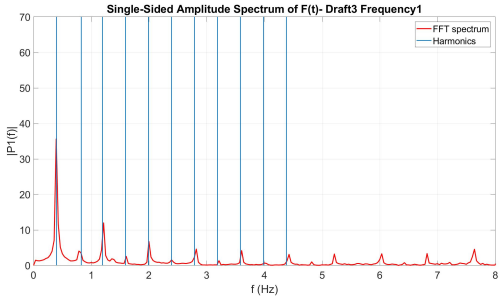

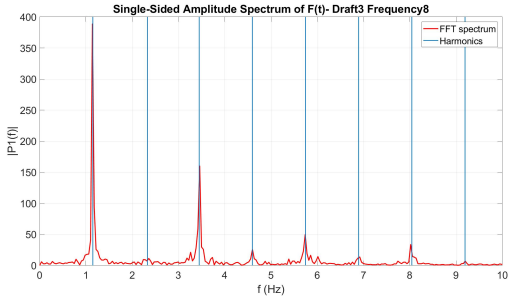

Figure C.9: Draft 3 FFT spectrum frequency 1 and frequency 8.

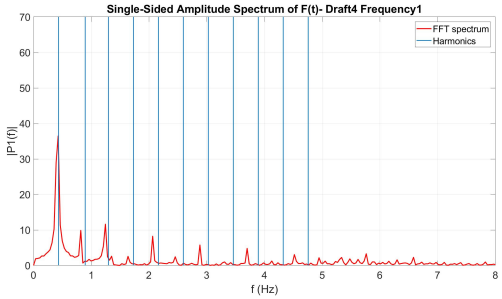

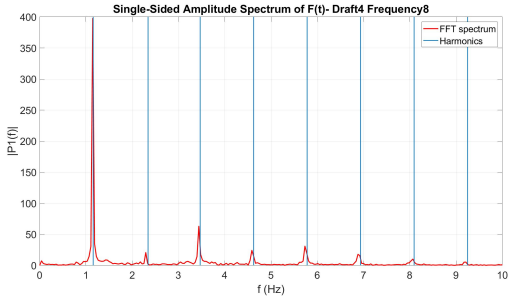

Figure C.10: Draft 4 FFT spectrum frequency 1 and frequency 8.

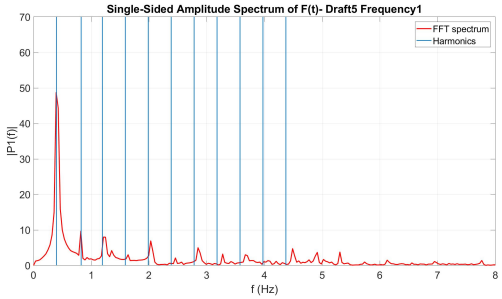

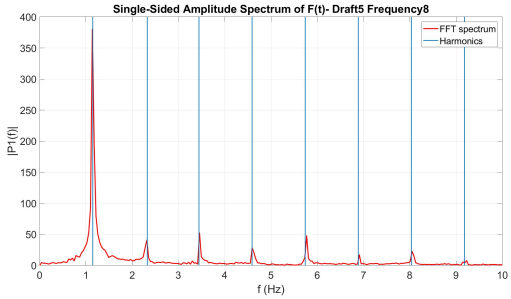

Figure C.11: Draft 5 FFT spectrum frequency 1 and frequency 8.

D

Matlab Scripts

Main file

```
%%  //\\ Jasper Stokkermans //\\ %%%
%  Thesis Boskalis: Added Mass SBJ
%=== Load, Filter and Plot data ===
%  ===  Draft 5   ===
%   ===  May 2018 ===

clc
clear all
close all
tic

%% ===== Load data =====

freq    = 1:8; series  = 1:3;
M_0     = 21.5;                     % [kg]
draft   = 5;
Draft   = (draft-1)*0.125;          % [m]

d=dir('C:\Users\STOK\OneDrive - boskalis.com\Thesis\2000_Matlab\Draft_5\*.csv');
input_ = cell(1,length(d));
for i = 1:length(d);
input_{i}  = d(i).name ;
pdd{i}     = d(i).folder;
end
fl  = input_; pd  = pdd{1};

input_ = cell(1,length(d));

%% Write matrices for loadcell, accelerometer1 and accelerometer2

r_loadcell_path          = cell(1,3);  % 3 = #redundancy series.      [rows = freq 1:8, ...
    cols = serie 1:3]
r_accelerometer1_path    = cell(1,3);
r_accelerometer2_path    = cell(1,3);

for ii = freq              % #freqs
for i = series         % #metingen per freq
d_f_l = 9*ii+i-9;
r_loadcell_raw{ii,i} =  d(d_f_l).name;
r_loadcell_path{ii,i} =  strcat(pd,'\',d(d_f_l).name);
d_f_a2 = 9*ii+i-3;
r_accelerometer2_raw{ii,i} =  d(d_f_a2).name;
r_accelerometer2_path{ii,i} =  strcat(pd,'\',d(d_f_a2).name);
d_f_a1 = 9*ii+i-6;
r_accelerometer1_raw{ii,i} =  d(d_f_a1).name;
r_accelerometer1_path{ii,i} =  strcat(pd,'\',d(d_f_a1).name);
end
```

```
47 end
48
49 % PERIOD    FREQ    M   M   M   M   M   M   M   M   M   M   M   M       FREQ        M
50 % (SECS)    (RAD/S) 11  22  33  44  55  66  13  15  24  26  35  46      (RAD/S) Hz  11
51
52 Theoretical =  csvread('z_D5.csv',0,1);
53 Th_AM       = [Theoretical(:,1) Theoretical(:,2)];
54 Th_Damp     = [Theoretical(:,1) Theoretical(:,3)];
55
56
57 clear d_f_l; clear d_f_a2; clear d_f_a1; clear input_; clear pd; clear pdd;
58 %% Read date to serial string - Loadcell
59
60 flNm                    = r_loadcell_path;
61 flNm2                   = r_accelerometer2_path;
62 flNm3                   = r_accelerometer1_path;
63 R_data_loadcell         = cell(8,3);
64 R_data_accelerometer2   = cell(8,3);
65 R_data_accelerometer1   = cell(8,3);
66 x_zero_crossing         = cell(8,3);
67 t_zero                  = cell(8,3);
68 t_z                     = cell(8,3);
69 V_max                   = cell(8,3);
70 r_loadcell_data         = cell(8,3);
71 r_loadcell_data_cut     = cell(8,3);
72 f_avg                   = cell(8,3);
73 T_avg                   = cell(8,3);
74
75 %%  Add date string to matrix
76 for ii      = freq;             % #freqs
77 for i   = series;           % #metingen per freq
78
79 [r_loadcell_data{ii,i}, msg]    = data_read1(flNm{ii,i});
80 assignin('base','data', r_loadcell_data(ii,i))    % copy data to workspace
81 R_data_loadcell{ii,i} = [r_loadcell_data{ii,i}.cols    r_loadcell_data{ii,i}.dateser];
82 end
83 end
84
85 %% Find V_max, t_cut and reflection time
86
87 for ii          = freq;             % #freqs
88 for i   = series;           % #series
89
90 V_max{ii,i}                     = 0.973.*max(R_data_loadcell{ii,i}(:,4));
91 [t_cut{ii,i}  V_cut{ii,i}]      = find(R_data_loadcell{ii,i}(:,4) > ...
       V_max{ii,i},1,'first');
92 r_loadcell_data_cut{ii,i}       = r_loadcell_data{ii,i}.cols(t_cut{ii,i}:end,:);      % ...
       new dataset with first part removed
93
94 re{ii,i}            = r_loadcell_data{ii,i}.cols(2,1);          % time resolution per ...
       test
95 res                 = cell2mat(re(1));                          % time resolution sensor
96 clear V_cut V_max msg;
97
98 % Now find first zero up crossing Loadcell and Displacement
99
100 x_zero_crossing{ii,i} = detrend((r_loadcell_data_cut{ii,i}(:,3)))/100; % [m]
101
102
103 t_z{ii,i} = crossing(x_zero_crossing{ii,i}(1:end));
104
105 t_zero{ii,i} = t_z{ii,i}+t_cut{ii,i}(1)';
106
107 % Show difference in initial frequency and actual frequency
108 T_avg{ii,i}            = mean(diff(t_zero{ii,i}))*res*2;        % sine has 2 zero ...
       crossings
109 f_act{ii,i}             = 1./T_avg{ii,i};
110
111 %----
112 if t_zero{ii,i}(1,1) < t_cut{ii,i}  % error message if crossing is before cutoff time
113 error('zero crossing is in build up range of signal!');
```

```
114 end
115 %----
116 if r_loadcell_data_cut{ii,i}((t_cut{ii,i}(1)-1),2)> 0  % zero up crossing, if ...
        t_cut-1>0, go to next zero crossing
117 t_zero = t_zero(1);
118 end
119 %----
120 if abs(r_loadcell_data_cut{ii,i}(t_cut{ii,i},3)-mean(r_loadcell_data_cut{ii,i}(:,3)))> 5
121 error('Volt (r_loadcell_data_cut(:4)) is a noisy signal! review V_max= 97.5%');
122 end
123 end
124 zero_cross_freq(ii)          = mean([f_act{ii,1} f_act{ii,2} f_act{ii,3}]);
125 end
126 f_act_ = cell2mat(f_act);
127
128 T           = [2.46 2.24 2.01 1.79 1.57 1.34 1.12 0.89];        %[s] range of periods, ...
        find real periods from fft and insert here!
129 % draft dependent,T = 8x1 matrix
130 t_refl{1,1}         = reflection_time(T);
131
132 %% FFT spectrum: f1
133
134 figure('units','normalized','outerposition',[0 0 1 1])
135 for      f = 1 %freq;
136 for s = 1 %series;
137 Y_f = fft(detrend((r_loadcell_data_cut{f,s}(:,2))).*9.81);      % [N] .*9.81 from kg to N
138 Y_x = fft(detrend((r_loadcell_data_cut{f,s}(:,3))));            % displacement
139 L = length(r_loadcell_data_cut{f,s}(:,2));
140
141 P2          = abs(Y_f/L);
142 P1          = P2(1:L/2+1);
143 P1(2:end-1) = 2*P1(2:end-1);
144
145 %Define the frequency domain f and plot the single-sided amplitude spectrum P1.
146 fr = 1/res*(0:(L/2))/L;
147
148 pks = findpeaks(P1);
149 [pks,locs]       = findpeaks(P1);
150 [pks,locs,w,p]   = findpeaks(P1);  %[peakvalue, location peak, width peak, prominence of ...
        peaks]
151 X                = [pks,locs,w,p];
152 HZ               = sortrows(X, 'descend'); clear X
153
154 Dominant_FFT_fr = HZ(1,2)/res*(0:(L/2))/L;
155 Dominant_FFT_freq = Dominant_FFT_fr(2);
156
157 initial_freq             = [0.41 0.45 0.50 0.56 0.64 0.75 0.89 1.12]
158 zero_cross_freq;
159 Dominant_FFT_freq;
160
161 plot(fr,P1,'r','LineWidth',2)
162 line([Dominant_FFT_fr(2)-res Dominant_FFT_fr(2)-res], [0 70],'LineWidth',1.5);
163 line([2*Dominant_FFT_fr(2)-res     2*Dominant_FFT_fr(2)-res], [0 70],'LineWidth',1.5);
164 line([3*(Dominant_FFT_fr(2)-res)  3*(Dominant_FFT_fr(2)-res)], [0 70],'LineWidth',1.5);
165 line([4*(Dominant_FFT_fr(2)-res)  4*(Dominant_FFT_fr(2)-res)], [0 70],'LineWidth',1.5);
166 line([5*(Dominant_FFT_fr(2)-res)  5*(Dominant_FFT_fr(2)-res)], [0 70],'LineWidth',1.5);
167 line([6*(Dominant_FFT_fr(2)-res)  6*(Dominant_FFT_fr(2)-res)], [0 70],'LineWidth',1.5);
168 line([7*(Dominant_FFT_fr(2)-res)  7*(Dominant_FFT_fr(2)-res)], [0 70],'LineWidth',1.5);
169 line([8*(Dominant_FFT_fr(2)-res)  8*(Dominant_FFT_fr(2)-res)], [0 70],'LineWidth',1.5);
170 line([9*(Dominant_FFT_fr(2)-res)  9*(Dominant_FFT_fr(2)-res)], [0 70],'LineWidth',1.5);
171 line([10*(Dominant_FFT_fr(2)-res) 10*(Dominant_FFT_fr(2)-res)], [0 70],'LineWidth',1.5);
172 line([11*(Dominant_FFT_fr(2)-res) 11*(Dominant_FFT_fr(2)-res)], [0 70],'LineWidth',1.5);
173 xlim([0 8])
174
175 end
176 end
177 grid on
178 titel1 = strcat('Single-Sided Amplitude Spectrum of F(t)- Draft ', num2str(draft),' ...
        Frequency1');
179 title(titel1)
180 legend('FFT spectrum','Harmonics')
```

```
181 xlabel('f (Hz)')
182 ylabel('|P1(f)|')
183 set(gca,'fontsize',20)
184 saveas(gcf, titel1,'jpg');
185
186 P1          = P2(1:L/2+1);
187 P1(2:end-1) = 2*P1(2:end-1);
188
189
190 %% FFT spectrum: f8
191
192 figure('units','normalized','outerposition',[0 0 1 1])
193 for      f = 8 %freq;
194 for s = 1 %series;
195 Y_f = fft(detrend((r_loadcell_data_cut{f,s}(:,2))).*9.81);      % [N] .*9.81 from kg to N
196 Y_x = fft(detrend((r_loadcell_data_cut{f,s}(:,3))));            % displacement
197 L = length(r_loadcell_data_cut{f,s}(:,2));
198
199 P2          = abs(Y_f/L);
200 P1          = P2(1:L/2+1);
201 P1(2:end-1) = 2*P1(2:end-1);
202
203 %Define the frequency domain f and plot the single-sided amplitude spectrum P1.
204 fr = 1/res*(0:(L/2))/L;
205
206 pks = findpeaks(P1);
207 [pks,locs]       = findpeaks(P1);
208 [pks,locs,w,p]   = findpeaks(P1);  %[peakvalue, location peak, width peak, prominence of ...
    peaks]
209 X                = [pks,locs,w,p];
210 HZ               = sortrows(X, 'descend'); clear X
211
212 Dominant_FFT_fr = HZ(1,2)/res*(0:(L/2))/L;
213 Dominant_FFT_freq = Dominant_FFT_fr(2);
214
215 initial_freq             = [0.41 0.45 0.50 0.56 0.64 0.75 0.89 1.12]
216 zero_cross_freq;
217 Dominant_FFT_freq;
218
219 plot(fr,P1,'r','LineWidth',2)
220 line([Dominant_FFT_fr(2)-res Dominant_FFT_fr(2)-res], [0 400],'LineWidth',1.5);
221 line([2*Dominant_FFT_fr(2)-res   2*Dominant_FFT_fr(2)-res], [0 400],'LineWidth',1.5);
222 line([3*(Dominant_FFT_fr(2)-res)  3*(Dominant_FFT_fr(2)-res)], [0 400],'LineWidth',1.5);
223 line([4*(Dominant_FFT_fr(2)-res)  4*(Dominant_FFT_fr(2)-res)], [0 400],'LineWidth',1.5);
224 line([5*(Dominant_FFT_fr(2)-res)  5*(Dominant_FFT_fr(2)-res)], [0 400],'LineWidth',1.5);
225 line([6*(Dominant_FFT_fr(2)-res)  6*(Dominant_FFT_fr(2)-res)], [0 400],'LineWidth',1.5);
226 line([7*(Dominant_FFT_fr(2)-res)  7*(Dominant_FFT_fr(2)-res)], [0 400],'LineWidth',1.5);
227 line([8*(Dominant_FFT_fr(2)-res)  8*(Dominant_FFT_fr(2)-res)], [0 400],'LineWidth',1.5);
228 line([9*(Dominant_FFT_fr(2)-res)  9*(Dominant_FFT_fr(2)-res)], [0 400],'LineWidth',1.5);
229 line([10*(Dominant_FFT_fr(2)-res) 10*(Dominant_FFT_fr(2)-res)], [0 400],'LineWidth',1.5);
230 line([11*(Dominant_FFT_fr(2)-res) 11*(Dominant_FFT_fr(2)-res)], [0 400],'LineWidth',1.5);
231 xlim([0 10])
232
233 end
234 end
235 grid on
236 titel1 = strcat('Single-Sided Amplitude Spectrum of F(t)- Draft', num2str(draft),' ...
    Frequency8');
237 title(titel1)
238 legend('FFT spectrum','Harmonics')
239 xlabel('f (Hz)')
240 ylabel('|P1(f)|')
241 set(gca,'fontsize',20)
242 saveas(gcf, titel1,'jpg');
243
244 P1          = P2(1:L/2+1);
245 P1(2:end-1) = 2*P1(2:end-1);
246
247 %% ===== Least Squares Method - Fit F(t) =====
248
249 phi_deg      = zeros(8,3);
```

```
F_ampl      = zeros(8,3);

for f = freq;
for s = series;

F_t         = -(detrend((r_loadcell_data_cut{f,s}(:,2)*9.81)));      % [N] 2= Force, 3 = ... displacement
t           = r_loadcell_data_cut{f,s}(:,1);
W           = 2*pi*f_act{f,s};                % omega in rad/sec

A           = [cos(W.*t), -sin(W.*t)];
b           = inv(A'*A)*(A'*F_t);             % =(A'*A)\(A'*F_t);        %b1 = F^ ... cos(phi);  b2 = F^ sin(phi)

phi         = atan2(b(2),b(1));               % Radians   % phi          = atan(b(2)/b(1));
phi_deg     = phi*180/pi;

F_ampl      = b(1)/cos(phi);                  % is equal to: F_ampl2     = b(2)/sin(phi)

if F_ampl <0    % amplitude must be a positive value, introduces a phaseshift of 180deg ... is F_ampl is negative.
F_ampl = abs(F_ampl);
phi  = phi+pi;
end

phi_deg     = phi*180/pi;
error       = norm(A*b-F_t);

figure('units','normalized','outerposition',[0 0 1 1])
plot(t, F_ampl.*cos(W.*t+phi),'LineWidth', 1.5)                         % plot fit F
hold on
plot(t, F_t,'r','LineWidth', 1.5)                                       % plot F(t)
plot(r_loadcell_data_cut{f,s}(:,1),x_zero_crossing{f,s}*100,'k','LineWidth', 1.5);    % ... plot displacement(t)
grid on
set(gca,'fontsize',20)
hold off
legend('Fit Force','Force [N]', 'Displacement [cm]')
set(gca,'fontsize',20)
xlabel('Time(s)')
ylabel('[N], [cm]')
xlim([2 31])
titel2 = strcat('Draft ',num2str(draft),' Fit F(t) - Frequency = ', num2str(f), ', ... Serie = ', num2str(s));
title(titel2)
saveas(gcf, titel2,'jpg');

phi_deg_(f,s) = phi_deg;
F_ampl_(f,s)  = F_ampl;
error_(f,s)   = error;
end
end

phi_deg_
F_ampl_
error_
F_ampl_avg = mean(F_ampl_(8,:))
%% ==== Least Squares Method - Fit x(t) ===

phi_x_deg   = ones(8,3);
x_ampl      = ones(8,3);

for f = freq;
for s = series;

x_t         = detrend(r_loadcell_data_cut{f,s}(:,3))/100;      % [m] 2= Force, 3 = ... displacement
t           = r_loadcell_data_cut{f,s}(:,1);          % [s]
W           = 2*pi*f_act{f,s};                        % omega in rad/sec

A_x           = [cos(W.*t), -sin(W.*t)];
```

```
315 b_x             = inv(A_x'*A_x)*(A_x'*x_t);              % (A_x'*A_x)\(A_x'*x_t);
316
317 phi_x             = atan2(b_x(2),b_x(1));                % Radians
318 phi_x_deg         = phi_x*180/pi;
319
320 x_ampl            = (b_x(1)/cos(phi_x));
321
322 if x_ampl <0    % amplitude must be a positive value, introduces a phaseshift of 180deg ...
        is F_ampl is negative.
323 x_ampl = abs(x_ampl);
324 phi_x  = phi_x+pi;
325 end
326
327 phi_x_deg       = phi_x*180/pi;
328 error_x         = norm(A_x*b_x-x_t);
329
330 figure('units','normalized','outerposition',[0 0 1 1])
331
332 plot(t, x_ampl.*cos(W.*t+phi_x),'LineWidth', 1.5)        % plot fit F
333 hold on
334 plot(t,x_zero_crossing{f,s},'r','LineWidth', 1.5);       % plot displacement(t)
335
336 grid on
337 hold off
338 legend('Fit','Displacement [m]')
339 set(gca,'fontsize',20)
340 xlabel('Time (s)')
341 ylabel('Displacement [m]')
342 xlim([2 31])
343
344 titel3 = strcat('Draft ',num2str(draft),' Fit x(t) - Frequency = ', num2str(f), ', ...
        Serie = ', num2str(s));
345 title(titel3)
346 saveas(gcf, titel3,'jpg');
347
348 phi_x_deg_(f,s) = phi_x_deg;
349 x_ampl_(f,s)  = x_ampl;
350 error_x_(f,s)   = error_x;
351 end
352 end
353
354 phi_x_deg_
355 x_ampl_
356 error_x_
357 x_ampl_avg = mean(x_ampl_(8,:))
358
359 % Keulegan Carpenter Number      https://ocw.tudelft.nl/wp-content/uploads/Part_4.pdf
360 KC       = (2*pi*x_ampl_/0.5);
361 KC_      = mean(KC')'
362
363 %% ======= Retracing the Added Mass from F_ampl and phi =======
364
365 phi_diff = wrapTo360(phi_deg_-phi_x_deg_)                  % Phase difference
366 phi_diff_rad = (pi/180)*phi_diff;
367
368
369 for s = series
370 for f = freq
371
372 M_a_kg(f,s)         = ...
        -(cos(phi_diff_rad(f,s))/((2*pi*f_act{f,s})^2)*(F_ampl_(f,s)/(x_ampl_avg)))-M_0;  % ...
        in [kg]
373 M_a_kg_avg(:,f)     = mean(M_a_kg(f,:));
374 end
375
376 end
377
378 M_vol_kg     = (pi/4*(0.5)^2*1000*Draft)
379 M_a_kg_avg_ = M_a_kg_avg'
380 M_a_norm     = M_a_kg_avg_./M_vol_kg % [kg] normalised added mass
381
```

```
for f = freq
error_MA(f) = norm(M_a_kg(f,:)-M_a_kg_avg_(f,:));
end
%===== Plot Theroteical value Added mass =====
figure('units','normalized','outerposition',[0 0 1 1])
% plot(mean(f_act_')', M_a_kg,mean(f_act_')', M_a_kg_avg,'o','LineWidth', 1.5)  %Hz vs ... Added mass
plot(mean(f_act_')', M_a_kg_avg,'o','LineWidth', 1.5)  %Hz vs Added mass

hold on
errorbar(mean(f_act_')',M_a_kg_avg_, error_MA,'LineWidth', 3)
plot(Th_AM(:,1), Th_AM(:,2),'LineWidth', 1.5)  %Hz vs Added mass
plot(mean(f_act_')', M_a_kg_avg,mean(f_act_')', M_a_kg_avg,'o','LineWidth', 1.5)  %Hz ... vs Added mass
set(gca,'fontsize',20)

hold off
legend('Experiments','Average added mass','Potential theory added mass')
naam = strcat('Theoretical Added mass per frequency [Hz] for draft ', num2str(draft));
title(naam)
xlim([0.3 1.3])
ylim([0 250])
xlabel('[Hz]')
ylabel('Added mass [kg]')
saveas(gcf, naam ,'jpg');

figure('units','normalized','outerposition',[0 0 1 1])
plot(mean(f_act_')', M_a_kg_avg,'o','LineWidth', 1.5)  %Hz vs Added mass
hold on
errorbar(mean(f_act_')',M_a_kg_avg_, error_MA,'r','LineWidth', 3)
set(gca,'fontsize',20)

hold off
legend('Experiments','Average added mass')
naam = strcat('Added mass per frequency [Hz] for draft ', num2str(draft));
title(naam)
xlim([0.3 1.3])
ylim([0 250])
xlabel('[Hz]')
ylabel('Added mass [kg]')
set(gca,'fontsize',20)
saveas(gcf, naam );


%% Dimensionless added mass
for f = 1:8
error_MAD(f) = (norm(M_a_kg_avg_(f,:)-M_a_kg(f,:)))/M_vol_kg;
end

figure('units','normalized','outerposition',[0 0 1 1])
% plot(1./mean(f_act_')', M_a_norm  ,'LineWidth', 1.5)  %Hz vs Added mass

naam = strcat('Dimensionless Added mass per frequency [Hz] for draft ', num2str(draft));
title(naam)
xlim([0.3 1.3])
ylim([0 2.5])
xlabel('[Hz]')
ylabel('Dimensionless Added mass [-]')

hold on
errorbar(mean(f_act_'),M_a_norm, error_MAD,'r','LineWidth', 3)
legend('Dimensionless added mass')
set(gca,'fontsize',20)
hold off
saveas(gcf, naam );

%% ======= Retracing the Drag(B) from F_ampl and phi =======

for s = series
for f = freq

```

```
451 B(f,s)      = ...
        (sin(phi_diff_rad(f,s))/(2*pi*f_act{f,s}))*((F_ampl_(f,s)/9.81)/(x_ampl_avg)); % ...
        in [kg]
452 B_avg(:,f) =  mean(B(f,:));
453 end
454 end
455
456 % hold off
457
458 B_avg_ = B_avg';
459 for f = freq
460 error_B(f) = norm(B(f,:)-B_avg_(f,:));
461 end
462
463 %==== Plot Theroteical value Damping ====
464
465 figure('units','normalized','outerposition',[0 0 1 1])
466 errorbar(mean(f_act_')',B_avg_, error_B,'r','LineWidth', 2.5)
467
468 hold on
469
470 plot(mean(f_act_'),B)
471 plot(Th_Damp(:,end-1), Th_Damp(:,end),'LineWidth', 2) %Hz vs damping
472 plot(mean(f_act_')', B_avg_,'o','LineWidth', 2.5) %Hz vs damping
473 set(gca,'fontsize',20)
474 hold off
475 legend('Location','northwest')
476 legend('Average Damping','serie 1','serie 2','serie 3', 'Potential theory')
477 naam = strcat('Theoretical damping per frequency [Hz] for draft ', num2str(draft));
478 title(naam);
479 xlim([0.3 1.3])
480 ylim([0 150])
481 xlabel('[Hz]')
482 ylabel('Damping [kg/s]')
483 saveas(gcf, naam,'jpg');
484
485
486 figure('units','normalized','outerposition',[0 0 1 1])
487 errorbar(mean(f_act_')',B_avg_, error_B,'r','LineWidth', 2.5)
488
489 hold on
490 plot(mean(f_act_')', B_avg_,'o','LineWidth', 2.5) %Hz vs Added mass
491 legend('Location','northwest')
492 legend('Average Damping')
493 naam = strcat('Damping per frequency [Hz] for draft ', num2str(draft));
494 set(gca,'fontsize',20)
495 title(naam);
496 xlim([0.3 1.3])
497 ylim([0 150])
498 xlabel('[Hz]')
499 ylabel('Damping [kg/s]')
500 saveas(gcf, naam);
501
502 %% non-dimensional Damping
503 for f = 1:8
504 error_BD(f) = (norm(B_avg_(f,:)-B(f,:)))/(1025*Draft*(pi/4)*(0.5^2));
505 end
506 B_dim = B_avg_/(1025*(Draft*(pi/4)*(0.5^2)*((9.81/0.5)^0.5)));
507
508 figure('units','normalized','outerposition',[0 0 1 1])
509 %plot(mean(f_act_')', B_dim,'o','LineWidth', 2.5) %Hz vs Added mass
510 hold on
511 errorbar(mean(f_act_')',B_dim,error_BD/(1025*(Draft*(pi/4)*(0.5^2)*((9.81/0.5)^0.5))),'r','LineWidth',
        2.5)
512 legend('Location','northwest')
513 legend('Damping [-]')
514
515 naam = strcat('Dimensionless damping per frequency [Hz] for draft ', num2str(draft));
516 title(naam);
517 xlim([0.3 1.3])
518 ylim([0 2])
```

```
519 xlabel('[Hz]')
520 ylabel('Dimelsionless Damping [-] ')
521 set(gca,'fontsize',20)
522 saveas(gcf, naam);
523 saveas(gcf, naam, 'jpg');
524
525
526 %% Potential theory added mass
527 figure('units','normalized','outerposition',[0 0 1 1])
528 plot(Th_AM(:,end-1), Th_AM(:,end)/(M_vol_kg),'LineWidth', 2)  %Hz vs Added mass
529
530 naam = strcat('Potential theory, non-dimensional Added mass per frequency [Hz] for ...
        draft ', num2str(draft));
531 title(naam);
532 xlim([0.3 1.3])
533 ylim([0 0.5])
534 xlabel('[Hz]')
535 ylabel('Dimelsionless Damping [-] ')
536 set(gca,'fontsize',20)
537 legend('Location','northwest')
538 legend('Damping [-]',' ')
539 saveas(gcf, naam);
540 saveas(gcf, naam, 'jpg');
541
542 %% Potential theory damping
543 figure('units','normalized','outerposition',[0 0 1 1])
544 plot(Th_Damp(:,end-1), ...
        Th_Damp(:,end)/(1025*(Draft*(pi/4)*(0.5^2)*((9.81/0.5)^0.5))),'LineWidth', 2)  %Hz ...
        vs Added mass
545
546 naam = strcat('Potential theory, non-dimensional Damping per frequency [Hz] for draft ...
        ', num2str(draft));
547 title(naam);
548 xlim([0.3 1.3])
549 ylim([0 0.5])
550 xlabel('[Hz]')
551 ylabel('Dimelsionless Damping [-] ')
552 set(gca,'fontsize',20)
553 legend('Location','northwest')
554 legend('Damping [-]',' ')
555 saveas(gcf, naam);
556 saveas(gcf, naam, 'jpg');
557
558 toc
559
560 close all
```

Load data

```
1  %%%  \\ Jasper Stokkermans // %%%
2  %  Thesis Boskalis: Added Mass SBJ
3  %     ==== load data ====
4  %     ==== April 2018 ====
5
6  %load data, rewrite datestructure dd/mm/yyy hh:mm:ss to singular timestamp in seconds
7
8  function [data, msg] = data_read(flNm)
9  d=dir('C:\Users\STOK\OneDrive - boskalis.com\Thesis\2000_Matlab\Draft_5\*.csv');
10
11 data    = struct;
12 msg = '';
13
14 fid = fopen(flNm);
15
16 %%
17
18 if fid<0
19 msg = sprintf('Cannot open "%s"', flNm);
```

```
20 return
21 end
22
23 %|sec,kg,cm,Volt,Date,Time
24 %|0,-3.05E-02,3.38E+01,1.10E-02,3/16/2018,1:33:08 PM
25 %                                    M D  YYYY H:M:S
26
27 headerLn     = fgetl(fid);
28
29 colCnt       = 4;    % data only, no date
30 fmt          = repmat('%f,',1,colCnt);
31 fmt          = [fmt '%d%d%d,%d%d%d %*2c'];
32 delimiter    = ' /:';    % allows for multiple, possible delimiters
33
34 [dataC, pntr]    = textscan(fid, fmt, 'Delimiter', delimiter);
35
36 %fgetl(fid)     % TEST
37
38 fclose(fid);
39
40 % -- post-processing --
41 data.cols    = [dataC{1:colCnt}];
42
43 % collect remaining columns (and convert from decimal (int32 <--> %d) to double %f
44 datetime     = double([dataC{colCnt+1:end}]);
45
46 % convert "vector" to a serial date (per row)
47 data.dateser     = datenum(datetime(:, [3 1 2 4:6]));
48
49 datestr(data.dateser,0);
50
51 data.date    = [];
52
53 end
```

Zero Crossing

```
1  %%%  \\ Jasper Stokkermans // %%%
2  %  Thesis Boskalis: Added Mass SBJ
3  %   ==== Zero Crossing ====
4  %     ==== April 2018 ====
5
6  function [ind,t0,s0,t0close,s0close] = crossing(S,t,level,imeth)
7
8  % CROSSING find the crossings of a given level of a signal
9  %   ind = CROSSING(S) returns an index vector ind, the signal
10 %   S crosses zero at ind or at between ind and ind+1
11 %   [ind,t0] = CROSSING(S,t) additionally returns a time
12 %   vector t0 of the zero crossings of the signal S. The crossing
13 %   times are linearly interpolated between the given times t
14 %   [ind,t0] = CROSSING(S,t,level) returns the crossings of the
15 %   given level instead of the zero crossings
16 %   ind = CROSSING(S,[],level) as above but without time interpolation
17 %   [ind,t0] = CROSSING(S,t,level,par) allows additional parameters
18 %   par = {'none'|'linear'}.
19 %   With interpolation turned off (par = 'none') this function always
20 %   returns the value left of the zero (the data point thats nearest
21 %   to the zero AND smaller than the zero crossing).
22 %
23 %   [ind,t0,s0] = ... also returns the data vector corresponding to
24 %   the t0 values.
25 %
26 %   [ind,t0,s0,t0close,s0close] additionally returns the data points
27 %   closest to a zero crossing in the arrays t0close and s0close.
28
29
30 % check the number of input arguments
31 error(nargchk(1,4,nargin));
```

```
32
33 % check the time vector input for consistency
34 if nargin < 2 || isempty(t)
35 % if no time vector is given, use the index vector as time
36 t = 1:length(S);
37 elseif length(t) ~= length(S)
38 % if S and t are not of the same length, throw an error
39 error('t and S must be of identical length!');
40 end
41
42 % check the level input
43 if nargin < 3
44 % set standard value 0, if level is not given
45 level = 0;
46 end
47
48 % check interpolation method input
49 if nargin < 4
50 imeth = 'linear';
51 end
52
53 % make row vectors
54 t = t(:)';
55 S = S(:)';
56
57 % always search for zeros. So if we want the crossing of
58 % any other threshold value "level", we subtract it from
59 % the values and search for zeros.
60 S   = S - level;
61
62 % first look for exact zeros
63 ind0 = find( S == 0 );
64
65 % then look for zero crossings between data points
66 S1 = S(1:end-1) .* S(2:end);
67 ind1 = find( S1 < 0 );
68
69 % bring exact zeros and "in-between" zeros together
70 ind = sort([ind0 ind1]);
71
72 % and pick the associated time values
73 t0 = t(ind);
74 s0 = S(ind);
75
76 if strcmp(imeth,'linear')
77 % linear interpolation of crossing
78 for ii=1:length(t0)
79 if abs(S(ind(ii))) > eps(S(ind(ii)))
80 % interpolate only when data point is not already zero
81 NUM = (t(ind(ii)+1) - t(ind(ii)));
82 DEN = (S(ind(ii)+1) - S(ind(ii)));
83 DELTA =  NUM / DEN;
84 t0(ii) = t0(ii) - S(ind(ii)) * DELTA;
85 % I'm a bad person, so I simply set the value to zero
86 % instead of calculating the perfect number ;)
87 s0(ii) = 0;
88 end
89 end
90 end
91
92 % Addition:
93 % Some people like to get the data points closest to the zero crossing,
94 % so we return these as well
95
96 if any(ind==1)    % EDITED for if ind =1, resulted in error
97 ind(ind==1)=2;
98 end
99
100 [CC,II] = min(abs([S(ind-1) ; S(ind) ; S(ind+1)]),[],1);
101 ind2 = ind + (II-2); %update indices
102
```

```
t0close = t(ind2);
s0close = S(ind2);
```

Period Check

```
%%%  \\ Jasper Stokkermans // %%%
%  Thesis Boskalis: Added Mass SBJ
%   ==== Period check ====
%      ==== April 2018 ====


% pd - output phase difference (in radians)
% v - first sinusoidal signal
% i - second sinusoidal signal
% Note: v and i should have the same frequency
function pd=givepd(F,x)
L=length(F);
if(L~=length(x))
error('The length of the 2 sinusoidal input vectors is not same!!!');
end

% The following block calculates the FFT
NFFT = 2^nextpow2(L);
V = fft(F,NFFT)/L;                    %Fourier Transform of signal v

% The following block calculates the phase of the most significant
% frequency component
[value,index]=max(2*abs(V(1:NFFT/2+1)));
pV = angle(V(index));

% The following block calculates the FFT
NFFT = 2^nextpow2(L);
I = fft(x,NFFT)/L;                    %Fourier Transform of signal i

% The following block calculates the phase of the most significant
% frequency component
[value,index]=max(2*abs(I(1:NFFT/2+1)));
pI = angle(I(index));

% The following is the phase difference between the 2 signals
pd=pV-pI;

% The code below limits the output to pd={-pi,pi}radians
while 1
if pd>pi
pd=pd-2*pi;
elseif pd<-pi
pd=pd+2*pi;
else
break;
end
end

return;
end
```

Reflection times

```

%%%  \\ Jasper Stokkermans // %%%
%  Thesis Boskalis: Added Mass SBJ
%  ====  Reflection Time Tank ====
%      ==== April 2018 ====

function[t_refl] = reflection_time(T)
```

```
8
9  %%
10 % Phase velocity
11 % Based on 'deep' water limit
12
13 % T          = [2.46 2.24 2.01 1.79 1.57 1.34 1.12 0.89]       %[s] max range periods
14 d            = 1.12                      ; %[m] waterdepth tank
15 g            = 9.81                    ; %[m/s^2] gravity
16
17 lambda_0     = g.*T.^2/(2*pi)          %[m] deep water limit
18
19 k_0          = 2*pi./lambda_0          ; %[m^-1]
20 k_0d         = k_0*d                     %
21 deep         = d./lambda_0             ;
22
23 n            = 0.5*(1+k_0.*d./sinh(2*k_0*d))
24 c            = sqrt((g./k_0).*tanh(k_0.*d)) ;
25 cg           = n.*c                      %[m/s] Phase velocity
26
27 tank         = 10                      ; %[m] both sides from frame
28 t_refl       = 2*tank./cg                %[s] time to reflect waves back to structure
```

Hammer test FFT spectrum

```
1
2  %%%  \\ Jasper Stokkermans // %%%
3  %  Thesis Boskalis: Added Mass SBJ
4  %  ==== Hammer test FFT ====
5  %     ==== April 2018 ====
6
7  clear all
8  clc
9  close all
10 %% load data
11 % d=dir('G:\2000_Matlab\Hammer_test\*.csv')
12
13 d = dir('C:\Users\STOK\OneDrive - boskalis.com\Thesis\2000_Matlab\Hammer_test\*.csv'); ...
       % return the list of csv files
14
15 series = 1:3;
16 draft = 1:6;
17 p1 = (series(end)*draft(end));
18 % Time Stamp,Accelerometer X,Accelerometer Y,Accelerometer Z,Total Acceleration
19 % (s),(m.s^-2),(m.s^-2),(m.s^-2),(m.s^-2)
20 for p = 1:p1  % number of files to read,    all=    1:length(d)
21 m{p}    = dlmread(d(p).name);
22
23 end
24
25 s1 = 3.*draft-2;
26 s2 = 3.*draft-1;
27 s3 = 3.*draft;
28 %% ==== Plots ====
29 %Raw data plots
30
31 figure('units','normalized','outerposition',[0 0 1 1])
32 %series 1
33 for a = 1: length(s1);
34 t1 = (m{1,s1(a)}(:,1)-m{1,s1(a)}(1,1));
35 subplot(2,3,a)
36 % plot(t1, m{1,s1(a)}(:,2)    ,t2, m{1,s2(a)}(:,2),    t3, m{1,s3(a)}(:,2))
37 plot(t1, m{1,s1(a)}(:,2),'b','LineWidth',2)
38 xlim([1.6 3.1])
39 ylim([-35 50])
40
41 hold on
42
43 % series2
```

```
for b = 1:length(s2);
t2 = (m{1,s2(b)}(:,1)-m{1,s2(b)}(1,1));
subplot(2,3,b)
plot(t2, m{1,s2(b)}(:,2),'r','LineWidth',2)

%series3
for c = 1:length(s3);
t3 = (m{1,s3(c)}(:,1)-m{1,s3(c)}(1,1));
subplot(2,3,c)
plot(t3, m{1,s3(c)}(:,2),'k','LineWidth',2)
xlabel('Time [s]')
ylabel('Force [N]')
legend('Serie 1','Serie 2','Serie 3')
for ti = 1:6
subplot(2,3,ti)
titel = strcat('Hammer test per Draft :', num2str(ti) );
title(titel)

end
end
end
end
hold off

%% Analyse graphs - https://nl.mathworks.com/help/matlab/ref/fft.html

Fs = 100;            % Sampling frequency
T = 1/Fs;            % Sampling period
%L = 1500;           % Length of signal

% series1
figure('units','normalized','outerposition',[0 0 1 1])

for a = 1:length(s1);

F = fft(m{1,s1(a)}(:,2));
L = length(m{1,s1(a)});
t = (0:L-1)*T;        % Time vector

P2 = abs(F/L);
P11 = P2(1:L/2+1);
P11(2:end-1) = 2*P11(2:end-1);
s11 = Fs*(0:(L/2))/L;

subplot(2,3,a)
plot(s11,P11,'linewidth', 2)

title('Amplitude Spectrum of acceleration of serie 1')
xlim([0 2]) %xlim('auto')
ylim('auto')
xlabel('f (Hz)')
ylabel('|P1(f)|')
for ti = 1:6
subplot(2,3,ti)
titel = strcat('Hammer test FFT, serie 1, Draft :', num2str(ti) );
title(titel)
end
end

figure('units','normalized','outerposition',[0 0 1 1])
for b = 1:length(s2);

F = fft(m{1,s2(b)}(:,2));
L = length(m{1,s1(b)});
t = (0:L-1)*T;        % Time vector

P2 = abs(F/L);
P12 = P2(1:L/2+1);
P12(2:end-1) = 2*P12(2:end-1);
s22 = Fs*(0:(L/2))/L;

```

```
115 subplot(2,3,b)
116 plot(s22,P12,'linewidth', 2)
117
118 xlim([0 2]) %xlim('auto')
119 ylim('auto')
120 xlabel('f (Hz)')
121 ylabel('|P1(f)|')
122 for ti = 1:6
123 subplot(2,3,ti)
124 titel = strcat('Hammer test FFT, serie 2, Draft :', num2str(ti) );
125 title(titel)
126 end
127 end
128 figure('units','normalized','outerposition',[0 0 1 1])
129 for c = 1:length(s3);
130
131 F = fft(m{1,s3(c)}(:,2));
132 L = length(m{1,s3(c)});
133 t = (0:L-1)*T;        % Time vector
134
135 P2 = abs(F/L);
136 P13 = P2(1:L/2+1);
137 P13(2:end-1) = 2*P13(2:end-1);
138 s33 = Fs*(0:(L/2))/L;
139
140 subplot(2,3,c)
141 plot(s33,P13,'linewidth', 2)
142
143 xlim([0 2]) %xlim('auto')
144 ylim('auto')
145 xlabel('f (Hz)')
146 ylabel('|P1(f)|')
147 for ti = 1:6
148 subplot(2,3,ti)
149 titel = strcat('Hammer test FFT, serie 3, Draft :', num2str(ti) );
150 title(titel)
151 end
152 end
153
154 toc
```

D.1. Viscous effects on Damping force

```
1
2 %%% \\ Jasper Stokkermans // %%%
3 % Thesis Boskalis: Added Mass SBJ
4 % === Viscous Effects on drag force ===
5 %    === June 2018 ===
6 close all
7 clear all
8 clc
9
10
11 t = 0:0.01:10;
12 w = 2*pi*0.41;
13
14 x  = 0.8*sin(w*t);          % F
15 x2 = -0.2*sin(3*w*t);    % viscous
16 x3 = x+x2;
17
18 plot(t,x,t,x3, 'LineWidth',1.5)
19 legend('Drag signal without viscous effects', 'Drag signal with viscous effects')
20 title('Viscous effects on drag force signal')
21 xlabel('Time(s)')
22 ylabel('Force')
23 set(gca,'fontsize',20)
```

D.2. JONSWAP Spectrum

```
%%% \\ Jasper Stokkermans // %%%
% Thesis Boskalis: Added Mass SBJ
% ==== JONSWAP Spectrum ====
%     ==== March 2018 ====
close all;
clear;
clc;
%%
Hw=1; % wave height significant (m)
Tp=11:-1:3; % Peak period (s)

w=linspace(0.1,2.5,1000);
d_w = w(2)-w(1);
w = w + d_w .* rand(1,length(w)); % random selection of frequencies
w3=w;
Hz = w3/(2*pi);

%----- Jonswap spectrum ------
gama  = 3.3;
fp    = 2*pi./Tp;
fac1  = (320*Hw^2)./Tp.^4;
sigma = zeros (length(fp), length(w3));

sigma = (w<=fp').*0.07+(w>fp').*0.09;

Aa    = exp(-((w./fp'-1)./(sigma.*sqrt(2))).^2);
fac2  = w.^-5;
fac3  = exp(-(1950*w.^-4)./Tp'.^4);
fac31 = exp(-5/4*(w./fp').^-4);
fac4  = gama.^Aa;
S     = fac1'.*fac2.*fac3.*fac4;

%%
plot(Hz,S,'LineWidth',2.5);
hold on
line([0.048 0.048],ylim,'LineWidth',2.5),'k';
% line([0.175 0.175],ylim,'LineWidth',2.5);
line([0.302 0.302],ylim,'LineWidth',2.5);
hold off

xlabel('Hz [s^-1]');ylabel('Spectral (m^2.s)');
title('Energy density spectrum JONSWAP');

legend('Tp = 11','Tp = 10','Tp = 9','Tp = 8', 'Tp = 7','Tp = 6','Tp = 5','Tp = 4','Tp = ...
    3')
grid;
set(gca,'FontSize', 20);
graph1 = plot(figure1);
set(graph1,'LineWidth',2);
```

D.3. Merge of plots

```
%  //\\ Jasper Stokkermans //\\ %%%
%  Thesis Boskalis: Added Mass SBJ
% ==== Merge plots ====
%    ==== May 2018 ====

clc
clear all
close all
tic
%% Damping
% 1) Load saved figures
figure(1) = hgload('Damping per frequency [Hz] for draft1.fig');
```

```
figure(2) = hgload('Damping per frequency [Hz] for draft2.fig');
figure(3) = hgload('Damping per frequency [Hz] for draft3.fig');
figure(4) = hgload('Damping per frequency [Hz] for draft4.fig');
figure(5) = hgload('Damping per frequency [Hz] for draft5.fig');

% 2) Prepare subplots

figure
h(1)=subplot(1,1,1);

copyobj(allchild(get(figure(1),'CurrentAxes')),h(1));
copyobj(allchild(get(figure(2),'CurrentAxes')),h(1));
copyobj(allchild(get(figure(3),'CurrentAxes')),h(1));
copyobj(allchild(get(figure(4),'CurrentAxes')),h(1));
copyobj(allchild(get(figure(5),'CurrentAxes')),h(1));

grid on
title('Experiments Damping-Draft relation');
legend('Draft 1','Draft 2','Draft 3','Draft 4','Draft 5')

%% Added Mass

% 1) Load saved figures
figure(1) = hgload('Added mass per frequency [Hz] for draft1.fig');
figure(2) = hgload('Added mass per frequency [Hz] for draft2.fig');
figure(3) = hgload('Added mass per frequency [Hz] for draft3.fig');
figure(4) = hgload('Added mass per frequency [Hz] for draft4.fig');
figure(5) = hgload('Added mass per frequency [Hz] for draft5.fig');

% 2) Prepare subplots

figure%('units','normalized','outerposition',[0 0 1 1])
h(1)=subplot(1,1,1);

copyobj(allchild(get(figure(1),'CurrentAxes')),h(1));
copyobj(allchild(get(figure(2),'CurrentAxes')),h(1));
copyobj(allchild(get(figure(3),'CurrentAxes')),h(1));
copyobj(allchild(get(figure(4),'CurrentAxes')),h(1));
copyobj(allchild(get(figure(5),'CurrentAxes')),h(1));
title('Experiments Added mass-Draft relation');
ylim([-15 250])
grid on
legend('Draft 1','Draft 2','Draft 3','Draft 4','Draft 5')


%% Dimensionless Added Mass

% 1) Load saved figures
figure(6) = hgload('Dimensionless Added mass per frequency [Hz] for draft1.fig');
figure(7) = hgload('Dimensionless Added mass per frequency [Hz] for draft2.fig');
figure(8) = hgload('Dimensionless Added mass per frequency [Hz] for draft3.fig');
figure(9) = hgload('Dimensionless Added mass per frequency [Hz] for draft4.fig');
figure(10) = hgload('Dimensionless Added mass per frequency [Hz] for draft5.fig');

% 2) Prepare subplots

figure%('units','normalized','outerposition',[0 0 1 1])
h(2)=subplot(1,1,1);

copyobj(allchild(get(figure(6),'CurrentAxes')),h(2));
copyobj(allchild(get(figure(7),'CurrentAxes')),h(2));
copyobj(allchild(get(figure(8),'CurrentAxes')),h(2));
copyobj(allchild(get(figure(9),'CurrentAxes')),h(2));
copyobj(allchild(get(figure(10),'CurrentAxes')),h(2));
naam = 'Experiments Dimensionless Added mass-Draft relation';
title(naam);
ylim([0 2.2])
grid on

legend('Draft 1','Draft 2','Draft 3','Draft 4','Draft 5')
saveas(gcf, naam);
```

```
84  saveas(gcf, naam, 'jpg');
85
86  %% Potential Added Mass
87  % 1) Load saved figures
88  figure(11) = hgload('Potential theory, non-dimensional Added mass per frequency [Hz] ...
        for draft1.fig');
89  figure(12) = hgload('Potential theory, non-dimensional Added mass per frequency [Hz] ...
        for draft2.fig');
90  figure(13) = hgload('Potential theory, non-dimensional Added mass per frequency [Hz] ...
        for draft3.fig');
91  figure(14) = hgload('Potential theory, non-dimensional Added mass per frequency [Hz] ...
        for draft4.fig');
92  figure(15) = hgload('Potential theory, non-dimensional Added mass per frequency [Hz] ...
        for draft5.fig');
93
94  % 2) Prepare subplots
95
96  figure%('units','normalized','outerposition',[0 0 1 1])
97  h(2)=subplot(1,1,1);
98
99  copyobj(allchild(get(figure(11),'CurrentAxes')),h(2));
100 copyobj(allchild(get(figure(12),'CurrentAxes')),h(2));
101 copyobj(allchild(get(figure(13),'CurrentAxes')),h(2));
102 copyobj(allchild(get(figure(14),'CurrentAxes')),h(2));
103 copyobj(allchild(get(figure(15),'CurrentAxes')),h(2));
104 naam = 'Potential theory Dimensionless Added mass-Draft relation';
105 title(naam);
106 ylim([0 2.2])
107 grid on
108 legend('Draft 1','Draft 2','Draft 3','Draft 4','Draft 5')
109 saveas(gcf, naam);
110 saveas(gcf, naam, 'jpg');
111
112 %% Potential Damping
113 % 1) Load saved figures
114 figure(16) = hgload('Potential theory, non-dimensional Damping per frequency [Hz] for ...
        draft1.fig');
115 figure(17) = hgload('Potential theory, non-dimensional Damping per frequency [Hz] for ...
        draft2.fig');
116 figure(18) = hgload('Potential theory, non-dimensional Damping per frequency [Hz] for ...
        draft3.fig');
117 figure(19) = hgload('Potential theory, non-dimensional Damping per frequency [Hz] for ...
        draft4.fig');
118 figure(20) = hgload('Potential theory, non-dimensional Damping per frequency [Hz] for ...
        draft5.fig');
119
120 % 2) Prepare subplots
121
122 figure%('units','normalized','outerposition',[0 0 1 1])
123 h(2)=subplot(1,1,1);
124
125 copyobj(allchild(get(figure(16),'CurrentAxes')),h(2));
126 copyobj(allchild(get(figure(17),'CurrentAxes')),h(2));
127 copyobj(allchild(get(figure(18),'CurrentAxes')),h(2));
128 copyobj(allchild(get(figure(19),'CurrentAxes')),h(2));
129 copyobj(allchild(get(figure(20),'CurrentAxes')),h(2));
130
131 naam = 'Potential theory Dimensionless Damping-Draft relation';
132 title(naam);
133 ylim([0 0.4])
134 grid on
135 legend('Draft 1','Draft 2','Draft 3','Draft 4','Draft 5')
136 saveas(gcf, naam);
137 saveas(gcf, naam, 'jpg');
138 toc
139 close all
140
141 %% Dimensionless Damping
142
143 % 1) Load saved figures
144 figure(21) = hgload('Dimensionless damping per frequency [Hz] for draft1.fig');
```

```
figure(22) = hgload('Dimensionless damping per frequency [Hz] for draft2.fig');
figure(23) = hgload('Dimensionless damping per frequency [Hz] for draft3.fig');
figure(24) = hgload('Dimensionless damping per frequency [Hz] for draft4.fig');
figure(25) = hgload('Dimensionless damping per frequency [Hz] for draft5.fig');

% 2) Prepare subplots

figure%('units','normalized','outerposition',[0 0 1 1])
h(2)=subplot(1,1,1);

copyobj(allchild(get(figure(21),'CurrentAxes')),h(2));
copyobj(allchild(get(figure(22),'CurrentAxes')),h(2));
copyobj(allchild(get(figure(23),'CurrentAxes')),h(2));
copyobj(allchild(get(figure(24),'CurrentAxes')),h(2));
copyobj(allchild(get(figure(25),'CurrentAxes')),h(2));
naam = 'Experiments Dimensionless Damping-frequency relation';
title(naam);
ylim([0 0.6])
grid on

legend('Draft 1','Draft 2','Draft 3','Draft 4','Draft 5')
saveas(gcf, naam);
saveas(gcf, naam, 'jpg');
```

D.4. Non-linear Damping

```
%%% //\\ Jasper Stokkermans //\\ %%%
% Thesis Boskalis: Added Mass SBJ
% ==== Non-linear Damping ====
% ==== Viscous vs friction ====
% ==== May 2018 ====

clc
clear all
close all
tic

%% ==== Load data ====

freq    = 1:8; series  = 1:3;
M_0     = 21.5;                    % [kg]
draft   = 5;
Draft   = (draft-1)*0.125;         % [m]

d=dir('C:\Users\STOK\OneDrive - boskalis.com\Thesis\2000_Matlab\Draft_5\*.csv');
input_ = cell(1,length(d));
for i = 1:length(d);
input_{i}  = d(i).name ;
pdd{i}     = d(i).folder;
end
fl  = input_; pd  = pdd{1};

input_ = cell(1,length(d));

%% Write matrices for loadcell, accelerometer1 and accelerometer2

r_loadcell_path          = cell(1,3);  % 3 = #redundancy series.     [rows = freq 1:8, ...
    cols = serie 1:3]
r_accelerometer1_path    = cell(1,3);
r_accelerometer2_path    = cell(1,3);

for ii = freq              % #freqs
for i = series         % #metingen per freq
d_f_l = 9*ii+i-9;
r_loadcell_raw{ii,i} =  d(d_f_l).name;
r_loadcell_path{ii,i} =  strcat(pd,'\',d(d_f_l).name);
d_f_a2 = 9*ii+i-3;
r_accelerometer2_raw{ii,i} =  d(d_f_a2).name;
```

```
r_accelerometer2_path{ii,i} =  strcat(pd,'\',d(d_f_a2).name);
d_f_a1 = 9*ii+i-6;
r_accelerometer1_raw{ii,i} =  d(d_f_a1).name;
r_accelerometer1_path{ii,i} =  strcat(pd,'\',d(d_f_a1).name);
end
end

% PERIOD    FREQ    M   M   M   M   M   M   M   M   M   M   M   M       FREQ        M
% (SECS)    (RAD/S) 11  22  33  44  55  66  13  15  24  26  35  46      (RAD/S) Hz  11



clear d_f_l; clear d_f_a2; clear d_f_a1; clear input_; clear pd; clear pdd;
%% Read date to serial string - Loadcell

flNm                    = r_loadcell_path;
flNm2                   = r_accelerometer2_path;
flNm3                   = r_accelerometer1_path;
R_data_loadcell         = cell(8,3);
R_data_accelerometer2   = cell(8,3);
R_data_accelerometer1   = cell(8,3);
x_zero_crossing         = cell(8,3);
t_zero                  = cell(8,3);
t_z                     = cell(8,3);
V_max                   = cell(8,3);
r_loadcell_data         = cell(8,3);
r_loadcell_data_cut     = cell(8,3);
f_avg                   = cell(8,3);
T_avg                   = cell(8,3);

%%  Add date string to matrix
for ii      = freq;             % #freqs
for i   = series;           % #metingen per freq

[r_loadcell_data{ii,i}, msg]    = data_read1(flNm{ii,i});
assignin('base','data', r_loadcell_data(ii,i))    % copy data to workspace
R_data_loadcell{ii,i} = [r_loadcell_data{ii,i}.cols    r_loadcell_data{ii,i}.dateser];
end
end

%% Find V_max, t_cut and reflection time

for ii          = freq;             % #freqs
for i   = series;           % #series

V_max{ii,i}                     = 0.973.*max(R_data_loadcell{ii,i}(:,4));
[t_cut{ii,i}  V_cut{ii,i}]      = find(R_data_loadcell{ii,i}(:,4) > ...
    V_max{ii,i},1,'first');
r_loadcell_data_cut{ii,i}       = r_loadcell_data{ii,i}.cols(t_cut{ii,i}:end,:);      % ...
    new dataset with first part removed

re{ii,i}            = r_loadcell_data{ii,i}.cols(2,1);          % time resolution per ...
    test
res                 = cell2mat(re(1));                          % time resolution sensor
clear V_cut V_max msg;

% Now find first zero up crossing Loadcell and Displacement

x_zero_crossing{ii,i} = detrend((r_loadcell_data_cut{ii,i}(:,3)))/100; % [m]


t_z{ii,i} = crossing(x_zero_crossing{ii,i}(1:end));

t_zero{ii,i} = t_z{ii,i}+t_cut{ii,i}(1)';

% Show difference in initial frequency and actual frequency
T_avg{ii,i}             = mean(diff(t_zero{ii,i}))*res*2;       % sine has 2 zero ...
    crossings
f_act{ii,i}              = 1./T_avg{ii,i};

%----
```

```
109 if t_zero{ii,i}(1,1) < t_cut{ii,i} % error message if crossing is before cutoff time
110 error('zero crossing is in build up range of signal!');
111 end
112 %----
113 if r_loadcell_data_cut{ii,i}((t_cut{ii,i}(1)-1),2)> 0 % zero up crossing, if ...
        t_cut-1>0, go to next zero crossing
114 t_zero = t_zero(1);
115 end
116 %----
117 if abs(r_loadcell_data_cut{ii,i}(t_cut{ii,i},3)-mean(r_loadcell_data_cut{ii,i}(:,3)))> 5
118 error('Volt (r_loadcell_data_cut(:4)) is a noisy signal! review V_max= 97.5%');
119 end
120 end
121 zero_cross_freq(ii)          = mean([f_act{ii,1} f_act{ii,2} f_act{ii,3}]);
122 end
123 f_act_ = cell2mat(f_act);
124
125
126 %% FFT spectrum: f1
127
128 figure('units','normalized','outerposition',[0 0 1 1])
129 for      f = 1; %freq;
130 for s = 1; %series;
131 Y_f = fft(detrend((r_loadcell_data_cut{f,s}(:,2))).*9.81);      % [N] .*9.81 from kg to N
132 Y_x = fft(detrend((r_loadcell_data_cut{f,s}(:,3))));            % displacement
133 L = length(r_loadcell_data_cut{f,s}(:,2));
134
135 P2           = abs(Y_f/L);
136 P1           = P2(1:L/2+1);
137 P1(2:end-1) = 2*P1(2:end-1);
138
139 %Define the frequency domain f and plot the single-sided amplitude spectrum P1.
140 fr = 1/res*(0:(L/2))/L;
141
142 pks = findpeaks(P1);
143 [pks,locs]       = findpeaks(P1);
144 [pks,locs,w,p]   = findpeaks(P1); %[peakvalue, location peak, width peak, prominence of ...
        peaks]
145 X                = [pks,locs,w,p];
146 HZ               = sortrows(X, 'descend'); clear X
147
148 Dominant_FFT_fr = HZ(1,2)/res*(0:(L/2))/L;
149 Dominant_FFT_freq = Dominant_FFT_fr(2);
150
151 zero_cross_freq;
152 Dominant_FFT_freq;
153
154 plot(fr,P1,'r','LineWidth',2)
155 line([Dominant_FFT_fr(2)-res Dominant_FFT_fr(2)-res], [0 70],'LineWidth',1.5);
156 line([2*Dominant_FFT_fr(2)-res     2*Dominant_FFT_fr(2)-res], [0 70],'LineWidth',1.5);
157 line([3*(Dominant_FFT_fr(2)-res)   3*(Dominant_FFT_fr(2)-res)], [0 70],'LineWidth',1.5);
158 line([4*(Dominant_FFT_fr(2)-res)   4*(Dominant_FFT_fr(2)-res)], [0 70],'LineWidth',1.5);
159 line([5*(Dominant_FFT_fr(2)-res)   5*(Dominant_FFT_fr(2)-res)], [0 70],'LineWidth',1.5);
160 line([6*(Dominant_FFT_fr(2)-res)   6*(Dominant_FFT_fr(2)-res)], [0 70],'LineWidth',1.5);
161 line([7*(Dominant_FFT_fr(2)-res)   7*(Dominant_FFT_fr(2)-res)], [0 70],'LineWidth',1.5);
162 line([8*(Dominant_FFT_fr(2)-res)   8*(Dominant_FFT_fr(2)-res)], [0 70],'LineWidth',1.5);
163 line([9*(Dominant_FFT_fr(2)-res)   9*(Dominant_FFT_fr(2)-res)], [0 70],'LineWidth',1.5);
164 line([10*(Dominant_FFT_fr(2)-res) 10*(Dominant_FFT_fr(2)-res)], [0 70],'LineWidth',1.5);
165 line([11*(Dominant_FFT_fr(2)-res) 11*(Dominant_FFT_fr(2)-res)], [0 70],'LineWidth',1.5);
166 xlim([0 8])
167
168 end
169 end
170 grid on
171 titel1 = strcat('Single-Sided Amplitude Spectrum of F(t)- Draft ', num2str(draft),' ...
        Frequency1');
172 title(titel1)
173 legend('FFT spectrum','Harmonics')
174 xlabel('f (Hz)')
175 ylabel('|P1(f)|')
176
```

```
P1           = P2(1:L/2+1);
P1(2:end-1) = 2*P1(2:end-1);
%% Viscous vs Friction f1

[pks2,locs2] = findpeaks(P1);
PL = [pks2,locs2];
S  = sort(pks2);
A1 = max(P1)
A3 = S(end-1)

syms  A_f1 A_d1 ;

eqns = [A_f1*2/pi+A_d1*8/(3*pi)-A1==0  A_f1*-2/pi+8/(15*pi)*A_d1-A3==0];
vars = [A_f1 A_d1];
[sol_f, sol_d] = solve(eqns,vars);

A_f1 = double(sol_f)
A_d1 = double(sol_d)

%%  FFT spectrum: f8

figure('units','normalized','outerposition',[0 0 1 1])
for      f = 8 %freq;
for s = 1 %series;
Y_f = fft(detrend((r_loadcell_data_cut{f,s}(:,2))).*9.81);      % [N] .*9.81 from kg to N
Y_x = fft(detrend((r_loadcell_data_cut{f,s}(:,3))));            % displacement
L = length(r_loadcell_data_cut{f,s}(:,2));

P2           = abs(Y_f/L);
P1           = P2(1:L/2+1);
P1(2:end-1) = 2*P1(2:end-1);

%Define the frequency domain f and plot the single-sided amplitude spectrum P1.
fr = 1/res*(0:(L/2))/L;

pks = findpeaks(P1);
[pks,locs]       = findpeaks(P1);
[pks,locs,w,p]   = findpeaks(P1);  %[peakvalue, location peak, width peak, prominence of ...
    peaks]
X                = [pks,locs,w,p];
HZ               = sortrows(X, 'descend'); clear X

Dominant_FFT_fr = HZ(1,2)/res*(0:(L/2))/L;
Dominant_FFT_freq = Dominant_FFT_fr(2);

zero_cross_freq;
Dominant_FFT_freq;

plot(fr,P1,'r','LineWidth',2)
line([Dominant_FFT_fr(2)-res Dominant_FFT_fr(2)-res], [0 400],'LineWidth',1.5);
line([2*Dominant_FFT_fr(2)-res   2*Dominant_FFT_fr(2)-res], [0 400],'LineWidth',1.5);
line([3*(Dominant_FFT_fr(2)-res)  3*(Dominant_FFT_fr(2)-res)], [0 400],'LineWidth',1.5);
line([4*(Dominant_FFT_fr(2)-res)  4*(Dominant_FFT_fr(2)-res)], [0 400],'LineWidth',1.5);
line([5*(Dominant_FFT_fr(2)-res)  5*(Dominant_FFT_fr(2)-res)], [0 400],'LineWidth',1.5);
line([6*(Dominant_FFT_fr(2)-res)  6*(Dominant_FFT_fr(2)-res)], [0 400],'LineWidth',1.5);
line([7*(Dominant_FFT_fr(2)-res)  7*(Dominant_FFT_fr(2)-res)], [0 400],'LineWidth',1.5);
line([8*(Dominant_FFT_fr(2)-res)  8*(Dominant_FFT_fr(2)-res)], [0 400],'LineWidth',1.5);
line([9*(Dominant_FFT_fr(2)-res)  9*(Dominant_FFT_fr(2)-res)], [0 400],'LineWidth',1.5);
line([10*(Dominant_FFT_fr(2)-res) 10*(Dominant_FFT_fr(2)-res)], [0 400],'LineWidth',1.5);
line([11*(Dominant_FFT_fr(2)-res) 11*(Dominant_FFT_fr(2)-res)], [0 400],'LineWidth',1.5);
xlim([0 10])

end
end
grid on
titel1 = strcat('Single-Sided Amplitude Spectrum of F(t)- Draft', num2str(draft),' ...
    Frequency8');
title(titel1)
legend('FFT spectrum','Harmonics')
xlabel('f (Hz)')
ylabel('|P1(f)|')
```

```
246
247 P1           = P2(1:L/2+1);
248 P1(2:end-1) = 2*P1(2:end-1);
249 %% Viscous vs Friction f8
250
251 [pks2,locs2] = findpeaks(P1);
252 PL = [pks2,locs2];
253 S  = sort(pks2);
254 A1 = max(P1)
255 A3 = S(end-1)
256
257 syms  A_f8 A_d8 ;
258
259 eqns = [A_f8*2/pi+A_d8*8/(3*pi)-A1==0  A_f8*-2/pi+8/(15*pi)*A_d8-A3==0];
260 vars = [A_f8 A_d8];
261 [sol_f, sol_d] = solve(eqns,vars);
262
263 A_f8 = double(sol_f)
264 A_d8 = double(sol_d)
```

D.5. Results

All vectors and matrices must be read as [frequency x series];

$$[matrix] = \begin{bmatrix} f_1, serie_1 & f_1, serie_2 & f_1, serie_3 \\ f_2, serie_1 & f_2, serie_2 & f_2, serie_3 \\ f_3, serie_1 & f_3, serie_2 & f_3, serie_3 \\ f_4, serie_1 & f_4, serie_2 & f_4, serie_3 \\ f_5, serie_1 & f_5, serie_2 & f_5, serie_3 \\ f_6, serie_1 & f_6, serie_2 & f_6, serie_3 \\ f_7, serie_1 & f_7, serie_2 & f_7, serie_3 \\ f_8, serie_1 & f_8, serie_2 & f_8, serie_3 \end{bmatrix}$$

$$[vector] = \begin{bmatrix} f_1 \\ f_2 \\ f_3 \\ f_4 \\ f_5 \\ f_6 \\ f_7 \\ f_8 \end{bmatrix}$$

D.5.1. Draft 1 raw data

```
lambda_0 =

9.4484    7.8340    6.3078    5.0026    3.8485    2.8035    1.9585    1.2367


k_0d =

0.6650    0.8020    0.9961    1.2560    1.6326    2.2412    3.2082    5.0805


n =

0.6891    0.6681    0.6384    0.6025    0.5624    0.5253    0.5052    0.5002


cg =

2.0186    1.9056    1.7466    1.5525    1.3270    1.0867    0.8821    0.6950


t_refl =

9.9078   10.4956   11.4507   12.8825   15.0717   18.4036   22.6742   28.7758


initial_freq =

0.4100    0.4500    0.5000    0.5600    0.6400    0.7500    0.8900    1.1200


phi_deg_ =

-80.4377  -80.4377  -80.4377
-173.6235   33.7296  -10.9776
161.5670   21.2302 -107.3342
-92.0496  -14.4468  165.6863
11.8352 -125.3100 -173.3634
-145.0904  -73.8924  122.5751
-167.7532  -92.0421   28.5411
179.8264  -24.0408   58.5641
```

```
F_ampl_ =

30.0821   30.0821   30.0821
41.9426   41.2094   41.2661
41.2410   40.8922   40.9787
41.8095   41.8230   41.8760
44.1717   44.0417   44.0122
47.6909   47.4823   47.4138
52.9658   52.6127   52.7627
59.8678   59.7729   59.8240


error_ =

348.0885  348.0885  348.0885
504.9375  497.2454  497.6500
510.7746  509.5058  505.1198
509.1463  511.7336  515.5265
523.4996  525.8184  518.0636
515.9510  521.7189  515.7474
499.2212  499.1821  498.5052
494.5770  488.8433  491.3387


F_ampl_avg =

59.8216


phi_x_deg_ =

174.5913  174.5913  174.5913
87.1270  -66.0348 -110.5897
55.3139  -84.6378  146.6661
154.5526 -127.2813   52.7617
-108.9580  114.0706   65.7811
87.3693  158.3284   -5.2620
56.8861  132.3858 -106.8253
37.2678 -166.2479  -83.5857


x_ampl_ =

0.0373    0.0373    0.0373
0.0411    0.0411    0.0410
0.0410    0.0410    0.0411
0.0411    0.0411    0.0411
0.0411    0.0411    0.0411
0.0411    0.0411    0.0411
0.0412    0.0411    0.0411
0.0413    0.0413    0.0413


error_x_ =

0.0886    0.0886    0.0886
0.0378    0.0337    0.0428
0.0472    0.0450    0.0323
0.0403    0.0326    0.0394
0.0366    0.0476    0.0341
0.0362    0.0384    0.0371
0.0275    0.0569    0.0521
0.0530    0.0354    0.0387


x_ampl_avg =

0.0413
```

```
113
114 KC_ =
115
116 0.4687
117 0.5161
118 0.5160
119 0.5162
120 0.5161
121 0.5165
122 0.5173
123 0.5189
124
125
126 phi_diff =
127
128 104.9710  104.9710  104.9710
129 99.2495   99.7644   99.6121
130 106.2531  105.8680  105.9996
131 113.3978  112.8345  112.9246
132 120.7932  120.6194  120.8555
133 127.5403  127.7792  127.8370
134 135.3607  135.5721  135.3664
135 142.5586  142.2071  142.1498
136
137
138 M_vol_kg =
139
140 0
141
142
143 M_a_kg_avg_ =
144
145 6.8375
146 -5.7103
147 -3.3970
148 -2.5367
149 -1.6666
150 -1.2697
151 -0.3937
152 0.1717
153
154
155 M_a_norm =
156
157 Inf
158 -Inf
159 -Inf
160 -Inf
161 -Inf
162 -Inf
163 -Inf
164 -Inf
165
166 Elapsed time is 82.810383 seconds.
```

D.5.2. Draft 2 raw data

```
1
2 lambda_0 =
3
4 9.4484    7.8340    6.3078    5.0026    3.8485    2.8035    1.9585    1.2367
5
6
7 k_0d =
8
9 0.6650    0.8020    0.9961    1.2560    1.6326    2.2412    3.2082    5.0805
10
11
```

```
n =

0.6891    0.6681    0.6384    0.6025    0.5624    0.5253    0.5052    0.5002


cg =

2.0186    1.9056    1.7466    1.5525    1.3270    1.0867    0.8821    0.6950


t_refl =

9.9078   10.4956   11.4507   12.8825   15.0717   18.4036   22.6742   28.7758


initial_freq =

0.4100    0.4500    0.5000    0.5600    0.6400    0.7500    0.8900    1.1200


phi_deg_ =

-8.9447   -160.5403 -148.1603
-32.2402   21.8196   106.1192
 93.5501   85.8559  -107.6762
-73.3543   76.6879   89.2879
 147.6126 -55.1312   85.2054
 48.1491   156.4931 -34.4011
 124.0571  116.1460  43.9958
 136.0689  11.7766   83.6085


F_ampl_ =

33.2844   32.5926   32.5554
51.6618   51.2217   51.4326
58.3612   56.9980   58.0753
73.5701   73.2759   72.7961
92.3066   93.6208   94.1386
114.6699  114.6883  114.5559
144.5874  143.8682  144.5884
181.9269  181.8718  170.7614


error_ =

366.2827  347.4046  353.0079
529.0955  473.9764  536.1800
592.6031  597.9628  593.6168
593.5388  529.6904  593.4034
597.5734  587.3374  593.6331
643.4197  647.0593  654.0159
657.6976  679.2222  648.0106
622.3803  647.8707  665.0797


F_ampl_avg =

178.1867


phi_x_deg_ =

-120.2625  87.0285   99.2707
-141.7577 -87.4116  -3.3411
-24.2059  -32.6072   134.4820
 159.9752 -49.8586  -37.9968
 15.2054   172.6835 -47.0021
-87.2240   21.3829  -170.2892
-13.0104  -21.2535  -93.2873
 1.4552   -122.9382 -53.5027
```

```
x_ampl_ =

   0.0409    0.0409    0.0409
   0.0410    0.0410    0.0410
   0.0410    0.0410    0.0409
   0.0410    0.0410    0.0411
   0.0412    0.0412    0.0412
   0.0412    0.0412    0.0413
   0.0413    0.0413    0.0413
   0.0413    0.0413    0.0413


error_x_ =

   0.0474    0.0444    0.0380
   0.0392    0.0352    0.0477
   0.0442    0.0359    0.0445
   0.0405    0.0514    0.0421
   0.0380    0.0378    0.0384
   0.0315    0.0375    0.0307
   0.0400    0.0479    0.0348
   0.0328    0.0312    0.0369


x_ampl_avg =

   0.0413


KC_ =

   0.5142
   0.5149
   0.5148
   0.5156
   0.5177
   0.5180
   0.5189
   0.5189


phi_diff =

  111.3178  112.4312  112.5690
  109.5175  109.2312  109.4603
  117.7560  118.4631  117.8418
  126.6705  126.5465  127.2847
  132.4073  132.1854  132.2075
  135.3731  135.1102  135.8880
  137.0675  137.3995  137.2831
  134.6137  134.7148  137.1112


M_vol_kg =

   24.5437


M_a_kg_avg_ =

   23.3753
   18.2437
   21.5297
   26.9655
   30.4020
   31.0086
   32.9445
   37.2266
```

```
154
155 M_a_norm =
156
157 0.9524
158 0.7433
159 0.8772
160 1.0987
161 1.2387
162 1.2634
163 1.3423
164 1.5167
165
166 Elapsed time is 88.827474 seconds.
167 >>
```

D.5.3. Draft 3 raw data

```
1
2 lambda_0 =
3
4 9.4484    7.8340    6.3078    5.0026    3.8485    2.8035    1.9585    1.2367
5
6
7 k_0d =
8
9 0.6650    0.8020    0.9961    1.2560    1.6326    2.2412    3.2082    5.0805
10
11
12 n =
13
14 0.6891    0.6681    0.6384    0.6025    0.5624    0.5253    0.5052    0.5002
15
16
17 cg =
18
19 2.0186    1.9056    1.7466    1.5525    1.3270    1.0867    0.8821    0.6950
20
21
22 t_refl =
23
24 9.9078   10.4956   11.4507   12.8825   15.0717   18.4036   22.6742   28.7758
25
26
27 initial_freq =
28
29 0.4100    0.4500    0.5000    0.5600    0.6400    0.7500    0.8900    1.1200
30
31
32 phi_deg_ =
33
34  48.4831   83.3479  -129.7754
35 -45.1513  -91.2489   115.9955
36  117.4338 -74.5866  -33.4916
37  42.5941  -105.8893  118.3596
38  52.7729   142.6531  -52.2755
39 -153.7166 -131.1061 -125.8386
40  169.9846  50.2655  -116.1119
41  61.0618   115.9686   2.1534
42
43
44 F_ampl_ =
45
46 39.3128   39.5272   38.1906
47 67.3595   64.7277   65.1788
48 83.9885   84.4802   84.9446
49 118.4121  112.0823  117.9701
50 161.4661  160.1676  162.2748
51 214.9955  214.9904  212.9233
```

```
  348.4845  345.3586  337.3227
  398.3130  399.4775  385.2123


error_ =

1.0e+03 *

  0.4709    0.4584    0.4078
  0.5599    0.6299    0.6138
  0.7037    0.7267    0.7212
  0.7592    0.7265    0.7233
  0.8245    0.7864    0.8179
  0.9606    0.9714    0.9193
  3.7288    3.8000    3.7188
  4.5477    4.5992    4.3969


F_ampl_avg =

  394.3343


phi_x_deg_ =

 -75.1118  -41.6569  105.3909
-170.9792  145.6112   -7.1491
 -19.3273  148.8747 -169.5793
 -99.0294  113.5926  -19.6574
 -87.5828    2.0581  167.5891
  65.4621   88.1084   93.5582
  56.2788  -62.9043  130.3868
 -48.2930    6.8155 -107.4477


x_ampl_ =

  0.0409    0.0410    0.0407
  0.0411    0.0412    0.0411
  0.0412    0.0412    0.0412
  0.0413    0.0412    0.0413
  0.0414    0.0413    0.0413
  0.0414    0.0414    0.0414
  0.0405    0.0404    0.0405
  0.0405    0.0405    0.0405


error_x_ =

  0.0581    0.0370    0.0760
  0.0339    0.0340    0.0344
  0.0290    0.0433    0.0364
  0.0337    0.0398    0.0409
  0.0372    0.0376    0.0489
  0.0406    0.0411    0.0366
  0.0342    0.0585    0.0568
  0.0453    0.0546    0.0523


x_ampl_avg =

  0.0405


KC_ =

  0.5137
  0.5165
  0.5176
  0.5185
  0.5193
```

```
0.5206
0.5084
0.5087


phi_diff =

123.5949  125.0048  124.8337
125.8279  123.1399  123.1446
136.7611  136.5387  136.0876
141.6235  140.5181  138.0171
140.3558  140.5950  140.1354
140.8213  140.7855  140.6032
113.7057  113.1699  113.5012
109.3549  109.1531  109.6010


M_vol_kg =

49.0874


M_a_kg_avg_ =

64.2566
64.8586
73.3459
75.9852
79.4346
84.0098
47.5824
40.5820


M_a_norm =

1.3090
1.3213
1.4942
1.5480
1.6182
1.7114
0.9693
0.8267

Elapsed time is 95.790762 seconds.
>>
```

D.5.4. Draft 4 raw data

```

lambda_0 =

9.4484    7.8340    6.3078    5.0026    3.8485    2.8035    1.9585    1.2367


k_0d =

0.6650    0.8020    0.9961    1.2560    1.6326    2.2412    3.2082    5.0805


n =

0.6891    0.6681    0.6384    0.6025    0.5624    0.5253    0.5052    0.5002


cg =

```

```
 2.0186    1.9056    1.7466    1.5525    1.3270    1.0867    0.8821    0.6950


t_refl =

 9.9078   10.4956   11.4507   12.8825   15.0717   18.4036   22.6742   28.7758


initial_freq =

 0.4100    0.4500    0.5000    0.5600    0.6400    0.7500    0.8900    1.1200


phi_deg_ =

 -76.5056  -99.7820  -26.2785
  -5.9702   41.2941 -132.4882
 -37.6311  120.8145  101.4517
 124.5650   34.0532  175.0142
 -81.9363   89.5224  160.0413
 141.4347  -15.9759 -143.2288
  53.2213 -117.9685   59.6586
 -74.2985   91.3163  -65.5254


F_ampl_ =

  51.6717   52.0724   49.9816
  79.7110   74.5679   86.7564
 116.9330  116.4116  112.8627
 153.6312  182.0322  163.8045
 236.4572  221.1369  219.8514
 304.6184  307.3323  289.1897
 394.9873  398.5548  400.2556
 401.9248  402.4526  399.3172


error_ =

 1.0e+03 *

 0.5010    0.4737    0.4888
 0.6186    0.5732    0.6003
 1.2179    1.1246    1.1797
 0.9890    1.0484    0.9409
 1.0980    1.0254    0.9690
 1.1492    1.1880    1.1634
 1.8360    1.8091    1.7352
 2.0744    2.1546    2.0117


F_ampl_avg =

 401.2315


phi_x_deg_ =

 148.7964  125.4793 -162.9908
-149.3193  -93.6679   94.6846
 170.9755  -30.6242  -50.9743
 -25.7807 -112.1114   34.6681
 132.5427  -52.5916   12.2267
  -2.6928 -160.5230   71.4772
 -79.5353  109.7791  -72.4472
 156.7519  -37.2714  165.4960


x_ampl_ =

 0.0411    0.0411    0.0411
```

```
0.0415    0.0413    0.0414
0.0415    0.0415    0.0415
0.0415    0.0416    0.0415
0.0415    0.0415    0.0415
0.0416    0.0416    0.0416
0.0408    0.0407    0.0407
0.0408    0.0407    0.0407


error_x_ =

0.0470    0.0544    0.0480
0.0403    0.0323    0.0370
0.0606    0.0380    0.0504
0.0552    0.0347    0.0462
0.0348    0.0426    0.0474
0.0325    0.0523    0.0501
0.0354    0.0341    0.0325
0.0306    0.0453    0.0549


x_ampl_avg =

0.0407


KC_ =

0.5164
0.5200
0.5213
0.5218
0.5219
0.5227
0.5119
0.5119


phi_diff =

134.6980  134.7387  136.7123
143.3491  134.9620  132.8273
151.3934  151.4387  152.4259
150.3457  146.1647  140.3462
145.5210  142.1140  147.8147
144.1275  144.5471  145.2940
132.7566  132.2524  132.1058
128.9496  128.5876  128.9786


M_vol_kg =

73.6311


M_a_kg_avg_ =

114.4868
111.5817
128.5723
126.6301
127.8960
131.5402
111.7476
96.7242


M_a_norm =

1.5549
1.5154
```

```
1.7462
1.7198
1.7370
1.7865
1.5177
1.3136

Elapsed time is 87.418054 seconds.
```

D.5.5. Draft 5 raw data

```
lambda_0 =

9.4484    7.8340    6.3078    5.0026    3.8485    2.8035    1.9585    1.2367


k_0d =

0.6650    0.8020    0.9961    1.2560    1.6326    2.2412    3.2082    5.0805


n =

0.6891    0.6681    0.6384    0.6025    0.5624    0.5253    0.5052    0.5002


cg =

2.0186    1.9056    1.7466    1.5525    1.3270    1.0867    0.8821    0.6950


t_refl =

9.9078   10.4956   11.4507   12.8825   15.0717   18.4036   22.6742   28.7758


initial_freq =

0.4100    0.4500    0.5000    0.5600    0.6400    0.7500    0.8900    1.1200


phi_deg_ =

 87.9718    88.6609    58.4091
 55.5637    11.4371  -144.2810
-148.6333   29.9292  -138.5301
-10.0871  -119.8802    6.3383
 106.7357   170.0724    9.3357
-138.3873  -46.3685    39.3003
-122.4291   17.7651  -151.7445
-63.0969    82.5812    151.9657


F_ampl_ =

72.7686   65.9464   67.0368
112.9018  110.3817  100.3054
138.5234  138.9717  137.7991
236.4894  234.5861  243.9489
289.3685  289.5416  300.5671
370.8475  372.9448  372.8757
467.3316  463.9499  456.6662
463.6516  472.5861  468.2318


error_ =

1.0e+03 *
```

```
58
59  0.5329     0.5192     0.6756
60  0.7590     0.7366     0.7177
61  1.0743     1.0233     1.0026
62  1.1524     1.0985     1.2348
63  1.3038     1.5910     1.7055
64  1.5747     1.5544     1.5659
65  1.9904     2.2024     1.9787
66  2.3965     2.4979     2.2431
67
68
69  F_ampl_avg = 468.1565
70
71
72  phi_x_deg_ =
73
74  -54.8892   -50.4381    -75.1620
75  -90.9923   -136.0337    75.2335
76   58.9196   -126.1215    65.9773
77  -155.6851   99.4209    -138.6338
78  -35.8654    29.2386    -128.4744
79   77.0313    168.5428   -105.3727
80   101.1887  -118.3797    72.3643
81   163.3263  -49.9157     18.9999
82
83
84  x_ampl_ =
85
86  0.0413     0.0412     0.0411
87  0.0415     0.0415     0.0414
88  0.0416     0.0416     0.0416
89  0.0417     0.0416     0.0416
90  0.0416     0.0415     0.0415
91  0.0416     0.0416     0.0416
92  0.0409     0.0409     0.0409
93  0.0408     0.0408     0.0408
94
95
96  error_x_ =
97
98  0.0403     0.0590     0.0445
99  0.0340     0.0407     0.0407
100 0.0382     0.0345     0.0363
101 0.0408     0.0389     0.0471
102 0.0411     0.0418     0.0379
103 0.0550     0.0350     0.0521
104 0.0365     0.0379     0.0320
105 0.0353     0.0316     0.0372
106
107
108 x_ampl_avg = 0.0408
109
110
111 KC_ =
112
113 0.5177
114 0.5213
115 0.5229
116 0.5230
117 0.5219
118 0.5226
119 0.5137
120 0.5129
121
122
123 phi_diff =
124
125 142.8610   139.0990   133.5711
126 146.5559   147.4708   140.4855
127 152.4471   156.0507   155.4926
128 145.5980   140.6989   144.9721
```

```
129  142.6011   140.8338   137.8102
130  144.5813   145.0887   144.6729
131  136.3822   136.1448   135.8912
132  133.5768   132.4969   132.9658
133
134
135  M_vol_kg = 98.1748
136
137
138  M_a_kg_avg_ =
139
140  168.5983
141  180.1002
142  167.5454
143  187.6782
144  158.7253
145  167.9803
146  141.0109
147  127.7180
148
149
150  M_a_norm =
151
152  1.7173
153  1.8345
154  1.7066
155  1.9117
156  1.6168
157  1.7110
158  1.4363
159  1.3009
160
161  Elapsed time is 121.009360 seconds.
```

Bibliography

[1] 4C Offshore. Offshore Wind Support Structures, 2016, (Accessed: December 2017). URL http://www.4coffshore.com/windfarms/support-structures-for-offshore-wind-turbines-aid268.html.

[2] H.B. Amey and G.B.s Pomonik. Added Mass and Damping of Submerged Bodies Oscillating Near the Surface. *4th Offshore Technology Conference*, 1972. URL https://www.onepetro.org/conference-paper/OTC-1557-MS.

[3] T. Balkema. Hydrodynamic loads on an inclined cylinder in the wave zone. 2018.

[4] C. et al. Beels. Wave energy resource in the north sea. *7th European Wave and Tidal Energy Conference*, 2007.

[5] Boskalis. Boskalis annual report 2017, 2018 (Accessed: March 2018). URL https://boskalis.com/nl/pers/persberichten-en-bedrijfsnieuws/detail/boskalis-publiceert-jaarverslag-en-csr-verslag-2017.html.

[6] Chakrabarti. Hydrodynamics of offshore structures, 1987.

[7] Henrik Bisgaard Clausen and Ronnie Refstrup. Advanced framework for suction bucket jacket design. 2017.

[8] Gunther Clauss, Eike Lehmann, and C Ostergaard. Offshore structures, vol. 1: Conceptual design and hydrodynamics, 1992.

[9] Russell Davidson and James G Mackinnon. Regression Models 1.1. 1999.

[10] Wybren de Vries. Support Structure Concepts for Deep Water Sites (WP 4.2 Final Report). *Project UpWind*, 2011.

[11] João Gorenstein Dedecca, Rudi A. Hakvoort, and J. Roland Ortt. Market strategies for offshore wind in Europe: A development and diffusion perspective. *Renewable and Sustainable Energy Reviews*, 2016 (Accessed: October 2017). URL http://dx.doi.org/10.1016/j.rser.2016.08.007.

[12] N. T. Van Doorn. Environmental limitations in suction bucket based jacket foundation installation, using vertical lift-off from a jack-up vessel. 2016.

[13] Odd Faltinsen. *Sea loads on ships and offshore structures*, volume 1. Cambridge university press, 1993.

[14] Odd Magnus Faltinsen and Alexander N Timokha. *Sloshing*, volume 577. Cambridge university press Cambridge, 2009.

[15] David J Griffiths. *Introduction to quantum mechanics*. Cambridge University Press, 2016.

[16] GWEC Global Wind. offshore wind, 2017 (Accessed: October 2017). URL http://gwec.net/global-figures/global-offshore/.

[17] K W Hermans and J M Peeringa. Future XL monopile foundation design for a 10 MW wind turbine in deep water. 2016.

[18] R. S. Hoes. Spudcan Hydrodynamics - Analysis of hydrodynamic coefficients of spudcans in proximity of the seabed during jack-up installation. 2015.

[19] Leo H. Holthuijsen. Waves in oceanic and coastal waters. *Waves in Oceanic and Coastal Waters*, 2007.

[20] P.M. Jacobs. Evaluation of transient lift loads during a decommissioning operation with a crane vessel. 2017.

[21] Sheng-chao Jiang, Ying Gou, and Bin Teng. Water wave radiation problem by a submerged cylinder. *Journal of Engineering Mechanics*, 2013.

[22] Journee and Massie. *Offshore Hydrodynamics*. 2013.

[23] GH Keulegan and LH Carpenter. Forces on cylinders and plates in an oscillating fluid. *National Bureau of Standards*, 1956. doi: 10.6028/jres.060.043. URL http://scholar.google.com/scholar?hl=en{&}btnG=Search{&}q=intitle:Forces+on+Cylinders+and+Plates+in+an+Oscillating+Fluid{#}0.

[24] Kristin Lewotsky. Understanding power factor and harmonics, 2017, (Accessed: January 2018). URL https://www.motioncontrolonline.org/content-detail.cfm/Motion-Control-Technical-Features/Understanding-Power-Factor-and-Harmonics/content_id/1545.

[25] Mocean. DONG - Air-vent dimensioning analysis for suction buckets. 2015.

[26] 4C Offshore. Aberdeen offshore windfarm eowdc uk, 2017 (Accessed: November 2018). URL http://www.4coffshore.com/windfarms/aberdeen-offshore-wind-farm-(eowdc)-united-kingdom-uk47.html.

[27] SPT Offshore. Suction piles for wind turbines, 2017 (Accessed: November 2017). URL http://www.sptoffshore.com/en/solutions/suction-piles-for-wind-turbines1/suction-piles-for-wind-turbines-siwt(accessedNovember2017).

[28] Shell. Shell scenarios energy models - energy resource database, 2018 (Accessed: March 2018). URL https://www.shell.com/energy-and-innovation/the-energy-future/scenarios/shell-scenarios-energy-models/energy-resource-database.

[29] Limited SMart Wind. Hornsea Offshore Wind Farm - Project Two. 5(January), 2015, accessed Aug 2017. URL https://infrastructure.planninginspectorate.gov.uk/wp-content/ipc/uploads/projects/EN010033/EN010033-000545-7.4.3.2SubseaNoiseTechnicalReport.pdf.

[30] Ken Takagi and Junya Dobashi. Influence of trapped air on the slamming of a ship. *Journal of ship research*, 47, 2003. ISSN 00224502. URL http://www.ingentaconnect.com/content/sname/jsr/2003/00000047/00000003/art00001.

[31] UpWind. Design limits and solutions for very large wind turbines, 2017.

[32] Adriaan Pieter Van't Veer. *Behaviour of catamarans in waves.* PhD thesis, TU Delft, Delft University of Technology, 1998.

[33] V. Venugopal, K. S. Varyani, and P. C. Westlake. Drag and inertia coefficients for horizontally submerged rectangular cylinders in waves and currents. *Proceedings of the Institution of Mechanical Engineers Part M: Journal of Engineering for the Maritime Environment*, 2009.

[34] Det Norske Veritas. DNV H103 - Modelling and Analysis of Marine Operations. (April), 2011.

[35] WindEurope. Financing and investment trends Financing and investments trends. 2016 (Accessed: October 2017). URL https://windeurope.org/about-wind/reports/financing-investment-trends-2016/.

[36] WindPower. Ten of the biggest turbines, 2017 (Accessed: November 2017). URL https://www.windpowermonthly.com/10-biggest-turbines.